AD A105495

AFWAL-TR-81-2082
Volume II

INVESTIGATION OF PLASMA EXCITATION
Volume II: Microwave Plasmas

V. E. Merchant
Universal Energy Systems, Inc.
3195 Plainfield Road
Dayton OH 45432

August 1981

Final Report for Period 7 June 1977 to 20 September 1980

Approved for Public Release; Distribution Unlimited

Aero Propulsion Laboratory
Air Force Wright Aeronautical Laboratories
Air Force Systems Command
Wright-Patterson Air Force Base, Ohio 45433

0 14

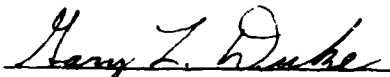This technical report has been reviewed and is approved for publication.
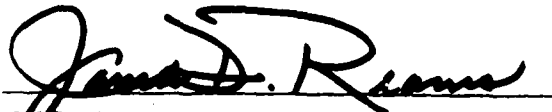
GARY A. DUKE, Capt, USAF
Project Engineer

ROBERT R. BARTHELEMY
Chief, Energy Conversion Branch
Aerospace Power Division

FOR THE COMMANDER

JAMES D. REAMS
Chief, Aerospace Power Division

| REPORT DOCUMENTATION PAGE | READ INSTRUCTIONS BEFORE COMPLETING FORM |
|---|---|

| 1. REPORT NUMBER | 2. GOVT ACCESSION NO. | 3. RECIPIENT'S CATALOG NUMBER |
|---|---|---|
| AFWAL-TR-81-2082, Volume II | AD-A105495 | |

| 4. TITLE (and Subtitle) | 5. TYPE OF REPORT & PERIOD COVERED |
|---|---|
| INVESTIGATION OF PLASMA EXCITATION. Volume II, Microwave Plasmas. | Final Report. 7 June 1977 — 20 Sept 1980 |
| | 6. PERFORMING ORG. REPORT NUMBER |
| | 707-2-F |

| 7. AUTHOR(s) | 8. CONTRACT OR GRANT NUMBER(s) |
|---|---|
| V.E. Merchant | F33615-77-C-3113 |

| 9. PERFORMING ORGANIZATION NAME AND ADDRESS | 10. PROGRAM ELEMENT, PROJECT, TASK AREA & WORK UNIT NUMBERS |
|---|---|
| Universal Energy Systems, Inc. 3195 Plainfield Road Dayton, OH 45432 | Program Element; 61102F Proj/Task/W.U.: 2301/S218 |

| 11. CONTROLLING OFFICE NAME AND ADDRESS | 12. REPORT DATE |
|---|---|
| AF Wright Aeronautical Laboratories (AFWAL/POOC) Wright Patterson AFB, Ohio 45433 | August 1981 |
| | 13. NUMBER OF PAGES |
| | 109 |

| 14. MONITORING AGENCY NAME & ADDRESS(If different from Controlling Office) | 15. SECURITY CLASS. (of this report) |
|---|---|
| | Unclassified |
| | 15a. DECLASSIFICATION/DOWNGRADING SCHEDULE |

16. DISTRIBUTION STATEMENT (of this Report)

Approved for public release; distribution unlimited.

17. DISTRIBUTION STATEMENT (of the abstract entered in Block 20, if different from Report)

18. SUPPLEMENTARY NOTES

19. KEY WORDS (Continue on reverse side if necessary and identify by block number)

Microwave Plasmas
Mercury
Mercury Bromide
Xenon
Hydrogen Chloride
Thallium Iodide
Sulfur
Ultra-violet spectra
Pulsed Discharges

20. ABSTRACT (Continue on reverse side if necessary and identify by block number)

Two different commercially available microwave applications were used to excite plasmas in electrodeless discharge tubes. Plasmas in a variety of gases and gas mixtures were investigated, including mercury, mercury bromide, xenon and hydrogen chloride, thallium iodide and mercury, thallium iodide and xenon, and sulfur. Approximately 35% of the total emission from tubes containing mercury and metallic halide additives occured in the ultra-violet (220-350 nm). However, extensive self-trapping occurred, and the emission was greatest in tubes with low partial pressures, about 100 Torr of the component

DD FORM 1473 EDITION OF 1 NOV 65 IS OBSOLETE
1 JAN 73

materials. Pulsed discharges in mercury bromide produced emission from mercurous bromide, but the application of continuous microwave power resulted in total dissociation and the observed emission was due to atomic mercury.

Pulsed microwave discharges in tubes containing xenon and hydrogen chloride resulted in emission from two bands of the xenon cholride excimer. No excimer emission was seen from discharge tubes containing xenon and thallium iodide, or mercury and thallium iodide. In both cases, the density of the volatile component could not be increased with the available equipment to the value necessary for excimer formation. Discharges in tubes containing sulfur resulted in emission from diatomic sulfur which extended from 280 nm to 500 nm. Techniques were devised for determining the rotational temperature and the vibrational populations distribution of the electronically excited $S_2$. Continuous power loadings as high as 160 KW/liter were achieved in sulfur discharge tubes.

TABLE OF CONTENTS

## LIST OF FIGURES

LIST OF FIGURES (continued)

LIST OF FIGURES (continued)

## LIST OF TABLES

# SECTION I

## INTRODUCTION

A microwave excited plasma is capable of providing electrical energy to a gas without using metallic electrodes. This eliminates the contamination due to degassing and sputtering of the electrodes and allows a more complete characterization of the discharge. In addition, microwave excitation can be used to study discharges in gases which would corrode metal electrodes. This section of the technical report describes an investigation of microwave excited discharges in a variety of gases. In many cases, the materials investigated were solids at room temperature and required extensive heating to produce the gas phase. These included mercury and a mixture of mercury and metallic halide additives which were shown to be efficient emitters of ultraviolet radiation when in a microwave discharge. The investigation also included several materials which are candidates for efficient visible or ultraviolet lasers.

The equipment used to excite and diagnose microwave discharges is described in Section III of this report. A procedure for a detailed analysis of the rotational and vibrational population distribution of microwave excited sulfur molecules is presented in Section IV. Section V describes the results obtained with different gas fills of the discharge tubes, followed by a discussion of the impurities observed in sulfur discharges.

# SECTION II

## MATERIALS INVESTIGATED

### 1. MERCURY VAPOUR

The need for pulsed ultraviolet sources for photolysis has demanded
emphasis on a new regime in pulsed light sources requiring higher tempera-
tures and efficiencies for the production of electromagnetic radiation
with wavelengths of 220 nm to 350 nm [1]. These new demands raise some
questions as to whether the traditional xenon flash tubes would be the
most effective source. It seems that other modes of excitation and other
gases might be more suitable.

A recent commercially available development in cw ultraviolet
sources using a 2.45 GHz microwave excited mercury arc tube has lead to
efficiencies at least equivalent to the direct electric mercury arc with
much longer lifetimes (3000 hours warranty) for the electrodeless
tubes [2]. An air cooled twin antenna irradiator in its commercial
form deposits 120 watts per centimeter along a 25 cm, 8 mm i.d. tube.
With a microwave power input of 3000 watts from 65% efficient magnetrons,
the uv output in the region of interest was about 1000 watts, resulting
in an overall efficiency somewhat better than 20%.

Before the advent of the xenon flash tube which proved so superior
in the visible spectrum, some work was done with pulsed electric dis-
charge mercury tubes [3]. These studies were done with cold tubes with
an average temperature close to ambient. The tubes contained an excess
of condensed mercury in a few torr of argon. When excited with a high
voltage pulse with a half-width of about 3 μsec at a one megawatt power

2

level, a corresponding width for the light pulse was produced with an output of 30 lumens per watt and thus an efficiency of up to one-half that of the cw irradiator produced light.

For these reasons a feasibility test on the pulsed ultraviolet production from microwave excited plasmas had been undertaken [4]. As a starting point, the commercially available mercury filled tubes were tested with the twin antenna irradiator. This report describes the continuation of this work with a microwave irradiation system somewhat modified from that described in reference [4].

The results presented in Section V indicate that strong self absorption of the radiation emitted by mercury atoms was taking place. Additional discharge tubes with doping compounds added to the mercury were tested. The dopants, $SnI_2$ and $MnI_2$, are efficient radiators in the 220-350 nm wavelength region. The vapor pressure of the additives, shown as a function of temperature in Figure 1, is sufficiently low that self trapping is not a problem. The vapor pressure of mercury and of the additives is controlled by the temperature of the inside wall at the coldest spot on the discharge tube.

For mercury and mercury-metal halide electric arc lamps, Waymouth [5,6] describes a calculation of the temperature as a function of discharge tube radius from the steady state energy balance equation. Local thermodynamic equilibrium was assumed in order to use the Saha equation to describe the temperature dependence of the electron density. A calculated temperature profile illustrated in Figure 2 characterizes an arc that is "wall stabilized," that is, it has a relatively steep temperature gradient at the walls. If the arc axis should move from the

3
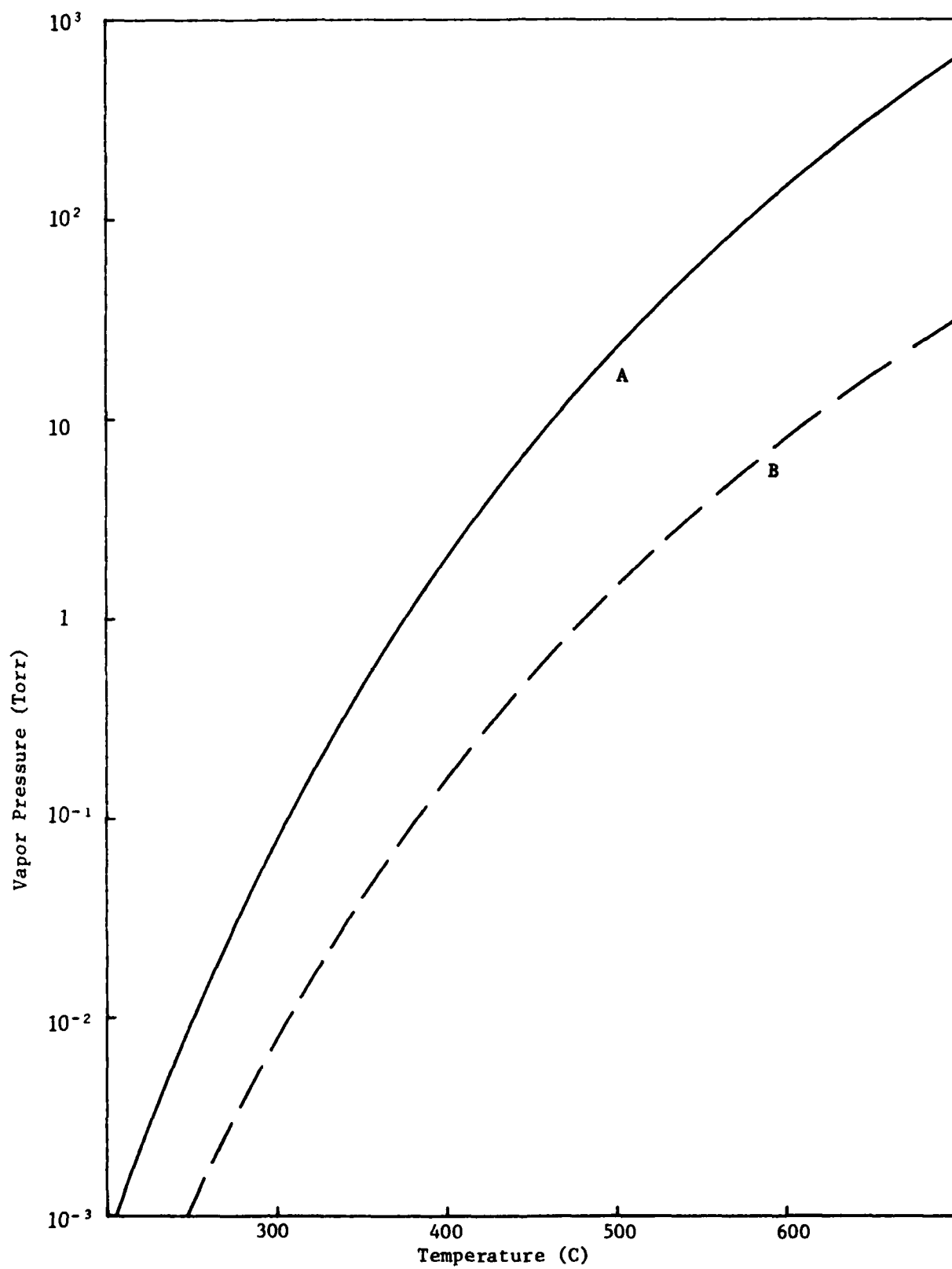
FIGURE 1    Vapor Pressure of (A) SnI$_2$ and (B) MnI$_2$.

4
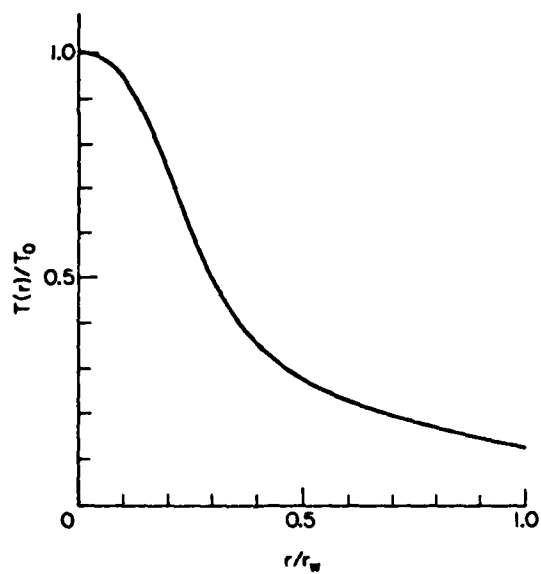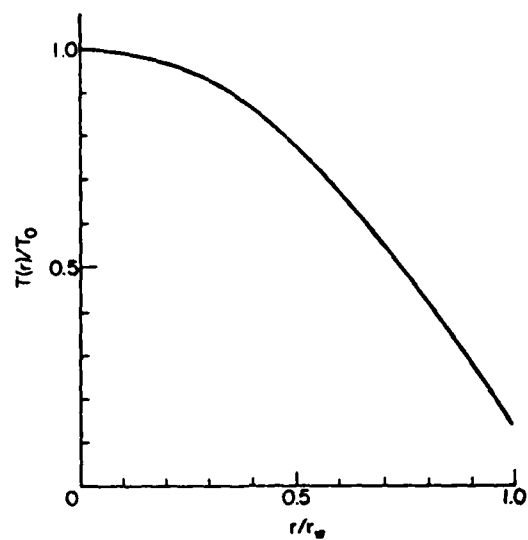
FIGURE 2    Radial temperature profile of (A). Wall-
            stabilized arc such as that of a high pressure
            mercury lamp, and (B) a non-wall-stabilized
            arc.

5

center toward one side, the temperature gradient on that side would steepen. This increases the heat conduction loss and tends to cool the arc on that side. The temperature gradient on the other side would become less steep, resulting in less heat conduction loss which would permit the arc temperature to rise somewhat. The effects of the changes in the heat conduction loss therefore partly cancel the initial motion of the arc column. This serves to stabilize the arc against motion in the tube. By contrast, a temperature profile such as is shown in Figure 2(B) would be unstabilized. A relatively large motion of the arc core in the tube causes little or no change in heat conduction loss and the walls exert no stabilizing influence on the arc. The arc position is therefore strongly affected by convection and turbulence and generally wanders erratically around the cross section.

A wall stabilized arc in a single component discharge occurs when

$$\bar{V} > V_i/2$$

where $V_i$ is the ionization potential and $\bar{V}$ is the average excitation potential. The total optical output per radiating atom can be approximately expressed as a single exponential [5]:

$$P_R \sim Ce^{-e\bar{V}/kT}$$

For a gas in equilibrium the validity of this expression has been checked and $\bar{V}$ has been evaluated for various emitters. Resonance lines are not considered because they are so strongly self absorbed that they contribute little to the total radiation output. For mercury $\bar{V} > V_i/2$ and a well stabilized discharge is observed. Additives added to the mercury will lower the average excitation potential and a non-wall stabilized discharge may result. Such is the case for $HgBr_2$ discharges.

6

## 2. MERCURY BROMIDE

Mercurous bromide fluoresces at about 500 nm when mercuric bromide is dissociated by irradiation with ultraviolet light or by an electrical discharge. Photo dissociation [7] and electric discharge [8,9] lasers at the fluorescing wavelength have been produced in HgBr. Moreover, it has been found that the laser emission is enhanced by the addition of nitrogen to the gas mix [10,11]:

$$e + N_2(X) \rightarrow N_2(A)$$

or

$$e + N_2(X) \rightarrow N_2(B,C)$$

followed by

$$N_2(B,C) \rightarrow N_2(A)$$
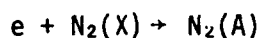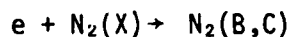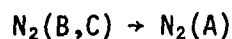
Then dissociative excitation transfer to HgBr takes place

$$N_2(A) + HgBr_2 \rightarrow HgBr(B) + Br + N_2(X)$$
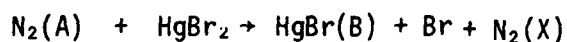
A high density of excited HgBr molecules can be produced in this way. The excited HgBr(B) decay to the ground state

$$HgBr(B) \rightarrow HgBr(X) + h\nu$$
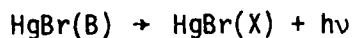
radiating at 502 nm with a lifetime of 24 ns [12], or lasing in the presence of an optical cavity. The mercurous bromide recombines with the free bromide

$$HgBr + Br \rightarrow HgBr_2$$
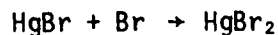
Thus, the system is cyclic and does not consume the active molecule.

*Two discharge tubes containing mercurous bromide, one with and one without nitrogen, were available and the visible emission from these tubes induced by a microwave discharge was studied.*

Mercury bromide is a solid at room temperature. The discharge tubes required heating to produce a significant vapor pressure of $HgBr_2$. The vapor pressure curve is presented in Figure 3.

## 3. XENON CHLORIDE

Rare gas halide excimers lasers (13) are the most common ultra-violet lasers available at this time. This class of lasers is however adversely effected by contamination, and only the XeCl laser has been shown to be capable of long term sealed operation [14]. Microwave discharges were investigated in several mixtures of HCl, xenon, and neon which were prepared in a discharge tube sealed with a teflon valve. In an electron beam assisted discharge, energy deposition occurs mainly through dissociative attachment to vibrationally excited HCl [15]

$$e + HCl \rightarrow HCl(V) + e$$
$$e + HCl(V) \rightarrow H + Cl^-$$
$$Xe + Cl^- \rightarrow XeCl(B) + e$$
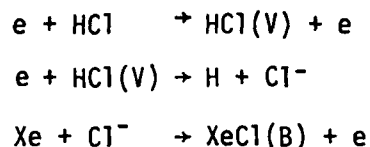
The XeCl(B) decays to a dissociative ground state in $10^{-8}$ seconds [13]. The same excitation pathway may be applicable to the experiments described here.

## 4. THALLIUM-MERCURY

Many of the efficient electronic transition lasers to date have been excimers, in particular the noble gas-halogen excimers such as that

8
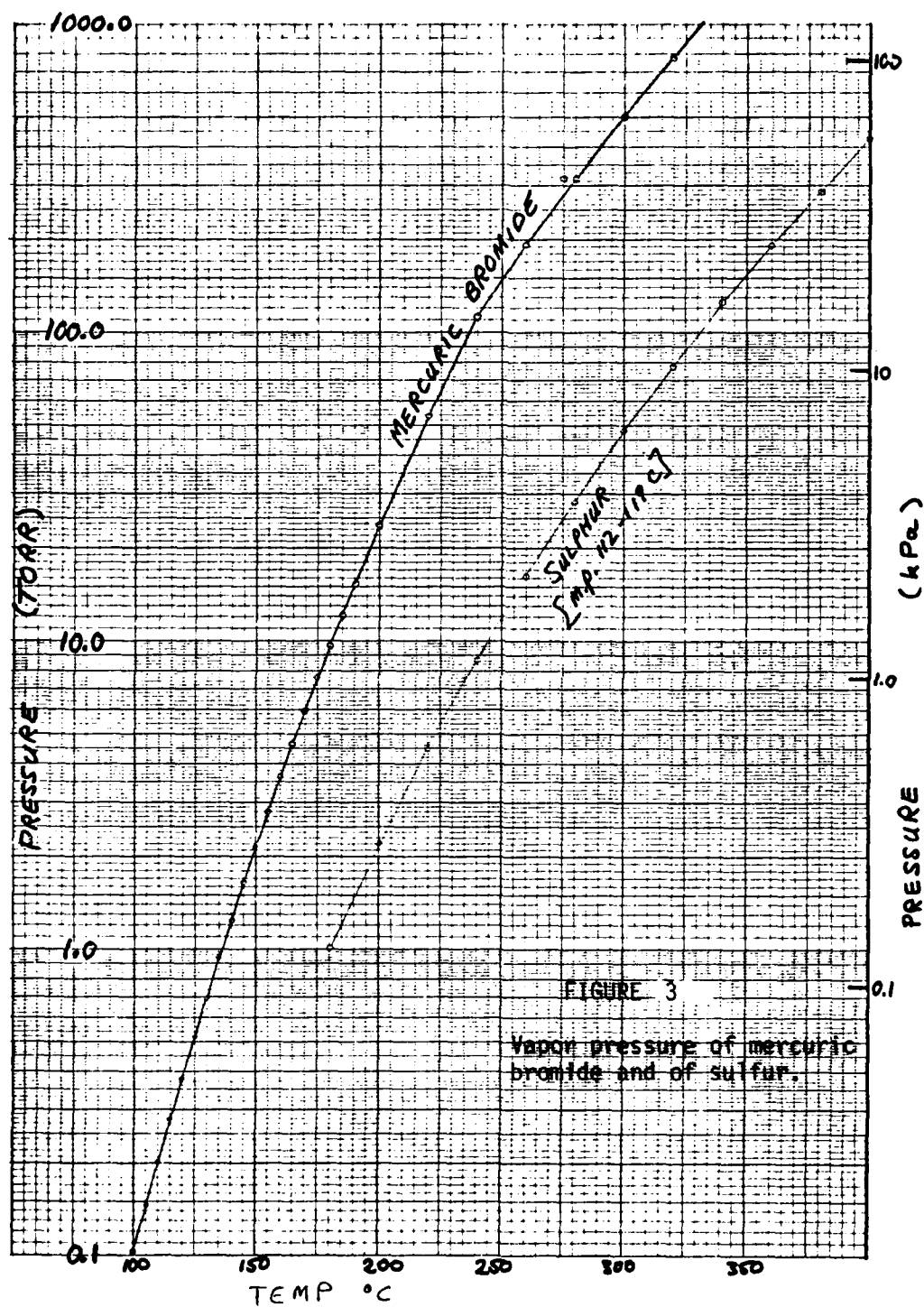
FIGURE 3

Vapor pressure of mercuric bromide and of sulfur.

9

described in the previous section. These and related lasers depend on the production of noble gas metastable atoms of 8 eV or higher energy for their excitation. With such a high initial energy input per molecule, any laser could be efficient only if the lasing band is in the ultra-violet. In order to produce a high efficiency electronic transition laser in the visible, atoms with relatively low lying electronic levels are much more suitable. Since the first excited state of mercury is at 5 eV it can transfer energy relatively efficiently to metal atoms radiating in the visible. Moreover mercury acts much like a noble gas in many respects, perhaps because of the shielding effect of its closed 5d shell, but is twice as polarizable as the rare gas molecules. Therefore, mercury provides strong bands when combined with other metal atoms. Strong Tl-Hg band emission at 459 and 656 nm has been observed in electron beam initiated discharges in TlI and Hg mixtures [16]. This band emission has also been observed from arc discharges [17], uv preionized discharges [18], and RF discharges [19]. A plausible model for the dominant kinetic processes leading to the formation of excited TlHg molecules is presented in reference [16].

Discharge tubes containing thallium iodide and mercury were available. Thallium iodide is used as a source of thallium atoms because its vapor pressure, presented Figure 4, is considerably lower than that of thallium metal. Many of the excited electronic levels of TlI are repulsive, as shown Figure 5. Excited Tl atoms can be produced by electron impact excitation of TlI to repulsive states that dissociate into excited states of the Tl and I atoms, by photodissociation of TlI

10

FIGURE 4

Vapor pressure of thallium iodide

Temperature (Celcius)

Pressure (Torr)

11
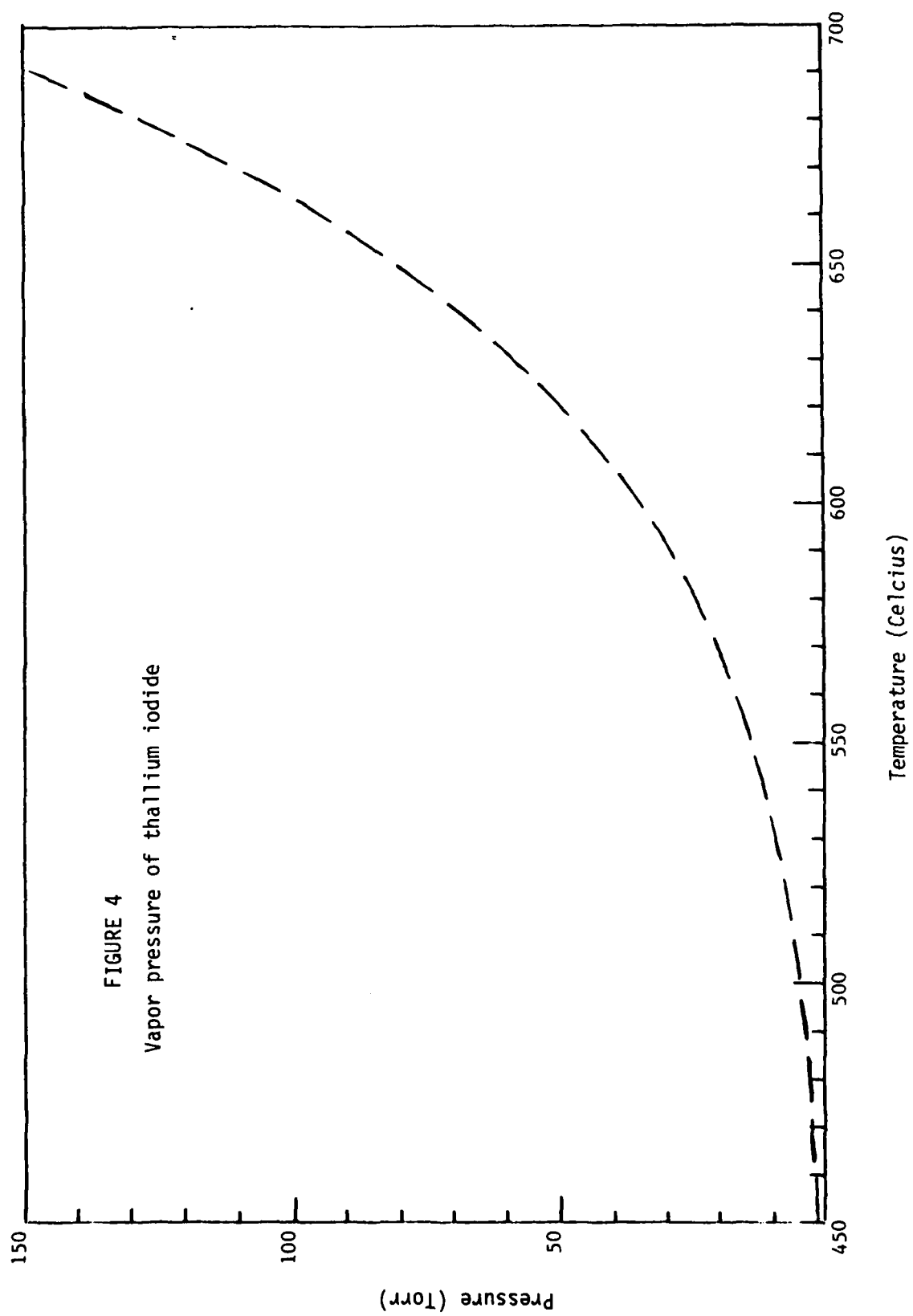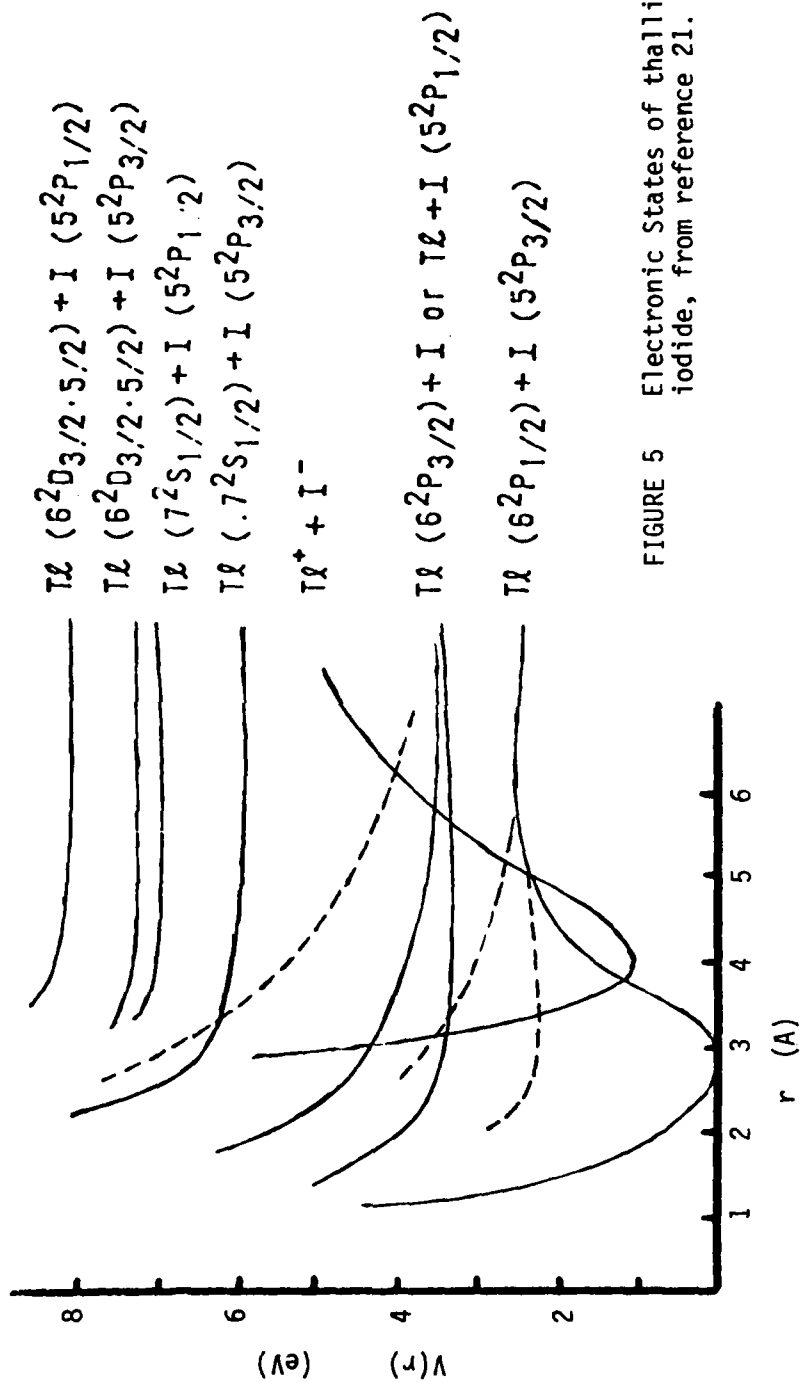
FIGURE 5    Electronic States of thallium
            iodide, from reference 21.

by radiation generated in the discharge, or by resonant energy transfer from mercury metastables to repulsive excited states of TlI. There is insufficient data available to determine the relative importance of the different methods of producing excited thallium atoms.

Ground state thallium recombines with iodine primarily on the vessel wall [20].

## 5. THALLIUM XENON

The thallium xenon system is an interesting visible laser candidate [21,22]. In an electron beam initiated discharge, very strong emission was observed on thallium atomic lines and on TlXe bands at 365, 430, and 600 nm. As in the thallium-mercury experiments, thallium iodide is used as the source of the thallium atoms, lowering the temperature required to produce an appreciable vapor pressure. Nevertheless, a temperature of 440 C was required to produce an appreciable ($10^{16}$ $cm^{-3}$) density of TlI. The design of a test cell for studying electron beam initiated discharges at the high operating temperatures presented formidible engineering problems [22]. To avoid these difficulties, it was desirable to study the optical emission from microwave excited plasmas in electrodeless discharge tubes.

## 6. SULFUR

Recently the $S_2$ molecule has been made to lase in an optically pumped configuration [23,24]. The $S_2$ was formed in a cell heated to 500° C which is sufficient to dissociate a large fraction of the $S_8$ molecules [25]. Optical pumping by a nitrogen laser (337.1 nm), a

frequency doubled dye laser (209 to 305 nm) or an argon ion laser (363.8 nm) produced lasing action over the range 365 to 570 nm. An $S_2$ laser may be a viable alternative to laser or flashlamp pumped liquid dye lasers, since the $S_2$ emission bands cover a wider wavelength range than that of any single dye. A gaseous laser shows promise of maintaining medium homogeneity under higher power pumping than is possible with a liquid laser. Moreover, a gas laser may be electrically pumped eliminating the need for a laser pump.

Stable electrical discharges were achieved in sulfur tubes [26,27] operated at a considerably lower temperature (0-250° C) than that used in the pumping experiments. The $S_2$ (B→X) band emission was observed in great detail. In these experiments interaction between the sulfur vapour and the electrodes formed low vapor pressure metallic sulfides and eventually limited the lifetime of the discharge tubes. A microwave discharge in an electrodeless sulfur tube would overcome this limitation.

The vapor pressure of sulfur as a function of temperature is given Figure 3. The sulfur vapour in equilibrium with the solid is a mixture of sulfur atoms and molecules ranging from $S_2$ to $S_8$ [28,29] , but predominantly $S_8$. As shown in Figure 6, it is apparent that as the temperature is increased a larger fraction of the sulfur is in the form $S_2$. When the temperature is increased beyond that necessary to vaporize all the solid sulfur in a given sample, a much larger fraction of the sulfur will be dissociated into $S_2$ [25]. At pressures of a few torr and temperatures of about 600 C, the sulfur vapor is almost entirely in the form of $S_2$.

14
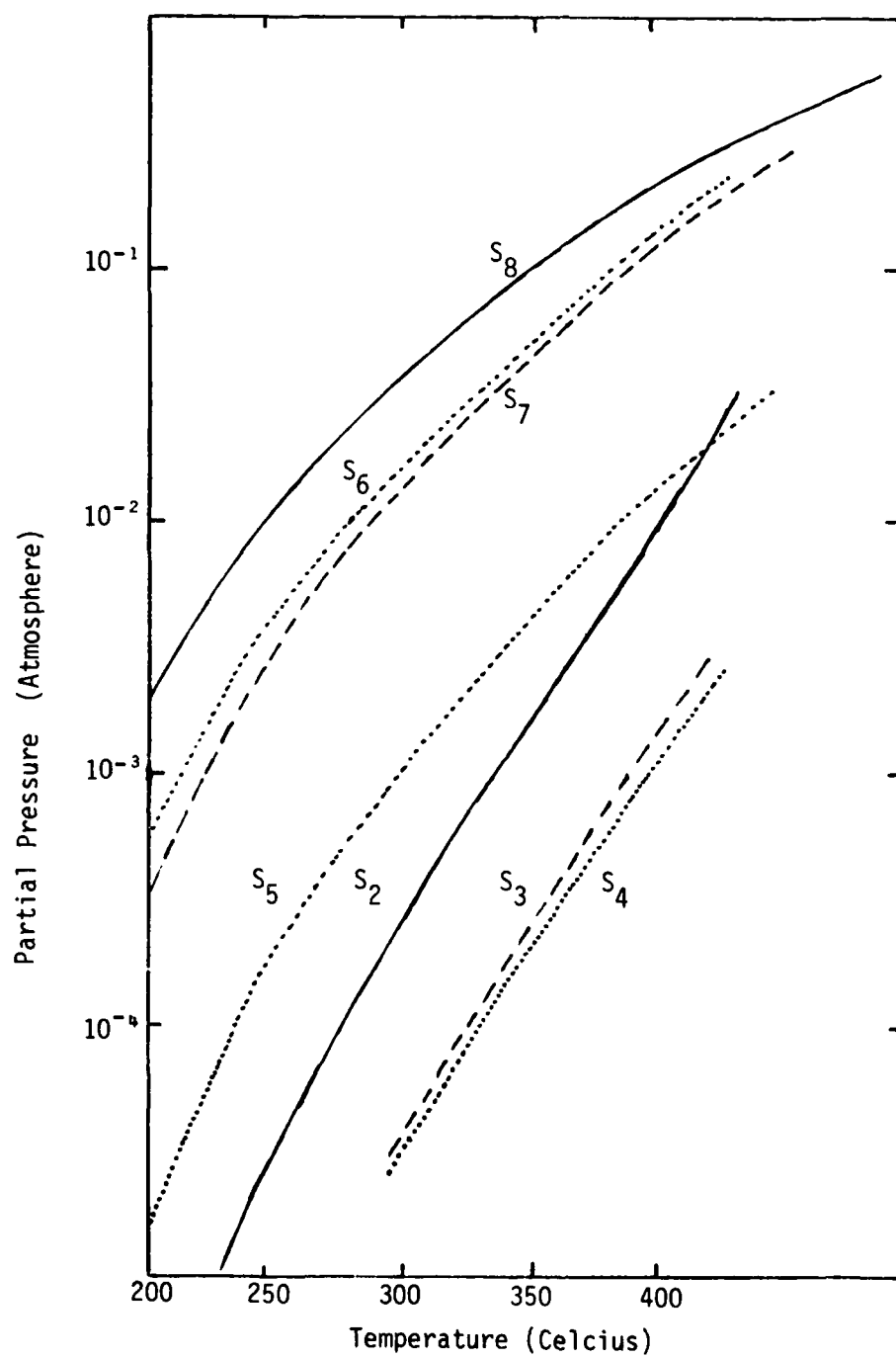
FIGURE 6    Partial pressures of sulfur in
saturated vapor.

15

The potential energy curves of low-lying electronic states of diatomic sulfur are illustrated in Figure 7. The ground state $X\ ^3\Sigma_g^-$ is formed from two ground state sulfur atoms. The $B''\ ^3\pi_u^-$ is also formed from two ground state atoms but is an excited state. The 1u state is an unbound state and represents two ground state atoms coming together with no bond forming. Finally, the $B\ ^3\Sigma_u^-$ state is made up of one excited atom and one ground state atom forming an excited molecule. The levels $v' \leq 9$ of the $B\ ^3\Sigma_u^-$ state are bound and strongly perturbed [30]. The levels $v' \geq 10$ are not observed in emission, probably due to strong predissociation by the 1u state of $S_2$ [31]. The potential energy curves of the two states are fortunately displaced in their relative internuclear position so that the lowest vibrational levels of the $B\ ^3\Sigma_u^-$ excited state lie above high vibrational levels of the ground $X\ ^3\Sigma_g^-$ state which are not populated at temperatures as high as 600° C. The Franck-Condon factors of the B-X transition are as large as 0.1 for many bands and cover broad spectral ranges before diminishing [32]. The measured fluorescence lifetime of the individual states is approximately 45 ns [33]. The bands associated with this system extend from 280 to 700 nm. Emission from the $B''\ ^3\Sigma_u^-$ state to ground has recently been observed [26,27] but appears to be much weaker than that from the $B\ ^3\Sigma_u^-$ state.

The emission intensity on an optically thin molecular band [34] is given by

$$I_{v'v''} = K\,N_v(v')R_e^2(T_{v'v''})q_{v'v''}/\lambda_{v'v''}^4 . \tag{1}$$

Here K is a constant which allows for units, $N_v(v')$ is the relative
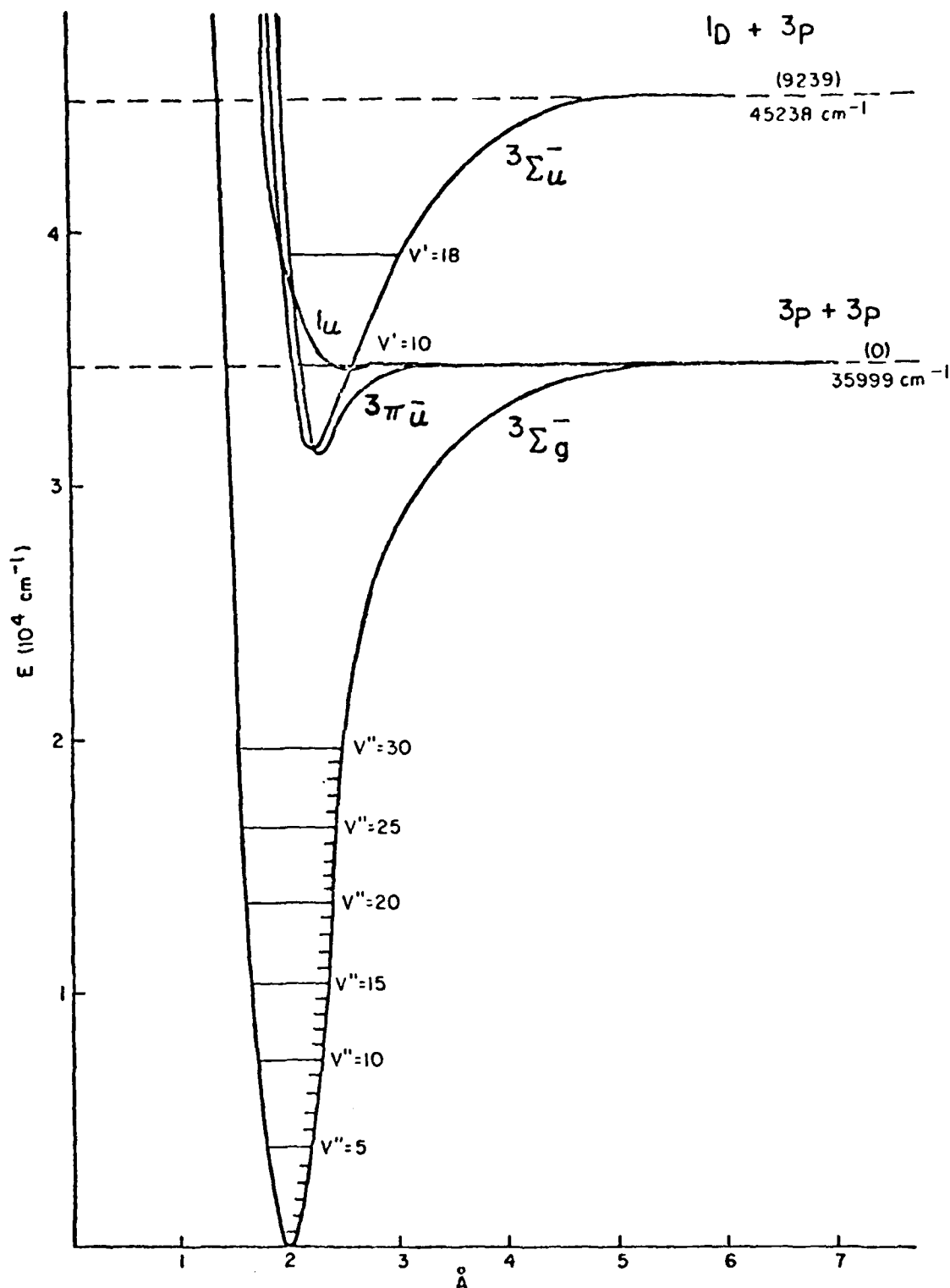
Some of the Approximate Potential Energy Curves of the
S₂ Molecule.

FIGURE 7

population of the vibrational level in the excited electronic state from which the emission occurs, and $q_{v'v''}$ is the Franck-Condon factor for the transition of wavelength $\lambda_{v'v''}$. $R_e(r)$ is the electronic transition dipole moment which in the above formula is evaluated at the r-centroid for the transition. For diatomic sulfur, $R_e$ is independent of $v'$ and $v''$ [32]. Thus, the spontaneous emission is proportional to $q_{v'v''}/\lambda_{v'v''}^4$. This factor is summed over all vibrational levels of the ground state which can make a contribution in a given 10 nm interval. For example, the points plotted at 300 nm represent transitions which occur between 295 and 305 nm and which are listed in Table 1. The sum over $v'$ is plotted in Figure 8 as a function of wavelength for different values of the excited state vibrational quantum number $v'$. With the aid of these functions, the observed spectrum as a function of wavelength can be deconvoluted to find the populations $N_v(v')$ of the vibrational levels of the excited electronic state, as described in a later section.

Absorption and stimulated emission is proportional to $q_{v'v''}/\lambda_{v'v''}$. This function is plotted in Figure 9 for the B-X transition of diatomic sulfur. For a given $v'$, the peak of the stimulated emission probability is shifted to the red with respect to that for the spontaneous emission probability because of the different dependence on wavelength. The fluorescence observed from discharge excited sulfur peaks at wavelengths of about 300 nm. Stimulated emission from sulfur excited under the same conditions is expected to peak at wavelengths near 360 nm.

Rotation of the $S_2$ molecule and its contribution to the observed spectrum is discussed in detail in a later section, in which it is shown that the rotational band shape can be used to determine the gas temperature.

18

TABLE 1    B-X Transitions in Diatomic Sulfur Occurring
Between 295 nm and 305 nm

| $v'$ | $v''$ | $\lambda_{v'v''}$ | $1000 \times q_{v'v''}$ |
|---|---|---|---|
| 3 | 0 | 303.310 | 4 |
| 4 | 0 | 299.700 | 9 |
| 5 | 0 | 296.010 | 15 |
| 5 | 1 | 302.473 | 48 |
| 6 | 1 | 298.976 | 77 |
| 7 | 1 | 295.418 | 80 |
| 7 | 2 | 301.800 | 41 |
| 8 | 2 | 298.274 | 4 |
| 8 | 3 | 304.726 | 38 |
| 9 | 3 | 301.187 | 58 |
| | | nm | |
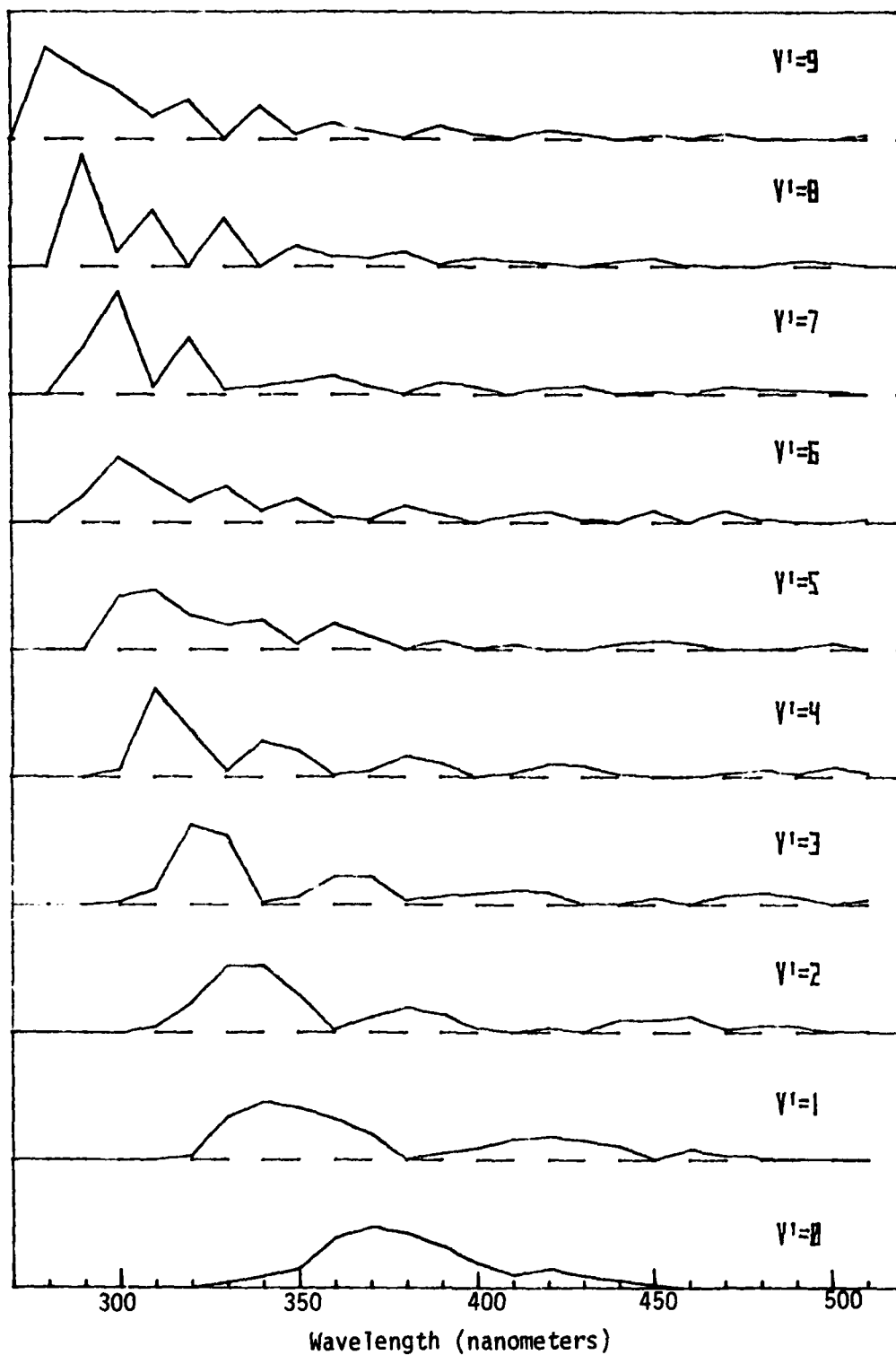
FIGURE 8   Probability of spontaneous emission from vibrational states of excited $S_2$.

20

V'=9

V'=8

V'=7

V'=6

V'=5

V'=4

V'=3

V'=2

V'=1

V'=0

Wavelength (nanometers)
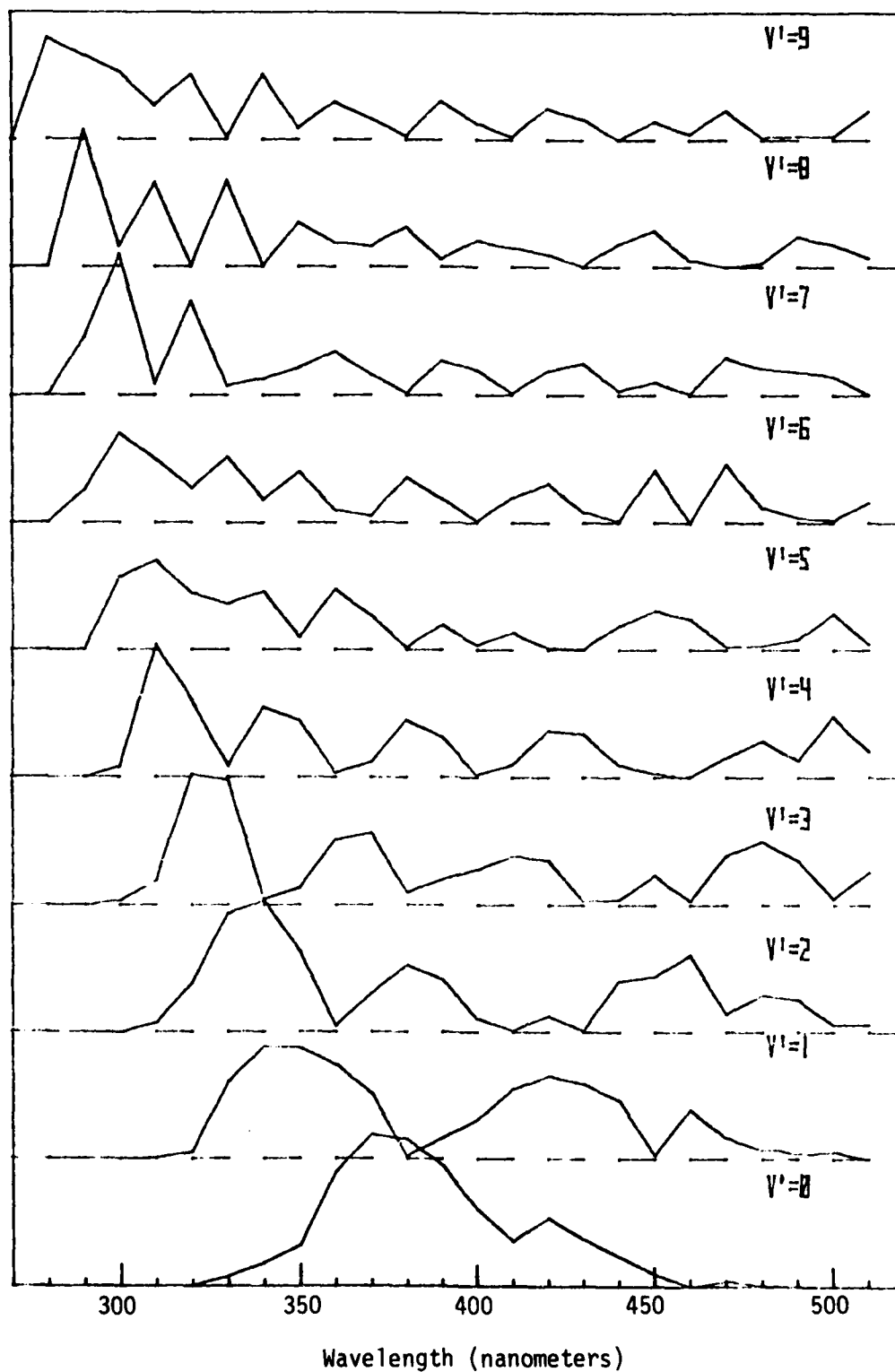
FIGURE 9    Probability of stimulated emission from
            excited states of $S_2$.

21

SECTION III

MICROWAVE APPLICATORS AND AUXILLIARY EQUIPMENT

## 1.  MICROWAVE APPARATUS

A variety of microwave equipment was available to study discharges.
This equipment has been described in reference 4 and in the manual prepared
for operation of the microwave irradiation facility [35].  The two applica-
tors which could be used in irradiation experiments were the Fusion Systems
twin antenna applicator in which the plasma tube forms a lossy central
conductor in a coaxial line and the interdigital applicator in which the
discharge is excited by evanescent fields near the applicator surface.
Figure 10 shows as an example the microwave equipment used with the sand-
wich applicator formed from two interdigital applicators.  Two continuous
and two pulsed microwave sources could be used.  Circulators and dummy
loads protected the sources from reflected and transmitted power not
absorbed by the plasma, and power meters monitored the reflected and
transmitted power.  A similar configuration was used with the Fusion Systems
applicator, as described in the references mentioned above.

## 2.  OPTICAL DIAGNOSTIC AND RECORDING EQUIPMENT

The optical components used to monitor the visible and ultraviolet
emission from plasma tubes is illustrated in Figure 11.  The output from
the photomultiplier was processed by the data collection system shown in
Figure 12 to separate out the pulsed and CW components of the emission.
Two computer programs PEAKPR and MERCHA were used predominately with
mercury and sulfur discharge tubes respectively and are described in

22
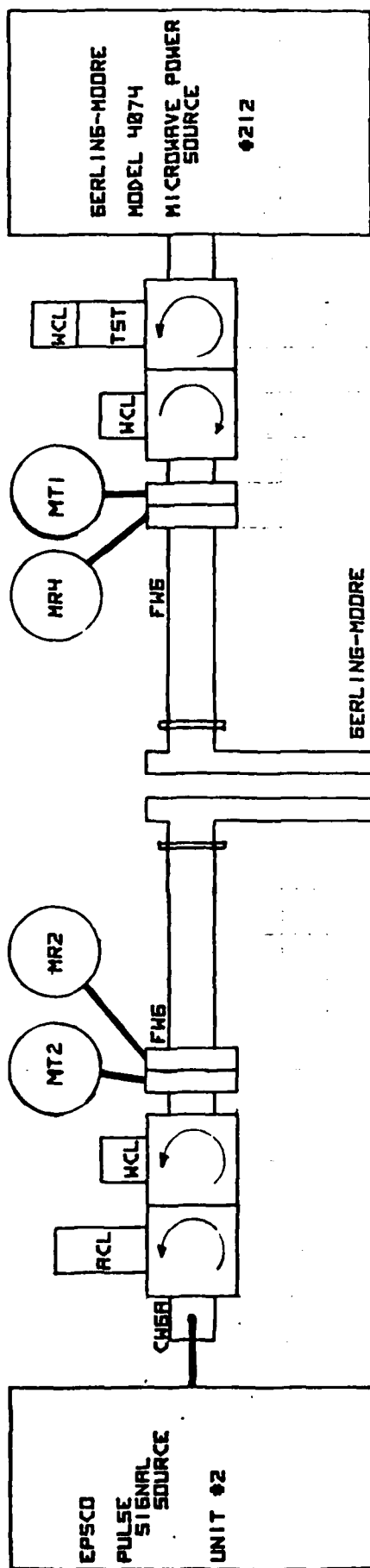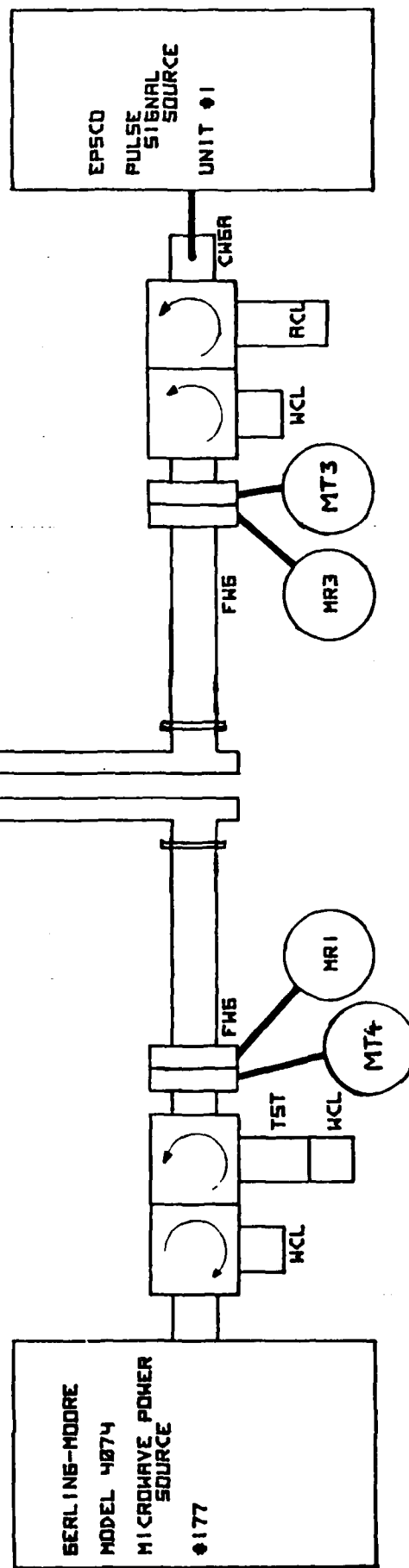
FIGURE 10 Experimental arrangement utilizing sandwich applicator

23

RCA 4840 Photomultiplier

Jarrell-Ash
Model 82-410
f/3.5 Ebert
Monochromator
with interchangeable
2360 mm$^{-1}$ and 1180 mm$^{-1}$
gratings

entrance slit

$d_s$

aperture (diameter a)

$d_a$

lens (focal length f)

filters (if used)
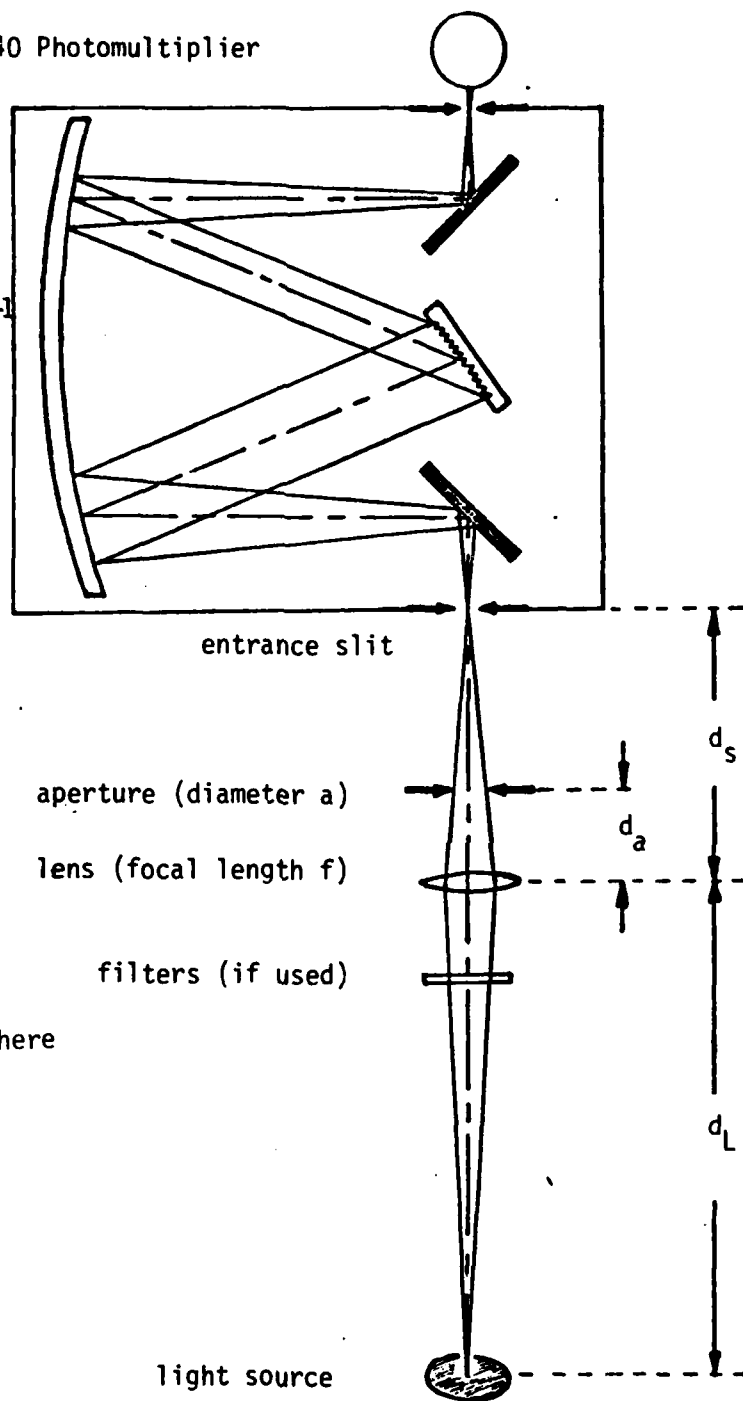
In experiments described here

$d_s$ = 6.76

$d_a$ = 1.14

$d_L$ = 86.2

a = 1.35

f = 6.27 cm

$d_L$

light source

FIGURE 11

SCHEMATIC DIAGRAM OF OPTICAL COMPONENTS

24
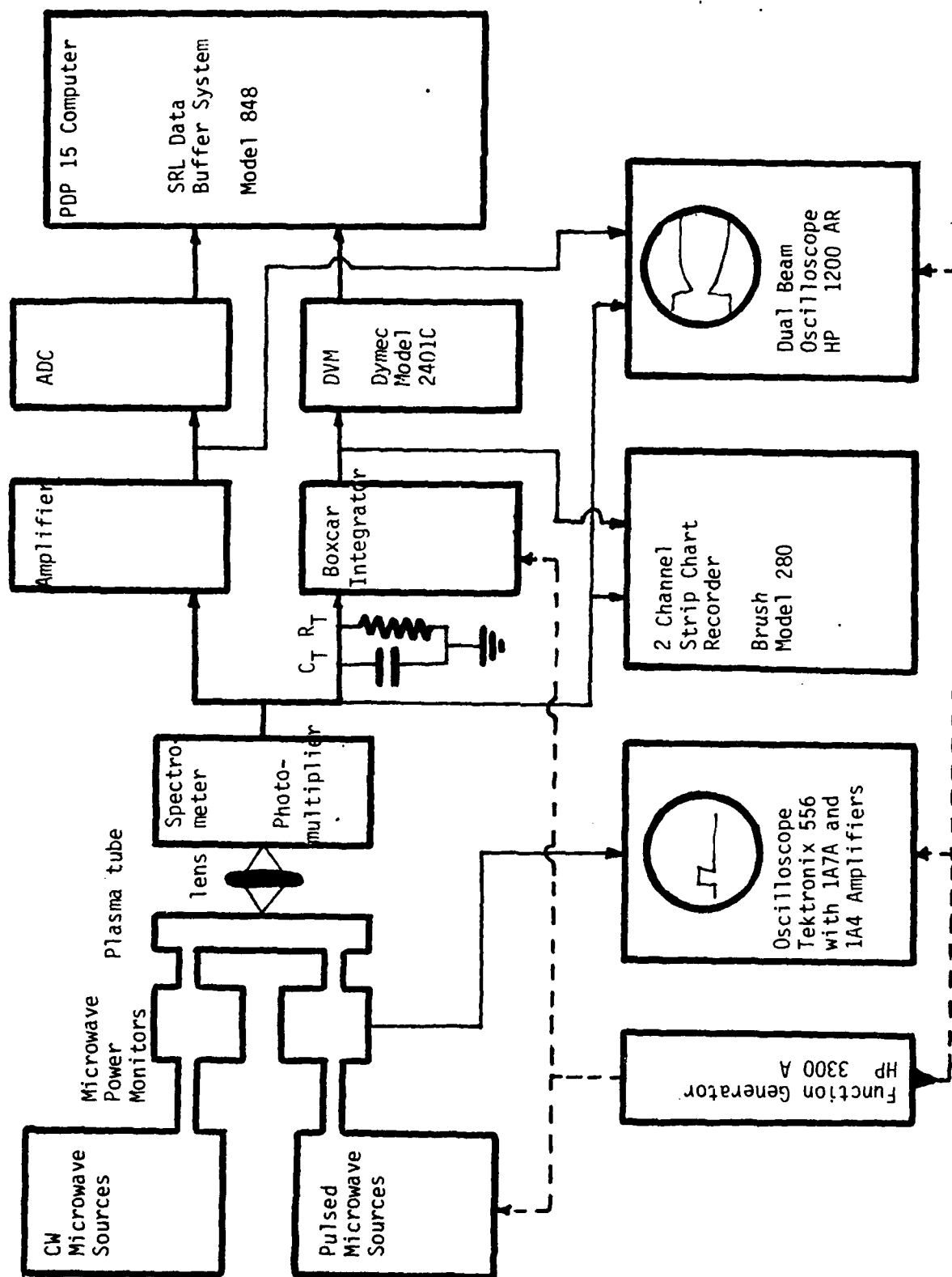
FIGURE 12   Components of the Data Collection System

detail in the manual for operating the microwave facility [35]. The computer programs corrected the photomultiplier readings for the background readings, made adjustments for the spectral sensitivity of the photomultiplier and spectrometer, and integrated the output of the discharge tubes over various spectral regions.

The programs required as input an analytical form of the spectral sensitivity curve. This was prepared by calibrating the spectrometer and photomultiplier with a tungsten lamp, as described in the report "Optical Calibration of Spectral Diagnostics for the Microwave Irradiation Facility."

3.   PREPARATION OF DISCHARGE TUBES

A vacuum station for fabrication of quartz discharge tubes has been assembled. The station has facilities for filling tubes from a stainless steel manifold connected to as many as four gas cylinders, and from a glass manifold connected to as many as four glass gas bottles. The base pressure of the system is approximately $1.5 \times 10^{-6}$ torr. A two inch oil diffusion pump provides vacuum pumping for the system.

In the duration of the contract about twenty five discharge tubes were fabricated. Most of these contained sulfur. The usual method for filling discharge tubes with sulfur involved preparing and cleaning a discharge tube, placing into the tube the desired amount of sulfur, and having the tube fused onto a vacuum fill station. The tube was evacuated, back filled with several torr of helium or some other buffer gas, then sealed and removed from the vacuum fill station.

A new technique for preparing sulfur discharge tubes has been tried and abandoned. The discharge tube was prepared, fused onto the vacuum

26

fill station, and then baked under vacuum for several hours to ensure its cleanliness. When the tube was returned to room temperature, sulfur was distilled from a reservoir attached to the vacuum fill station into the discharge tube which was then backfilled and sealed. To maintain the purity of the sulfur in the reservoir, the reservoir was valved off from the main part of the vacuum system when it was not required. A glass-teflon valve was used because of the corrosiveness of sulfur vapor. The valve was heated during the distillation process to prevent condensation of sulfur in the valve. The failure of this teflon valve under high temperature operation lead to the termination of the attempt to prepare ultraclean tubes by distillation. The heated valve allowed air to leak into the system during distillation. The presence of a background gas slowed down the distillation process and left impurities in the otherwise clean discharge tube.

The discharge tubes were typically 6 or 8 nm inside diameter with a one mm wall and 20 cm in length. However, both wider and narrower discharge tubes were made. Some discharge tubes with Brewster windows were prepared.

SECTION IV

ANALYSIS OF SULFUR DISCHARGES

## 1. THE SPECTRA OF SULFUR

The visible and ultraviolet emission from microwave excited

sulfur, shown in Figure 13, is identified as the B-X transition of $S_2$ [36].

The two peaks at low wavelength, shown in more detail in Figure 14 ,

correspond to B:v'=9 to X:v"=0 and B:v'=8 to X:v"=0 respectively, with

unresolved rotational structure.  It was found possible to determine the

temperature of the gas in situ by comparing the bandshape of the unresolved

structure with the results of a computer simulation.  The method for

determining temperature was the basis for a presentation at the 1979

annual meeting of the Optical Society of America [37] and has been

submitted for publication [38].

The distribution of population over the vibrational levels of the

electronically excited state has been determined.  The amount of radiation

emitted in 10 nm intervals between 275 nm and 515 nm is deconvoluted with

the known Franck Condon factors for transitions which can make a contri-

bution to each interval  (Figure 8)   to find the population of vibrational

states.  This procedure is described later in this section.

In all the peaks of the $S_2$ spectrum except the two at lowest wave-

lengths shown in  Figure 14, there are different but overlapping

vibrational transitions.  Numerous perturbations of the $B^3\Sigma_u$ state arise

by interaction with a $1_u$ state [31].  Rotationally resolved measurements

[31] using a 3.4 m spectrometer indicate that rotational lines greater

than $J' \gtrsim 36$ are not observed in v'=9 and greater than $J' \gtrsim 60$ are not

28

WAVELENGTH IN NANOMETERS
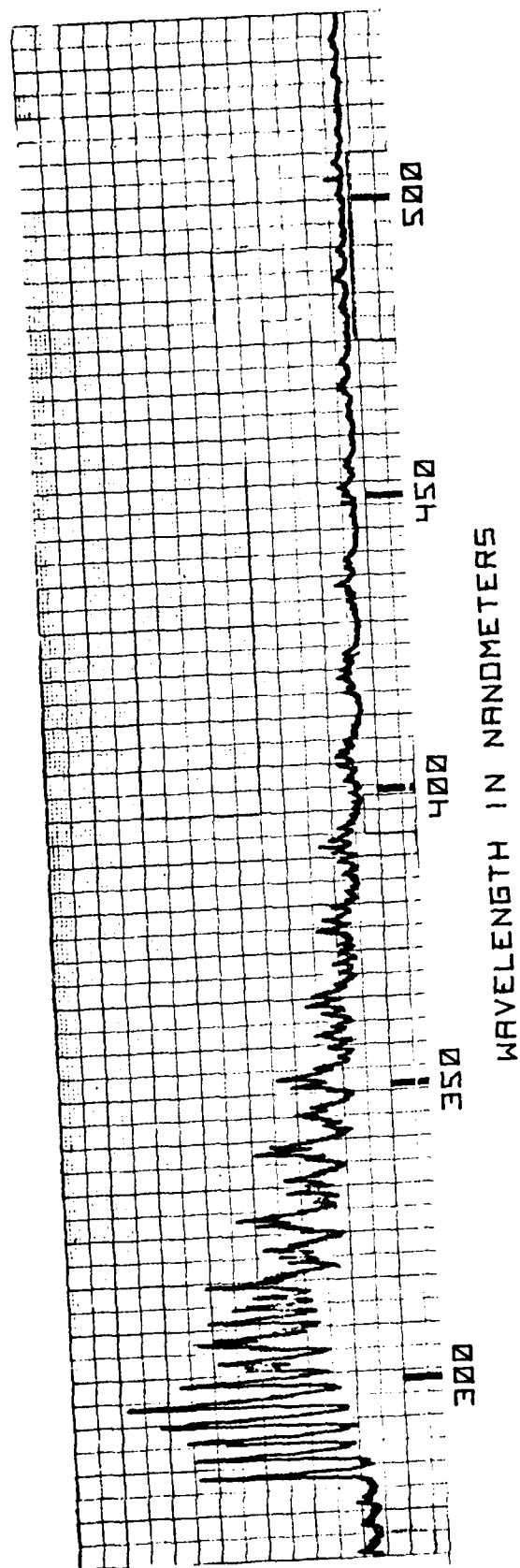
FIGURE 13    B-X emission spectra of microwave excited $S_2$.
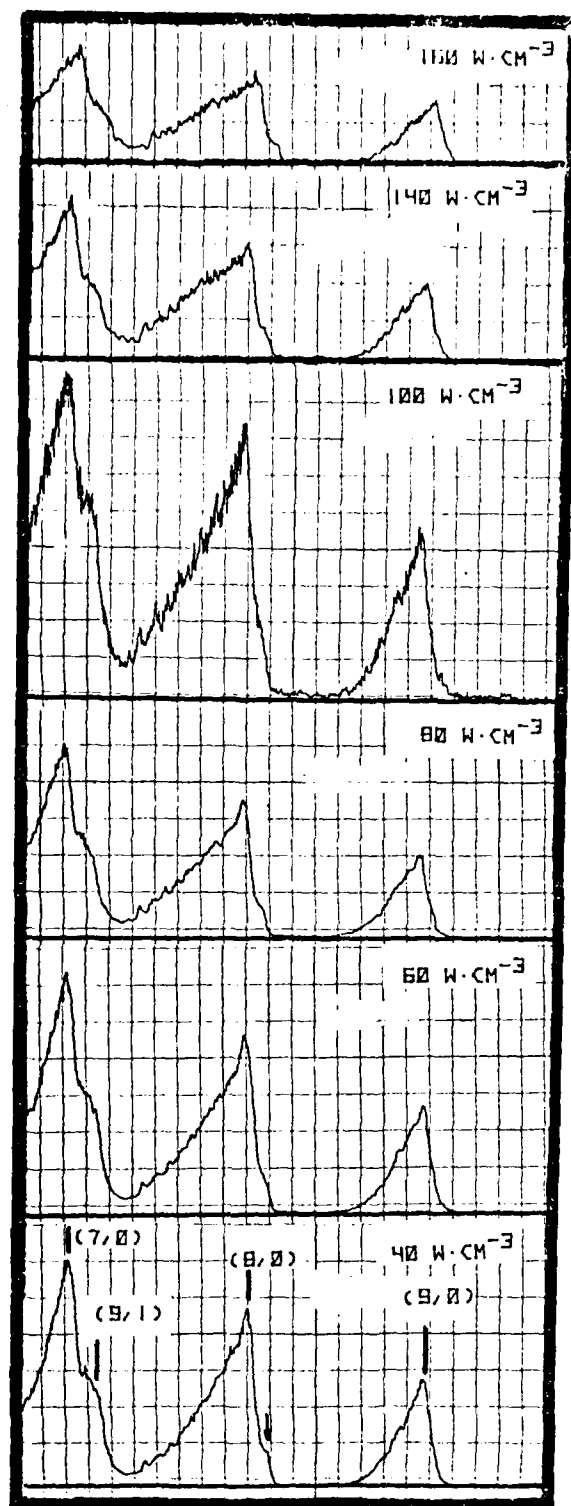
FIGURE 14 Emission on the range 281 nm to 293 nm (right side to
left side) from a tube containing 70 Torr of sulfur gas,
for a variety of absorbed power levels    The gas tempera-
tures, determined using the method described in the text,
increases from 102 C at 40 W/cm³ to 458 C at 140 W/cm³.

30

observed in v'=8. This is due to predissociation of the highly excited
levels for which the energy is greater than the dissociation energy of
$S_2$. Because the perturbations of the v'=8 level are less severe than
those of the v'=9 level, and because the B:v'=8 to X:v"=0 transition is
clearly separated from neighboring transitions, we choose to use the
width of this peak for temperature determination.

Both the B and X states of $S_2$ are $^3\Sigma^-$. Because of the second order
spin orbit interaction involving mixing of other electronic levels, the
coupling between the electronic spin angular momentum $\overline{S}$ and rotational
angular momentum $\overline{N}$ is intermediate between Hund's cases (a) and (b) [39].
For each state the levels with low N tend to belong to case (a) and
those with high N to case (b). For $^3\Sigma$ molecules belonging to case (b)
as well as those with intermediate coupling, each rotational level is a
triplet with values of the total angular momentum quantum number $J(\overline{J}=\overline{N}+\overline{S})$
equal to N-1, N, and N+1. The rotational levels of both the upper and
ground state are split with the splitting determined by a spin-rotation
coupling constant $\gamma$ and a spin-spin coupling constant $\lambda$ [40].

There are fourteen possible transitions to the ground state for each
value of the excited rotational quantum number N", as illustrated in
Figure 15. Only ten of the fourteen transitions will make a substantial
contribution to the emission. The fourteen transitions are listed
in Table 2 along with the designation of the triplet component of the
upper and lower states and the change in the rotational and total angular
momentum quantum numbers. Comparison of Figure 15 and Table 2 shows
that for the six strongest transitions there is no change of the spin

31
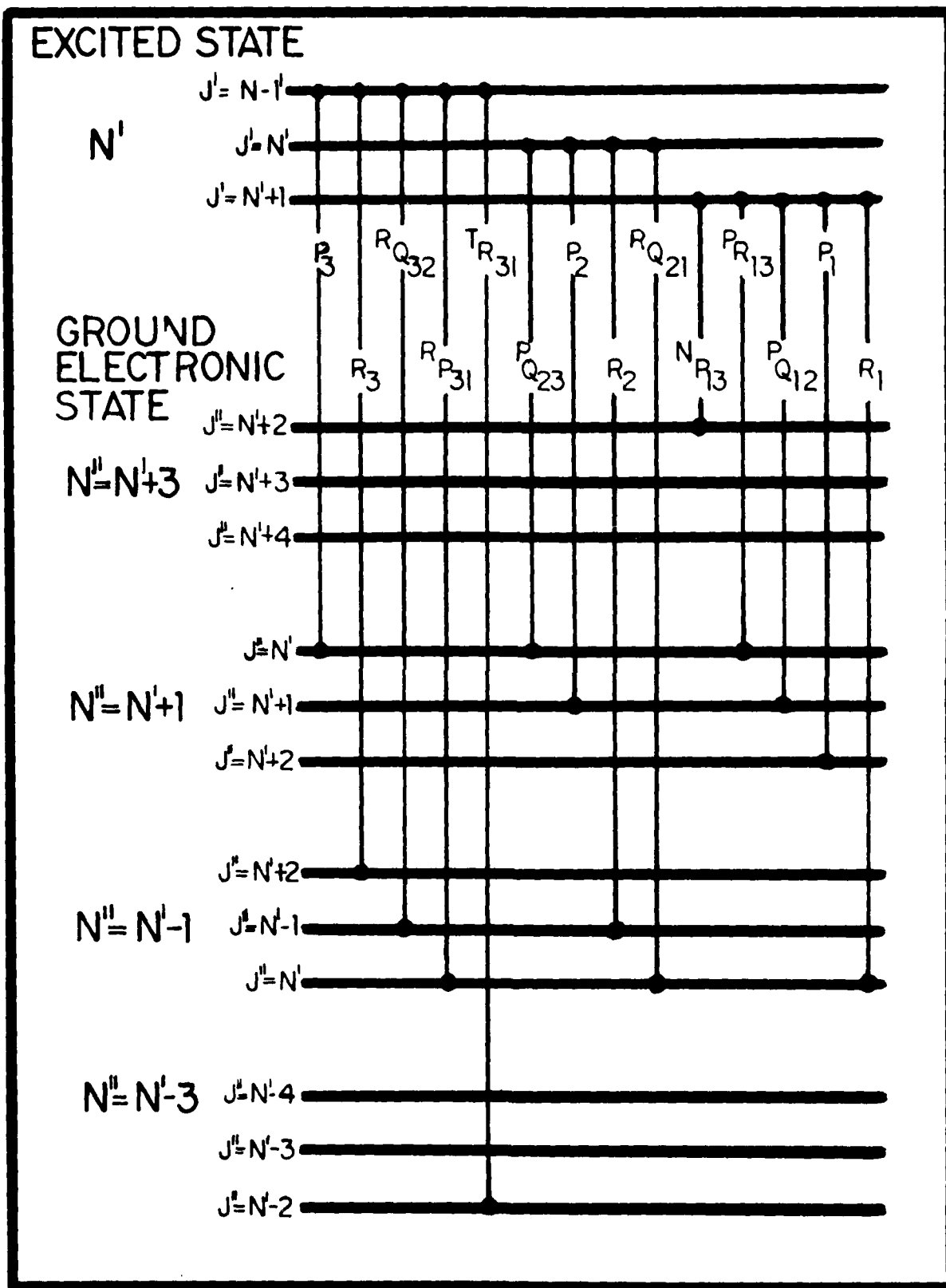
FIGURE 15  $^3\Sigma^-$ to $^3\Sigma^-$ transitions from an excited level with quantum number $N'$.

## TABLE 2

### Tabulation of the transitions originating from states with a given value of rotational quantum number N'.

| | | Upper Level | Lower Level | N"-N' ΔN | J"-J' ΔJ | TRANSITIONS WHICH DO NOT OCCUR FOR | | |
|---|---|---|---|---|---|---|---|---|
| | | | | | | N'=0 | N'=1 | N'=2 |
| 1 | $P_3$ | $F_3$ | $F_3$ | +1 | +1 | X | | |
| 2 | $R_3$ | $F_3$ | $F_3$ | -1 | -1 | X | X | X |
| 3 | $^R Q_{32}$ | $F_3$ | $F_2$ | -1 | 0 | X | X | |
| 4 | $^R P_{31}$ | $F_3$ | $F_1$ | -1 | +1 | X | | |
| 5 | $^T R_{31}$ | $F_3$ | $F_1$ | -3 | -1 | X | X | X |
| 6 | $^N P_{13}$ | $F_1$ | $F_3$ | +3 | +1 | | | |
| 7 | $^P R_{13}$ | $F_1$ | $F_3$ | +1 | -1 | X | | |
| 8 | $^P Q_{12}$ | $F_1$ | $F_2$ | +1 | 0 | | | |
| 9 | $P_1$ | $F_1$ | $F_1$ | +1 | +1 | | | |
| 10 | $R_1$ | $F_1$ | $F_1$ | -1 | -1 | X | | |
| 11 | $^P Q_{23}$ | $F_2$ | $F_3$ | +1 | 0 | X | | |
| 12 | $P_2$ | $F_2$ | $F_2$ | +1 | +1 | X | | |
| 13 | $R_2$ | $F_2$ | $F_2$ | -1 | -1 | X | X | |
| 14 | $^R Q_{21}$ | $F_2$ | $F_1$ | -1 | 0 | X | | |

33

quantum number. In the second group of four transitions, the spin quantum

number changes only by two units while the total angular momentum quantum

number changes by one unit. In the weakest group of four transitions,

the spin quantum number and the rotational quantum number each change

by one unit in the opposite sense and the total angular momentum quantum

number is unchanged. Further details, including formulae for the

rotational energy levels and the Hönl-London line strength factors, are

given by Tatum and Watson [40].

The coupling constants $\gamma''$ and $\lambda''$ for the ground state are well

known for all vibrational levels [30,41]. However, for the excited

state, the values for $\lambda'$ are found to depend strongly on the vibrational

level, with $\lambda' \simeq -4.7$ cm$^{-1}$ for v'=0,2, and 4; $\lambda' \simeq 9.5$ cm$^{-1}$ for v'=1,3, and 5;

and $\lambda' < 0$ for v'=6 and 7 [42]. The study of the rotational bandshape

presented here for the B:v'=8 to X:v'=0 transition suggests that $\lambda' \simeq -5$

is a suitable value for v'=8.

In diatomic sulfur there are only odd numbered rotational levels

in the ground state and even numbered rotational levels in the B state.

This is a consequence of symmetry of the eigenfunction with respect to

interchange of identical nuclei [39].

## 2. EMISSION INTENSITY FROM MOLECULES IN EQUILIBRIUM

An expression is derived for the wavelength dependence of the

emission from electronically excited $S_2$ molecules. Assuming rotational

equilibrium, the Boltzmann equation is used to describe the rotational

population in the excited state. Tnis occurs only if molecule-molecule

collisions dominate the kinetics of the excited state. That is,

34

rotational relaxation in collisions is more frequent than electron-molecule excitation, radiation from the excited state, and cascade electronic transitions into the B excited state. Since the radiative lifetime of the $S_2$:B state is about 40 ns [41], this condition implies an $S_2$ pressure of greater than four torr, assuming a collision frequency of $5 \times 10^9$ $sec^{-1}atm^{-1}$.

The power radiated from a unit volume of gas on the ith transition originating from the excited rotational state N' is

$$I_i(N') = KS_i(N') \exp[-E_i'(N')/kT] \tag{2}$$

Here $S_i(N')$ is the rotational line strength for the ith transition, as shown in Figure 16, and $E_i'$ is the rotational energy of the upper state for the ith transition. K is a factor which is dependent on temperature but approximately independent of N'. It is proportional to the Franck-Condon factor, the square of the electronic dipole moment, and the total population density of the excited state.

This transition occurs at a frequency

$$\nu_i(N') = \nu_e + \Delta\nu_{vib} + F_i'(N') - F_i''(N'') \tag{3}$$

which may be calculated with the formulae of Tatum and Watson [40] and the data of [41]. The transition has a line shape function $g[\nu, \nu_i(N')]$, so the intensity $I(\nu)$ of emission at a frequency $\nu$ is given by

$$I(\nu) = \sum_i \sum_{N'} I_i(N')g[\nu,\nu_i(N')] \tag{4}$$

For a spectrometer setting $\nu_s$, the response is determined by a slit response function $W[\nu,\nu_s]$. Then the observed signal is given by

35
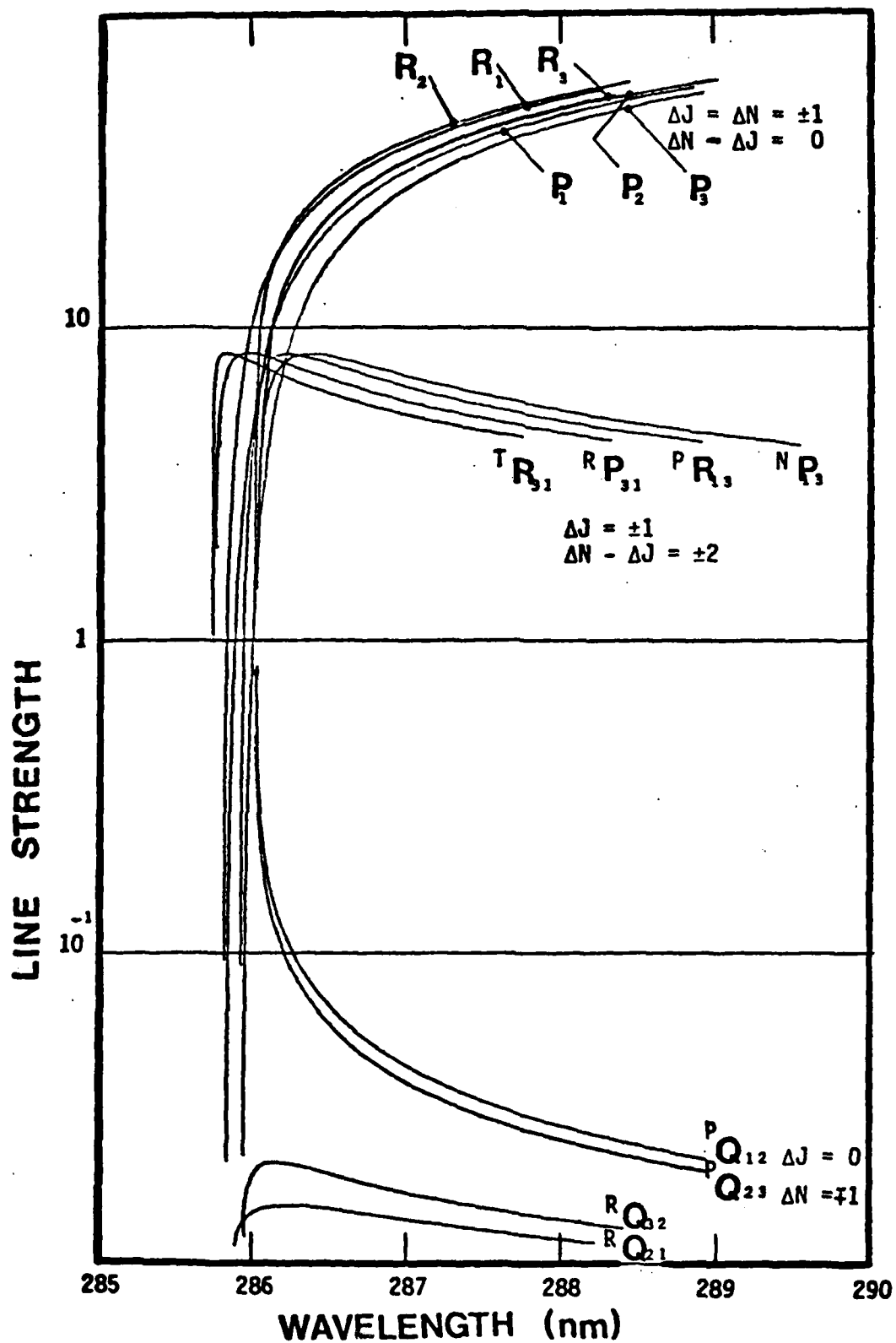
FIGURE 16    Line strength factors for electronic transitions in diatomic sulfur, as a function of the transition wavelength.

36

$$S(\nu_s) = \int_0^\infty d\nu W[\nu,\nu_s] \Sigma_i \Sigma_{N'} I_i(N') g[\nu,\nu_i(N')] \qquad (5)$$

For the apparatus used here, the slit response function has a halfwidth (FWHM) of about 20 $cm^{-1}$ while the natural linewidth of the transition is about 0.007 $cm^{-1}$ and the Doppler width at room temperature is about 0.055 $cm^{-1}$. Hence the line shape function is approximated by a delta function and

$$S(\nu_s) = \Sigma_i \Sigma_{N'} I_i(N') W[\nu_i(N'),\nu_s] \qquad (6)$$

## 3. EMISSION INTENSITY FROM LOW PRESSURE DISCHARGES

When rotational relaxation of excited state molecules is negligible, the rotational distribution of the $S_2$:B molecules is determined by the radiative transition rate, which depletes the excited state, and by the electron excitation rate. It is assumed that the dominant source of the $S_2(B)$ molecules, which are responsible for the observed emission, is electron excitation from ground state molecules.

$$S_2(X) + e \rightarrow S_2(B) + e \qquad (7)$$

This assumes that the cascade transitions

$$S_2(C,D,...) \rightarrow S_2(B) \qquad (8)$$

and excitation in dissociation of higher sulfur allotopes

37

$$S_n = e \rightarrow S_2(B) + e + \text{fragments} \qquad (9)$$

are negligible.

The electron excitation cross sections for the X to B transition process [7] are not known. As a first approximation, the electron excitation cross section can be considered to be proportional to the optical emission cross sections, which is proportional to the rotational line strength. Then the observed visible and ultraviolet emission takes place on the same transitions as used in excitation.

If $S_i(N')$ denotes the line strength for the $i^{th}$ transition into the N' level, and $E_j''(N')$ denotes the energy of the level from which this transition originates, then the excitation rate into a particular rotational sublevel (N',J') of the excited state is given by

$$R(N',J') = \sum_j{}' K\, S_j(N') \exp - \frac{E_j''(N')}{kT}$$

The prime on the summation is used to indicate that the summation is performed not over all the ten main transitions into the levels with a given value of N', but only those transitions into the particular N',J' sublevel. This is four transitions for $J'=N'\pm1$ and two for $J'=N'$.

This excited state now reradiates into the ground electronic state. The given excited state can radiate on any one of a number of transitions. The fraction of the power radiated on the $i^{th}$ transition is given by $S_i / \sum_j{}' S_j$.

Since rotational redistribution in collisions is assumed to be negligible, the rate of radiation from an N', J' level is equal to the

rate of excitation into the level. With the approximations described above, the power radiated on the $i^{th}$ transition originating from the excited rotational level N' is

$$I_i(N') = K \frac{S_i(N')}{\sum_j' S_j(N')} \sum_j' S_j(N')\exp -\frac{E_j''(N')}{kT} \qquad (10)$$

## 4. COMPUTATIONS

A computer program was written to calculate the transition frequencies and the intensities of the individual transitions, given by either equation [2] or [10]. It performed the summation (equation (6)) over the transitions weighted by the transition strength and the slit response function. The program provided a plot of emission intensity as a function of wavelength. The gas temperature and the spectroscopic constants $\lambda'$ and $\gamma'$ for which accurate values were not available, were adjustable parameters. The slit response function was digitalized and used as input to the computer program.

## 5. DEPENDENCE OF BANDSHAPE ON TEMPERATURE

For the $S_2$ transition of interest, the computed dependence of emission on wavelength and temperature is shown in Figure 17. Two different techniques were used to compare the computed curves with the experimental curves. The halfwidth is linearly dependent on temperature.

$$T = 565 \Delta\lambda_{FWHM} - 123 \qquad (11)$$

and

39
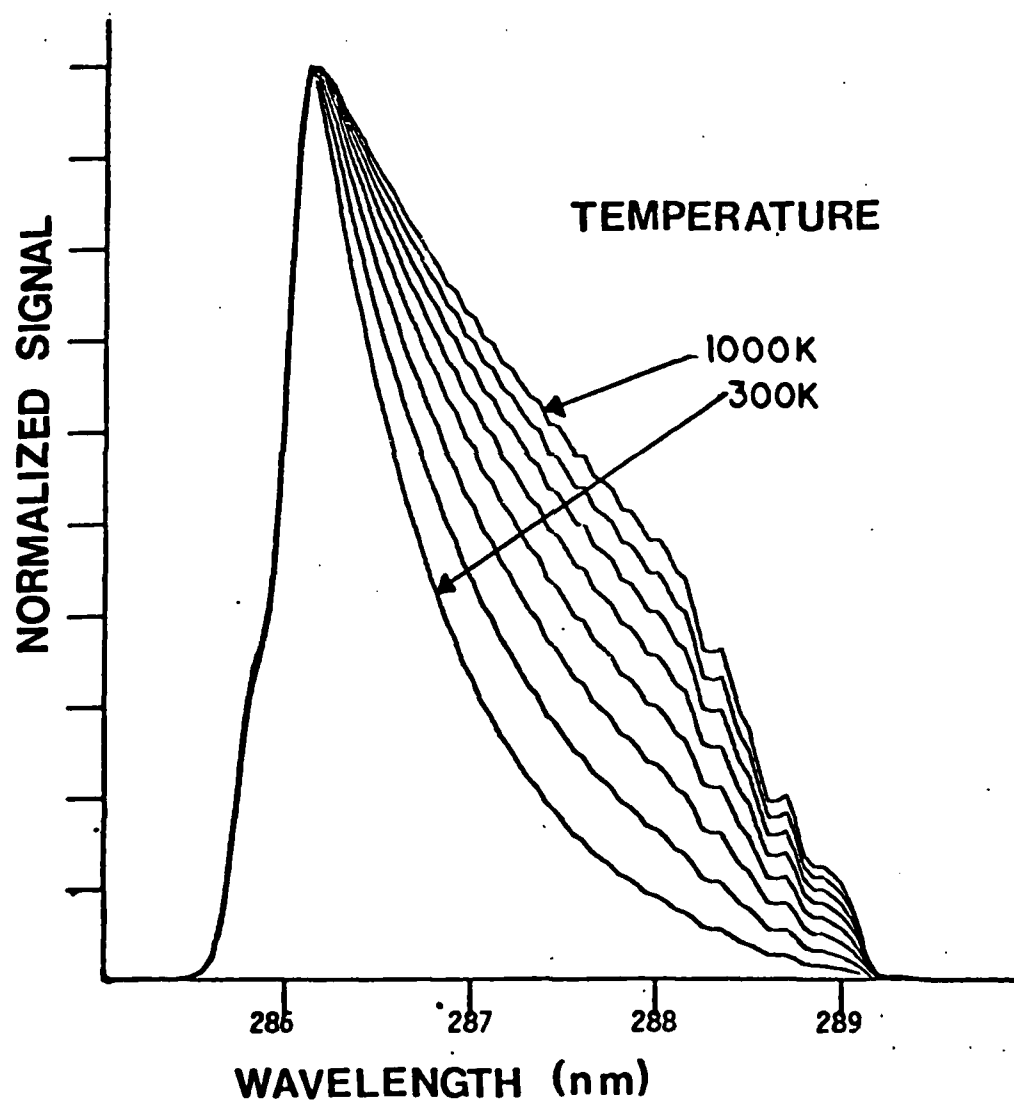
FIGURE 17    Computed dependence of emission on wavelength
and temperature for the $S_2$ B:v'=8 to X:v"=0
transition.

40

$$T = 752 \, \Delta\lambda_{FWHM} - 145 \tag{12}$$

where the halfwidth is in nanometers and the temperature is in Kelvin. Equation (11) applies to the high pressure case when rotational relaxation of the excited state occurs. Equation (12) applies to the low pressure case when radiative de-excitation of the excited state occurs more frequently than collisional relaxation. Thus, the halfwidth of the unresolved rotational structure can be used in temperature determinations for tubes containing a low pressure of sulfur gas, as well as those with a high pressure. This implies that the halfwidth of the emission can be used as an indication of relative temperature even in experimental situations which do not conform to the requirements of the two extreme cases considered here.

To provide greater accuracy, an alternative technique was developed to compare the experimental and calculated line profiles. It was found that the calculated intensities could be fitted to an exponential decay curve.

$$I(\lambda_W) = I_o e^{-\lambda_W/A}$$

for wavelengths $\lambda_W$ greater than that of the peak; i.e., in the range 286.5 nm to 288.0 nm. The exponential decay parameter is linearly related to the temperature parameter in the computations:

$$T(K) = 403 \, A(nm) - 11 \tag{13}$$

and

$$T(K) = 573 \, A(nm) + 20 \tag{14}$$

41

Equations (13) and (14) apply to the high and low pressure cases respectively.

As mentioned earlier, the values of the spin rotation coupling constant $\gamma'$ and the spin spin coupling constant $\lambda'$ have not been well determined for the $v'=8$ vibrational level in the B state of $S_2$. The results presented here have used the values $\lambda'=-4.9$ cm$^{-1}$ and $\gamma'=0.05$ cm$^{-1}$ which are similar to the values for other even numbered levels of the B state [30]. By varying the values of $\lambda'$ and $\gamma'$ used in the calculations, it was found that they did not greatly influence the halfwidth of the computed bandshapes. In particular, varying the parameter $\lambda'$ over the range -0.10 cm$^{-1}$ to 0.15 cm$^{-1}$ produced a negligible difference in the computed curves. The effect of varying the parameter $\lambda'$ in the range -15 cm$^{-1}$ to +10 cm$^{-1}$ is shown in Figure 18. Only for $\lambda' > 5$ cm$^{-1}$ is there a significant effect on the rotational bandwidth of the transition. However, the fainter head to the low wavelength side of the main head, indicated by an arrow in the spectra of Figure 14, is not predicted when using the values of $\lambda'$ which can make a significant difference to the temperature determination. This secondary head is due to the $T_{R_{31}}$ and $R_{P_{31}}$ bands (Figure 16) which are not distinct for positive values of $\lambda'$ [42]. Comparison of Figure 18 with the observed spectrum (Figure 14) indicates the value $\lambda' \simeq -5$ cm$^{-1}$ adequately describes the bandshape. This is in agreement with the value observed for $v'=0,2$, and 4 [30,41,42].

Thus comparison of the computed bandshapes with the spectrometer output allows a determination of the gas temperature. In addition, an approximate value for the spectroscopic constant $\lambda'$ has been ascertained.

6.    DISCUSSION OF IN SITU TEMPERATURE MEASUREMENT

The accuracy of the measured temperature values is limited in the

42
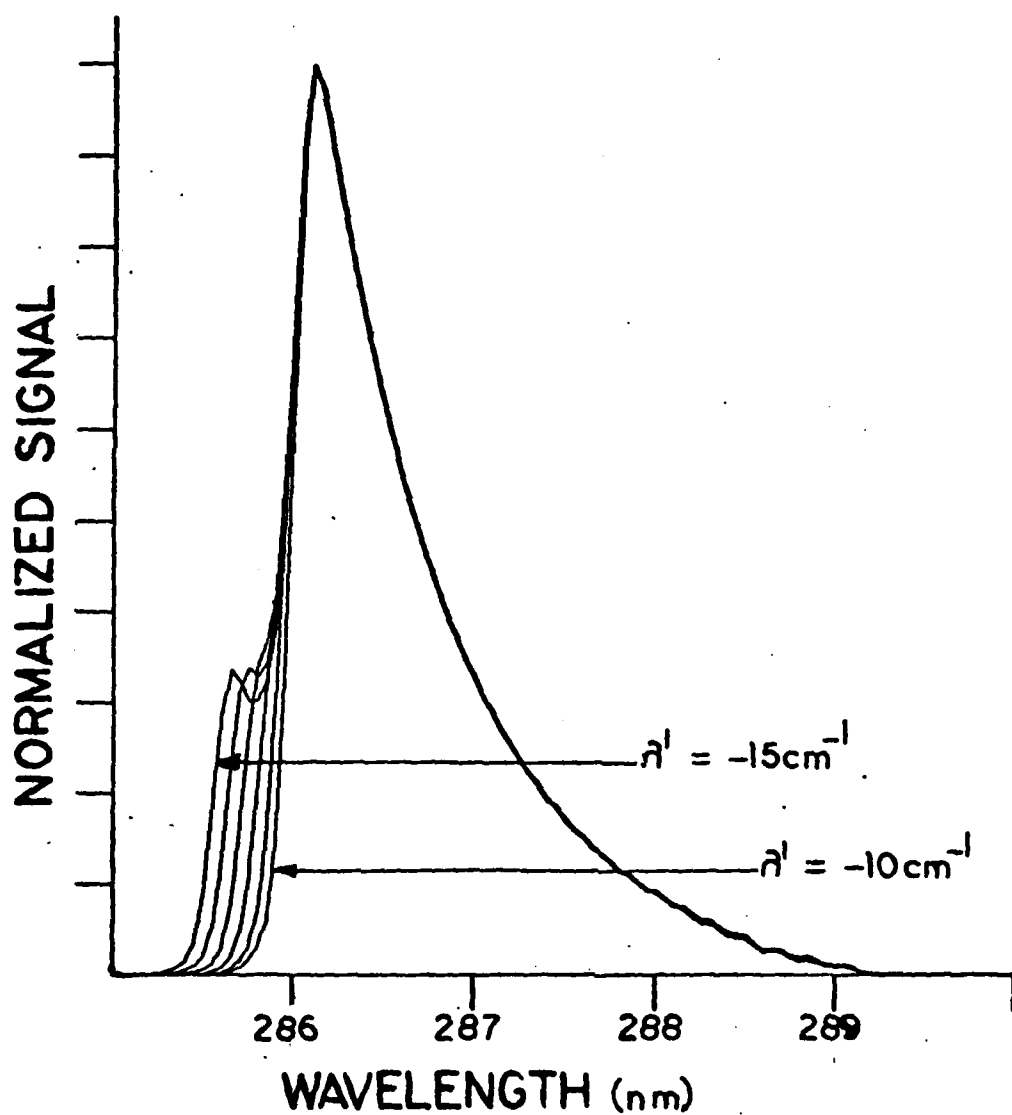
FIGURE 18    Effect of varying the parameter λ' over the range
+10 cm⁻¹ to -15 cm⁻¹ on the computed dependence of
emission on wavelength.

43

present case because only spatially integrated spectra have been observed. The radiation emitted by the hot gas in the center of the discharge tube will be absorbed by colder gas near the tube walls. Since the cooler gas will predominately absorb radiation originating from states with low values of N', this will depress the peak of the emission curve resulting in a wider halfwidth and an inflated temperature measurement. Radially resolved measurements would give more accurate temperature values and also an estimate of $S_2$ density as a function of radius. These measurements have not been performed to the present time.

The $S_2$ (B:v'=8) state is perturbed by a neighboring state, as mentioned in a previous section. This results in shifts of the rotational energy levels for particular values of the rotational quantum number [43], and deviation of the line strengths from the predicted values (Figure 16). Since the computed bandshape is a weighted average over many values of N', the shift of a few levels is not expected to make a significant difference. The distortion of the assumed Boltzmann distribution of rotational levels, due to predissociation of molecules with $J \geq 60$, will not be significant at the lower rotational levels from which emission influences the halfwidth of the curve in the temperature range of interest.

7. PROCEDURE FOR DETERMINING THE VIBRATIONAL POPULATION DISTRIBUTION OF ELECTRONICALLY EXCITED $S_2$

The spectra of $S_2$ in the range 280 - 370 nm is presented in Figure 19 which compares the emission from a pulsed only discharge to the emission from a pulsed plus continuous microwave discharge. Apart from the first few peaks, each peak is composed of several superimposed transitions and interpretation becomes more difficult. However, it can be seen that the maximum of the spectral emission envelopes is shifted

44
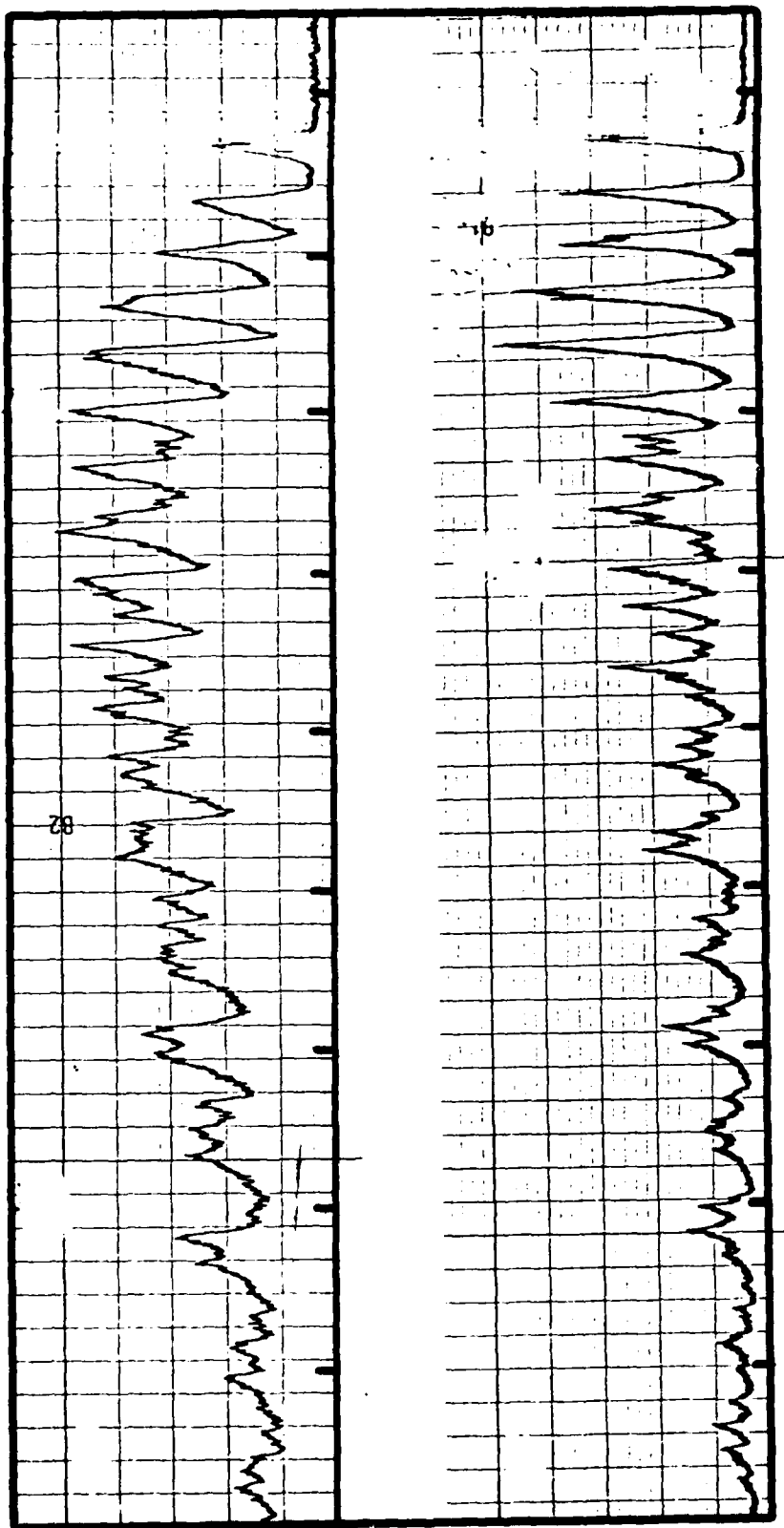
FIGURE 19    Emission spectra of $S_2$ in 280-370 nm range using

(1) pulsed only excitation of the plasma
tube, and

(2) pulsed plus 540 watts continuous excita-
tion

45

approximately 10 nm to the red when the continuous microwave excitation
is added to the pulsed excitation. This indicates a redistribution of
the vibrational population of the electronically excited state. The
emission with pulsed excitation favors more highly excited vibrational
levels than that with pulsed plus continuous excitation. A procedure
has been devised for extracting the relative populations of the vibra-
tional levels from the spectral distribution of the radiation.

The computer program MERCHA [35] used for data analysis integrates
the spectrometer output over various 10 nm wavelength intervals and
corrects for the sensitivity of the spectrometer and photomultiplier. In
each wavelength interval, several overalpping transitions make a contri-
bution. For example, in the 295 nm to 305 nm wavelength range, the
transitions listed in Table 1 make a contribution. The emission intensity
on the v'→v" transition is given by

$$I(v'v") = KN(v') \ \nu_{v'v"}^{4} \ [R_e(r_{v'v"})]^2 \ q_{v'v"} \tag{15}$$

where $q_{v'v"}$ is the Franck Condon (FC) factor, $R_e$ the electronic transition
dipole moment, $N(v')$ the population of the excited vibrational state,
and $\nu_{v'v"}$ the frequency of the transition. For diatomic sulfur, $R_e$ is
independent of $v'$ and $v"$ [32]. Then we can define an average signal for
each wavelength interval,

$$S(\Delta\lambda) = \sum_{v'v"} I(v',v") \tag{16}$$

The sum is over all quantum numbers for which the emission is in the
selected wavelength range. Then this signal is proportional to the

level populations and the Franck Condon factors. For example, in the 295 to 305 nm range,

$$S(295-305) = K[80N(7) + 15N(5) + 4N(8) + 77N(6) + 9N(4)$$
$$+ 58N(9) + 41N(7) + 48N(5) + 4N(3) + 38N(8)]/(300 \text{ nm})^4$$

Here we take N(v') to be a normalized population; i.e.,

$$\sum_{v'} N(v') = 1 \tag{17}$$

and incorporate all constant factors into K. In general, for the $j^{th}$ wavelength interval,

$$S_j = K \sum_{v'=0}^{9} Q_{jv'} N(v') \qquad j = 1 \text{ to } 24 \tag{18}$$

where $Q_{jv'}$ is the sum of all the FC factors from the v' level that can contribute in the $j^{th}$ wavelength interval, divided by the wavelength to the fourth power. In some cases more than one transition from a particular v' level can contribute to the wavelength interval. In the above equation, $S_j$ can be calculated from the computer integrated spectra and $Q_{jv'}$ from the published FC factors. Only the constant K and the normalized vibrational population N(v') are unknown. This equation can be inverted to tell us the vibrational population distribution.

There are 24 wavelength intervals and only 10 unknowns in the equation. The most straightforward inversion procedure involves minimizing the function

$$\sigma^2 = \sum_{j=1}^{24} (S_j - K \sum_{v'=0}^{9} Q_{jv'} N(v'))^2 \tag{19}$$

47

by the correct choice of K and the N(v'). However one wavelength interval
is determined totally by the population of the v'=9 level. No
transition except the v'=9 to v"=0 makes a contribution to the 275 to
285 nm wavelength interval. From equation (18),

$$K \, N(9) = S_1 / \, Q_{1,9} \tag{20}$$

Equation (18) can then be rewritten as

$$S_j{}' = S_j - \frac{Q_{j,9}}{Q_{1,9}} \, S_1 = K \sum_{v'=0}^{8} Q_{jv'} N(v') \quad j = 2 \text{ to } 24$$

Then the equation to be minimized becomes

$$\sigma^2 = \sum_{j=2}^{24} \{S_j{}' - K \sum_{v'=0}^{8} [Q_{jv'} N(v')]\}^2 \tag{21}$$

Diffe.entiating this equation by N(v') for v'=0 to 8 and interchanging
the order of summation leads to the result

$$N(i-1) = \frac{1}{K} \sum_{j=1}^{9} B_{ij} C_j \quad i = 1 \text{ to } 9 \tag{22}$$

or

$$\overline{N}' = \frac{1}{K} \overline{B} \, \overline{C} \tag{23}$$

where

$$B_{ki}^{-1} = \sum_{j=2}^{24} Q_{jk} \, Q_{ji} \tag{24}$$

is a 9 x 9 matrix, and $\overline{C}$ is a 9 x 1 matrix defined by

$$C_K = \sum_{j=2}^{24} Q_{jk} S_j{}' . \tag{25}$$

48

N' is a 9 x 1 matrix whose elements are equal to the first nine values of N(v'). The value of K can be found by normalization

$$K = K \sum_{v'=0}^{9} N(v') = \frac{S_1}{Q_{1,10}} + \sum_{j=1}^{9} C_j \sum_{i=1}^{9} B_{ij} .$$
(26)

A program in BASIC was written for the Hewlett Packard 9835 calculator to calculate the matrix $\overline{B}^{-1}$ from the known FC factors. This procedure and the matrix inversion must be done only once. For particular experimental conditions, the column matrix C is calculated from the published FC factors and from the integrated signals $S_j$ for each wavelength interval. The computation of the N(v') is then straightforward, using equations [26], [20], and [22] or [23].

One additional refinement on this technique was concerned with the construction of the 10 x 24 matrix Q. The computer program MERCHA integrates the spectrum over 10 nm intervals. Some vibrational transitions are located near the boundaries between the different intervals and because of the width of the vibrational transition, as given for example in Figure 17, could contribute to two different integrals. Therefore the Franck Condon factor for these transitions was broken into two parts and made a contribution to two elements of the Q matrix. The bandshape of Figure 17 and the band origins computed by Schlie [44] were used to estimate the division of the particular Franck-Condon factors. This neglects the temperature dependence of the bandshape and the variation of the rotational constants with vibrational states. Since the correction terms to the elements of the Q matrix were small, their dependence on temperature and vibrational state was not significant. The corrected

Q matrix is given in Table 3.

This process of reconstructing the vibrational population distribution from the spectral distribution of emission was tested in the following manner. If one assumes that all the electronically excited population is in one vibrational level, then the emission in each wavelength region is given by the appropriate column of the Q matrix. When these numbers were used as input to the vibrational analysis program, the computed population distribution was close to unity in the selected vibrational state and less than $10^{-3}$ in all other states.

As about half of the elements of the B matrix are negative, the calculation given in equation (22) involves the addition and subtraction of many terms, some of which may be nearly equal. Thus, minor inaccuracies may lead to significant discrepancies in the values for $N(v')$. Such minor inaccuracies are inherent in the measured Franck Condon factors and in the measured values for the spectrometer-photomultiplier calibration factor. Examples of the vibrational distribution computed by the technique described above are given in Figure 20. The dips observed in both curves for $v'=5$ and possibly that for $v'=2$ are considered to be not real but an artifact of the computing process due to the sources of inaccuracy mentioned above. Nevertheless, the computed $N(v')$ are useful to show general trends when values which are obviously inaccurate are neglected.

TABLE 3

The Q matrix used for determining vibrational
population distribution.

| wavelength interval (nm) | vibrational quantum number in excited electronic state | | | | | | | | | |
|---|---|---|---|---|---|---|---|---|---|---|
| | 0 | 1 | 2 | 3 | 4 | 5 | 6 | 7 | 8 | 9 |
| | Franck Condon factors summed over wavelength interval | | | | | | | | | |
| 285–295 | 0 | 0 | 0 | 0 | 0 | 0 | 977 | 1713 | 4162 | 2550 |
| 295–305 | 0 | 0 | 0 | 119 | 284 | 1991 | 2434 | 3814 | 560 | 1856 |
| 305–315 | 0 | 28 | 221 | 508 | 3272 | 2218 | 1580 | 292 | 2097 | 852 |
| 315–325 | 24 | 146 | 1099 | 2927 | 1757 | 1216 | 781 | 2087 | 24 | 1471 |
| 325–335 | 216 | 1576 | 2439 | 2571 | 237 | 944 | 1340 | 194 | 1770 | 43 |
| 335–345 | 441 | 2107 | 2470 | 115 | 1307 | 1092 | 439 | 303 | 19 | 1227 |
| 345–355 | 699 | 1911 | 1404 | 290 | 986 | 223 | 870 | 468 | 751 | 204 |
| 355–365 | 1798 | 1494 | 103 | 1021 | 76 | 953 | 198 | 682 | 381 | 594 |
| 365–375 | 2198 | 956 | 560 | 1043 | 219 | 498 | 96 | 301 | 304 | 314 |
| 375–385 | 1970 | 37 | 896 | 176 | 761 | 37 | 602 | 25 | 535 | 49 |
| 385–395 | 1505 | 255 | 664 | 309 | 509 | 310 | 299 | 420 | 98 | 476 |
| 395–405 | 893 | 450 | 160 | 407 | 30 | 60 | 20 | 290 | 300 | 190 |
| 405–415 | 483 | 743 | 18 | 513 | 130 | 181 | 263 | 18 | 200 | 36 |
| 415–425 | 675 | 823 | 162 | 444 | 461 | 22 | 387 | 239 | 126 | 313 |
| 425–435 | 434 | 696 | 17 | 45 | 404 | 10 | 97 | 292 | 7 | 195 |
| 435–445 | 260 | 509 | 444 | 48 | 166 | 212 | 14 | 39 | 198 | 7 |
| 445–455 | 100 | 34 | 449 | 237 | 32 | 312 | 418 | 102 | 293 | 147 |
| 455–465 | 0 | 372 | 583 | 34 | 6 | 234 | 0 | 11 | 51 | 48 |
| 465–475 | 37 | 152 | 132 | 347 | 142 | 26 | 409 | 262 | 0 | 210 |
| 475–485 | 10 | 61 | 245 | 420 | 242 | 29 | 101 | 176 | 29 | 24 |
| 485–495 | 0 | 32 | 204 | 277 | 106 | 67 | 31 | 144 | 187 | 25 |
| 495–505 | 0 | 41 | 46 | 39 | 356 | 211 | 12 | 111 | 133 | 22 |
| 505– 515 | 0 | 0 | 41 | 178 | 148 | 96 | 110 | 5 | 51 | 159 |
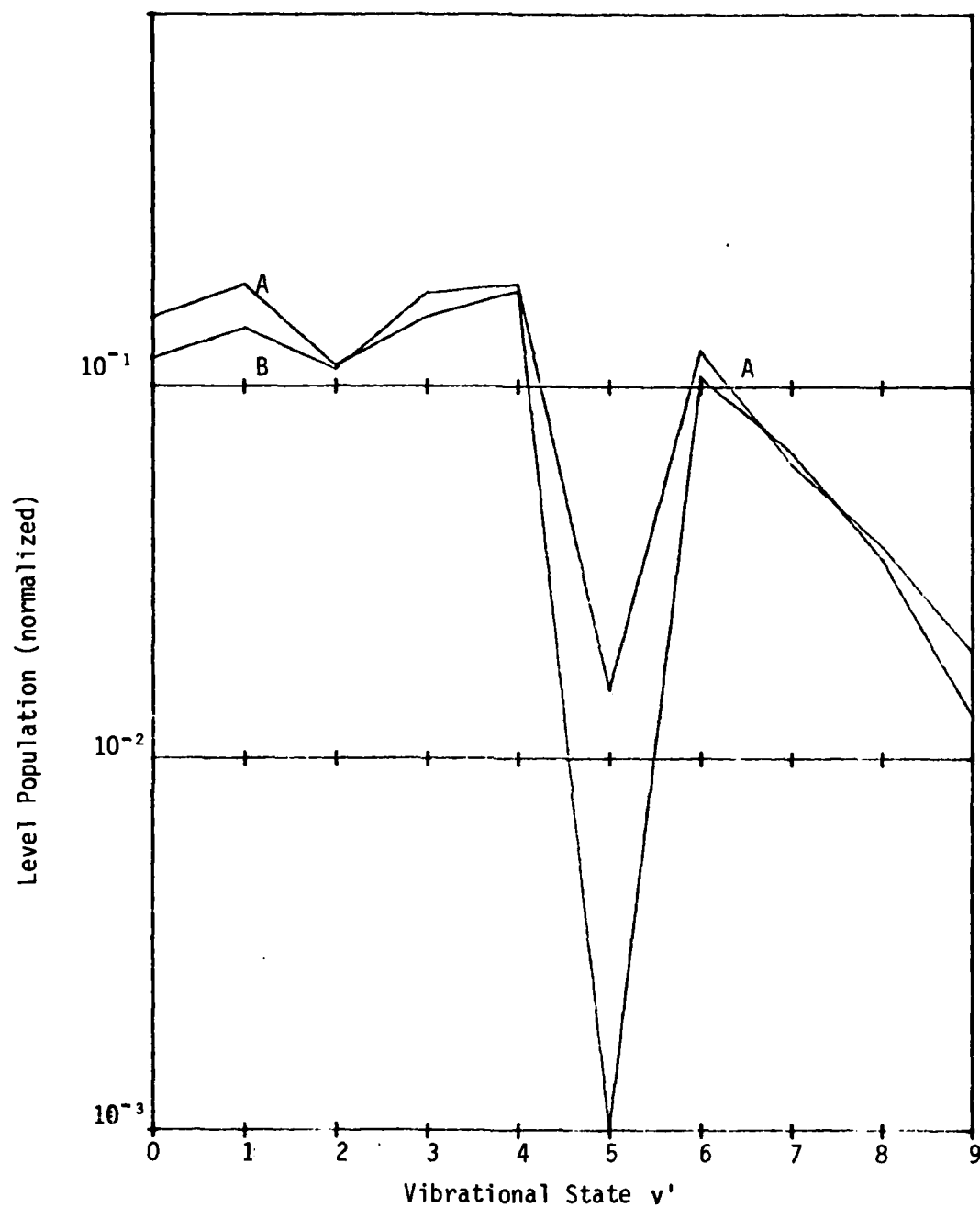
FIGURE 20        Computed vibrational distribution in the
                 B state of $S_2$: A discharge in 5 Torr of
                 sulfur with 50 Torr of (A) Argon or (B)
                 Helium.

52

# SECTION V

## CHARACTERISTICS OF MICROWAVE DISCHARGES AND
## THE RESULTANT OPTICAL EMISSION

### 1. MERCURY

When mercury discharge tubes were used with the sandwich applicator, the resulting plasma was spatially modulated with the spacing of the interdigital line. Hence most of the work with mercury discharge tubes was performed with the Fusion Systems twin antenna irradiator, in which a longitudinally uniform plasma could be obtained.

The twin antenna irradiator has two modes of operation with mercury tubes. Although there is an empty cavity mode, probably the half cylinder $TE_{111}$ mode, that is important for initial breakdown of the gas in the plasma tube, both operational modes appear to be coaxial with the mercury plasma in the discharge tube forming the center conductor element of the coax. The mode in which the cw discharge is normally operated is a very lossy TEM coaxial mode where the power input from each antenna is absorbed along the discharge tube in an e-folding length of about half the cavity length. In the other mode of operation, normally at lower power and pressure than the lossy coaxial mode, a coaxial cavity is formed with the mercury plasma as a much less lossy, effective center conductor providing the usual standing wave coaxial mode with, in this case, three antinodes, representing a cavity of three half wave lengths in length.

Sample spectra were recorded for a number of conditions to have available for comparison studies and to compare with the efficiencies reported for the twin antenna irradiator. In the lossy coaxial mode

53

with input powers up to 1200 watts the coupling is about 90% efficient. The spectra showed increasing band intensities in the 220 to 235 nm and 254 to 270 nm bands with increasing power and spectral efficiencies similar to those reported by Fusion Systems (2). Comparing these to standard direct electric mercury arc lamps, the temperatures, at the center, are about 7500° K; the electric fields are about 60 volts per centimeter; and the electron densities are about $10^{15}$/cc (5).

In the conductive coaxial mode the spectral efficiency is about 50% or higher, although the microwave power coupling is reduced to the order to 50 to 75%. This mode requires considerably more tube cooling to operate. Much of the radiant output is on the 253.7 nm line of mercury.

Several tests were made under various conditions. The cw sustainer discharge was operated in the conductive coaxial mode at low powers at a temperature near room temperature. Then the cw discharge was operated in the lossy coaxial mode at low powers and exit cooling air temperatures around 150° C. Finally the cw sustainer was operated at higher powers in the lossy coaxial mode with exit cooling air temperatures of about 210° C. For all these conditions, the peak pulsed microwave power was 3000 ± 200 watts with pulse lengths of 1, 2, and 4 µsec.

The relative spectral intensity in the pulse for the 220 to 350 nm region is plotted as a function of microwave sustainer power in Figure 21. For the upper plot, the discharge was in the conductive coaxial mode, while for the lower plot the discharge was in the lossy coaxial mode. For both modes the microwave pulse length was 4 µsec. In the

54

conductive coaxial mode the relative intensity initially increased, but then started to decrease as the sustainer power was increased, while for the lossy coaxial mode the intensity decreased continually as the sustainer power increased.

It is possible that the decrease in the intensity of the pulse output is due to resonance trapping in mercury. An examination of the ultraviolet pulse signal on an oscilloscope confirmed that for a micro-wave power pulse length of 4 $\mu$sec, the resulting ultraviolet pulse from the discharge had a half width of about 8 $\mu$secs, with a very long tail on the pulse. This indicates that, although the ultraviolet output may in fact be increasing as the sustainer power increases, the radiation from the discharge was not being emitted during the sample time but rather was being emitted over a relatively long period of time.

This indicates that a mercury plasma may not be suitable for generating high power ultraviolet pulses. An investigation was made of mercury discharge tubes with added doping compounds $SnI_2$ and $MnI_2$ which are known to improve the spectral response of mercury arc lamps. Figure 22 is a plot of relative intensity as a function of sustainer power for a 4 mm i.d. doped tube. The upper curve is the total light output from 200 to 600 nm while the lower plot is the output from 250 to 350 nm. This indicates that approximately 35% of the total output falls within the region of interest. However, neither the droplet of mercury or the dopant in the tube were completely vaporized even in the 1200 watt sustainer test.
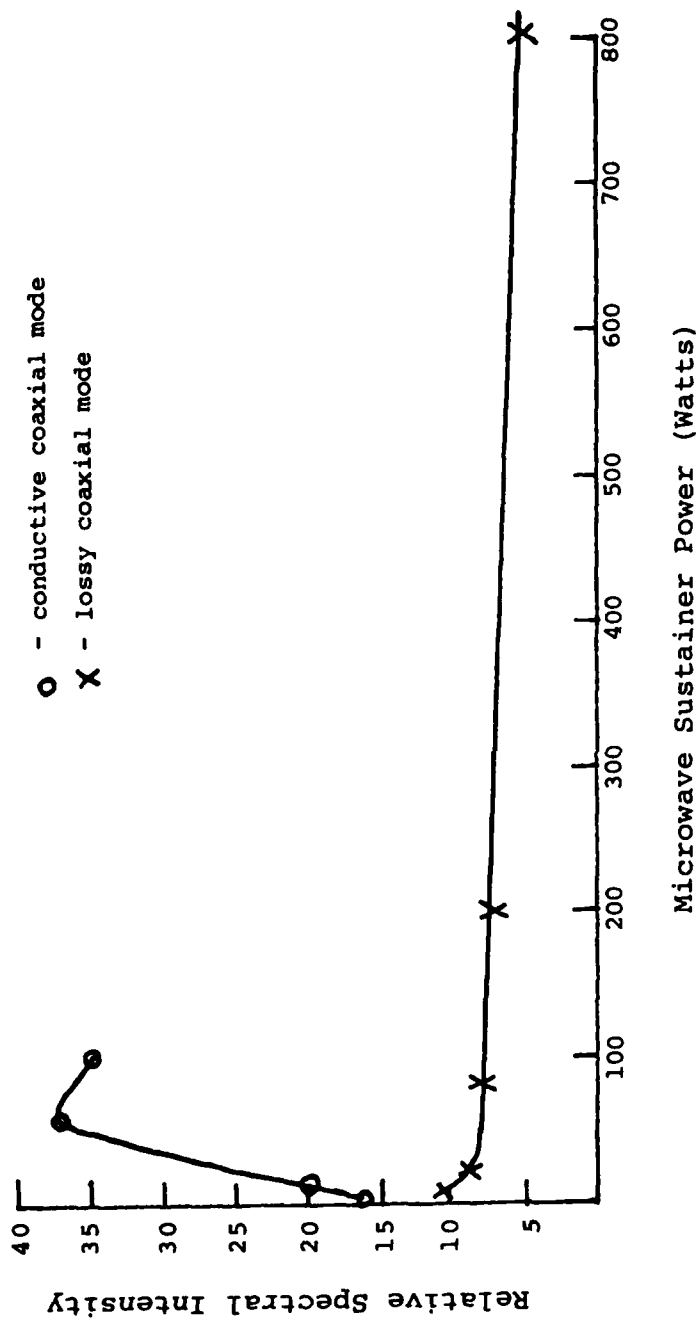
FIGURE 21    The Relative Spectral Intensity of the 220 nm to 350 nm Radiation as a Function of Microwave Sustainer Power for Two Modes of Operation of a Mercury Discharge.
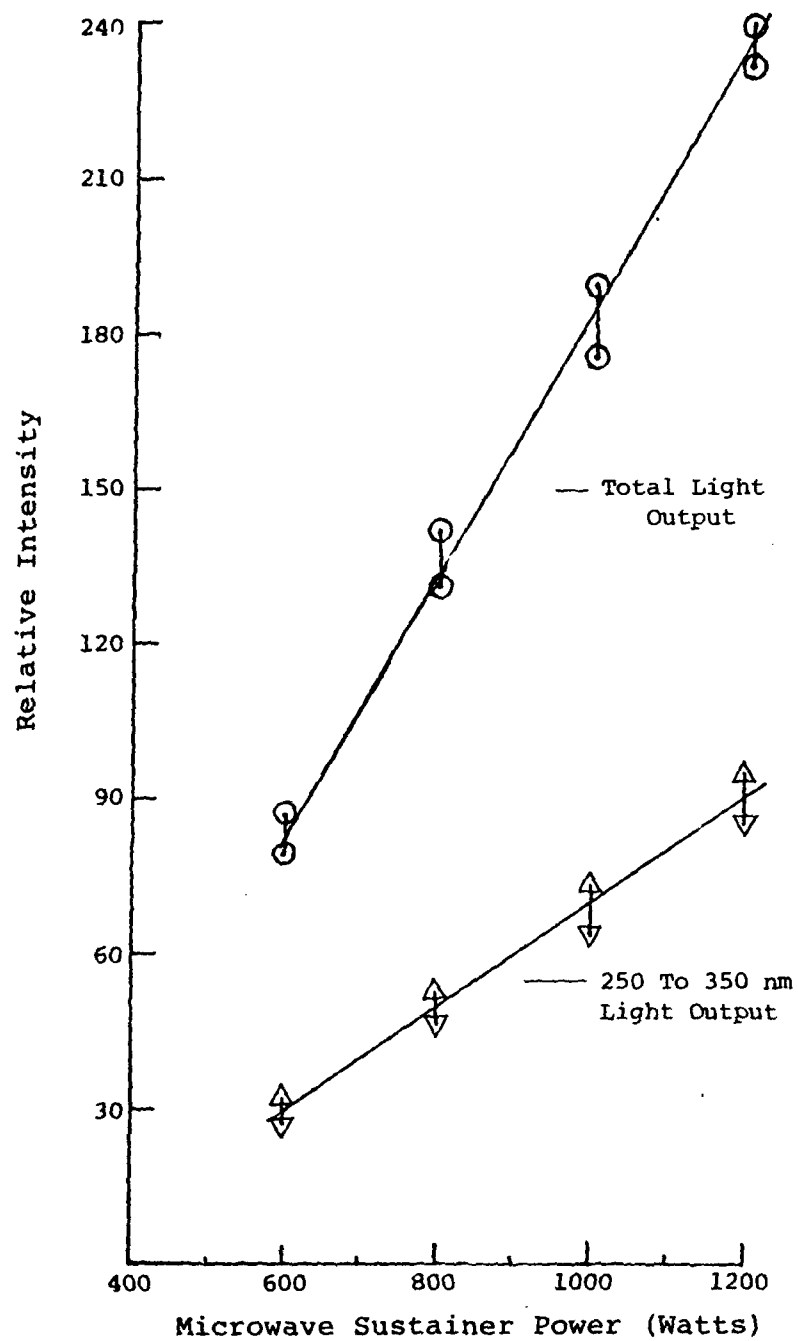
FIGURE 22    The Relative Light Intensity Output As
A Function Of Sustainer Power For The
Twin Antenna Irradiator

57

During the testing of the tube, the discharge appears constricted, so that there is a boundary layer of cooler gas around the discharge. This layer may act as an absorbing boundary and add to the problem of radiation trapping. The applied microwave power for these tests and those described following was about 3900 $\pm$ 200 W, while the pulsed microwave power transmitted through the irradiator was about 100 W, and the pulsed microwave power reflected back from the irradiator was about 200 W. For these tests then, about 3600 $\pm$ 200 W of pulsed microwave power was absorbed by the discharge. The pulsed microwave power was operated at 100 Hz with a pulse length of 4 $\mu$sec.

Measurement of the pulsed microwave power was accomplished by calibrating the output of the Hewlett Packard Model 420A crystal detectors on a Tektronix Type 556 dual beam oscilloscope with Tektronix Type 1A7A plug-ins. Exposures of the oscilloscope trace of the pulsed power is shown in Figure 23. The pulsed microwave power supply was operated at 100 Hz with a 4 $\mu$sec pulse length, and the sustainer power was 1200 W. The scope was operated in the single sweep mode with 2 $\mu$sec/vertical division and at 20 mv/horizontal division for traces A and B, and 10 mv/horizontal division for trace C. Figure 23A is the oscilloscope trace of the applied pulsed microwave power. Figure 23B is the reflected power, and Figure 23C is the transmitted power.

Two 4 mm i.d. tubes with a light fill and extra light fills of mercury doped with $SnI_2$ and $MnI_2$ and a back fill of argon were obtained from Fusion Systems Corporation and tested with the twin antenna irradiator. The extra light fill tubes would have a mercury pressure of 100 Torr when the mercury was completely vaporized. The tubes with light and heavy fill provided pressures of 1 and 15 at atmospheres respectively. Typical raw

58
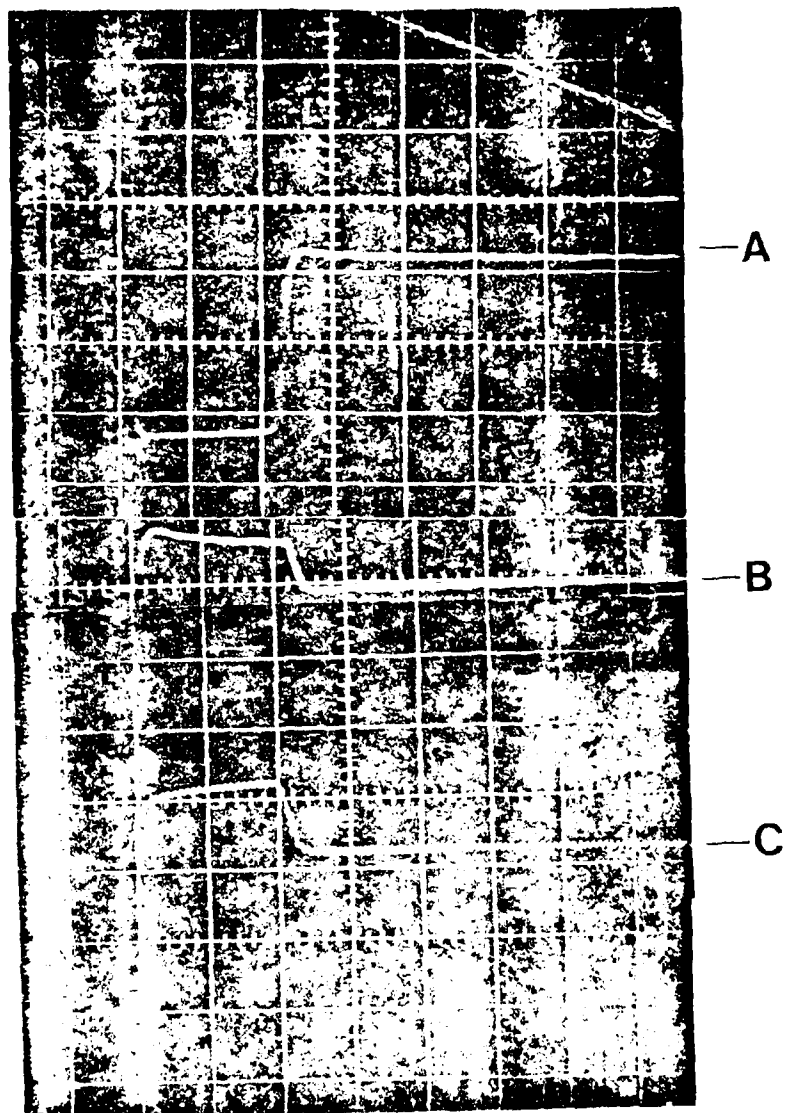
FIGURE 23 Exposures of Oscilloscope Traces of
Signal from Crystal Detector of Pulsed
Microwave Power.

spectra from the extra light filled tube are shown in Figure 24.
Figure 24A is the cw plus pulse output from the boxcar amplifier,
and Figure 24B is the cw output from the amplifier.

Figure 25 shows the results of the pulsed tests for the three
different fills for the discharge tubes. Figure 25A is a plot of the
total pulsed light output as a function of sustainer power and Figure
25B is a plot of the pulsed light output in the region of 250 to 350
nm as a function of sustainer power. While the percent of radiation in
the 250 to 350 nm region is about the same for all three fills, the
amount of pulsed radiation from the discharge in the 0.5 μsec sample
time is increasing significantly. However, the pulsed light output is
still below the cw output from the sustainer.

An examination of the cw and the cw plus pulsed outputs for the
313 nm and 365 nm Hg peaks was made. This is shown in Figures 26, 27
and 28. In each the upper spectrum is from the boxcar amplifier (cw +
pulsed output) and the lower spectrum is from the amplifier (cw output).
In Figure 26 the 365 nm Hg line shows more self absorbtion for the
pulsed plus cw (upper) spectrum than for the cw (lower) spectrum. For
Figure 27 the pulsed microwave power was turned off, and the shape of the
365 line is the same for both spectral plots, thus, the absorption seen in
the Figure 26 pulse + cw spectrum is a result of trapped pulse radiation
and not a function of the amplifier response. The self absorption of the 312.5
and 313.1 nm lines is shown in Figure 28. Again the self absorption is
greater for the pulse plus cw (upper) spectrum than for the cw (lower)
spectrum.

The self absorption that is shown by the mercury lines accounts

60
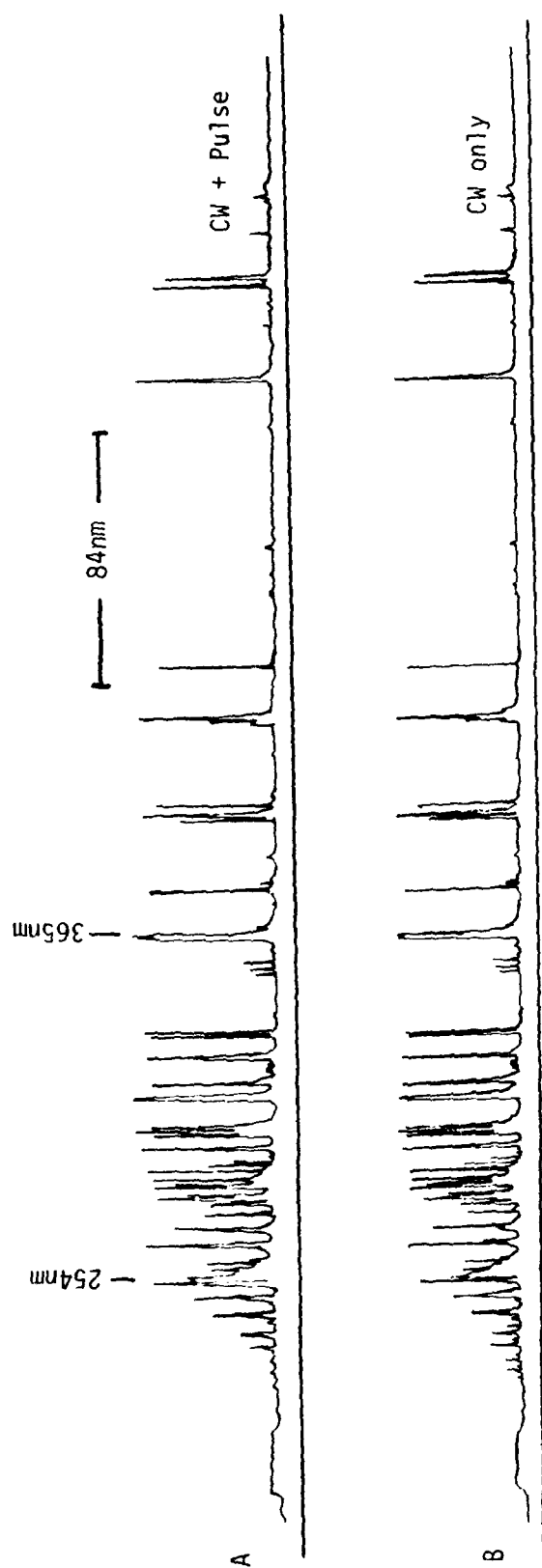
FIGURE 24    Spectrum induced by CW plus pulsed microwaves and by
CW microwaves alone from an extra light fill discharge
tube at 1200 Watt CW sustaines power.
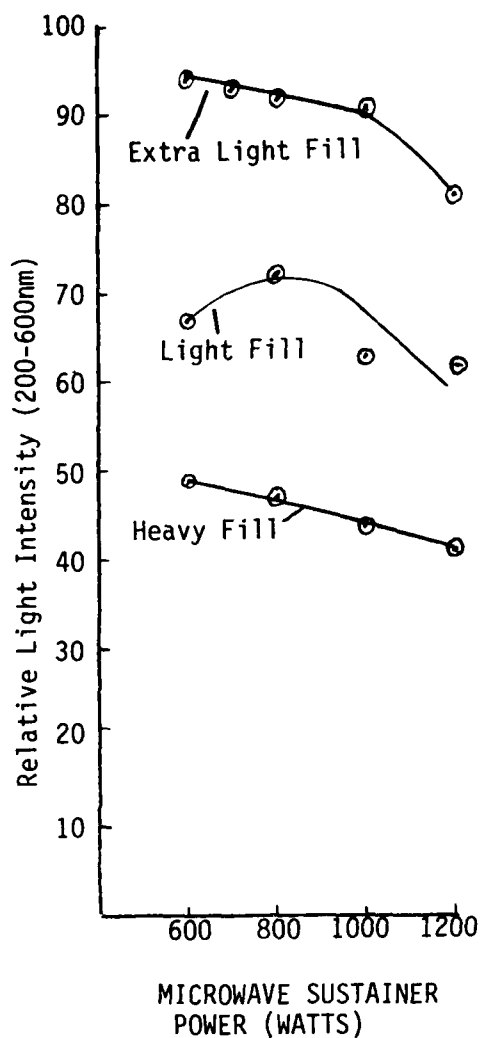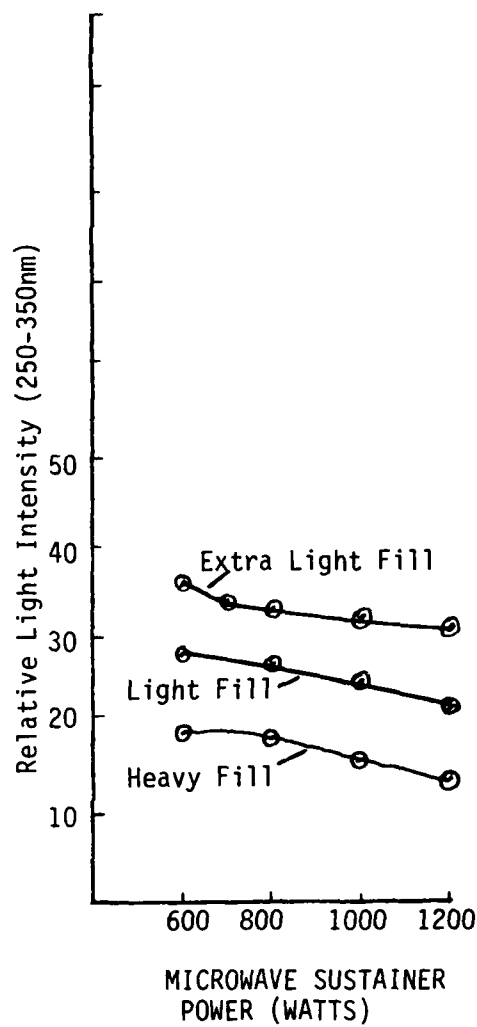
FIGURE 25   Relative Light Output as a Function of Microwave Power for Three Different Gas Fills.

62

CW + PULSE

4.2nm

365 Hg

CW
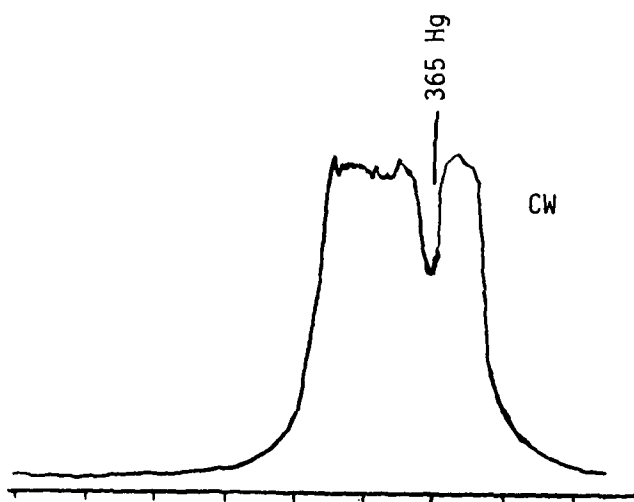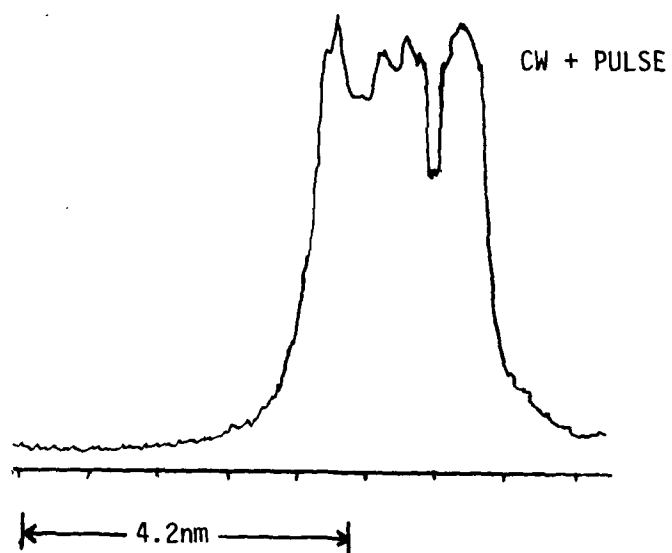
FIGURE 26   Self Absorption of 365nm Hg Line

63
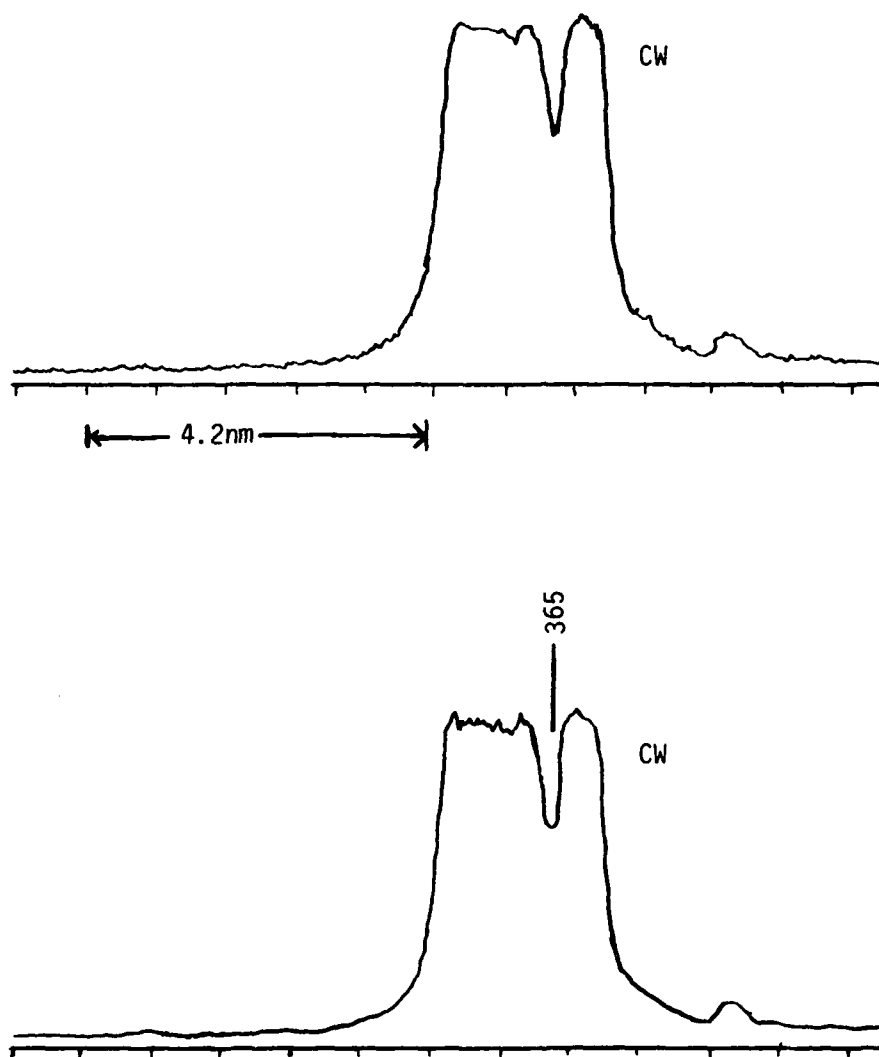
FIGURE 27 Self Absorption of the 365nm Hg Line with No Pulsed
Microwave Power.

64
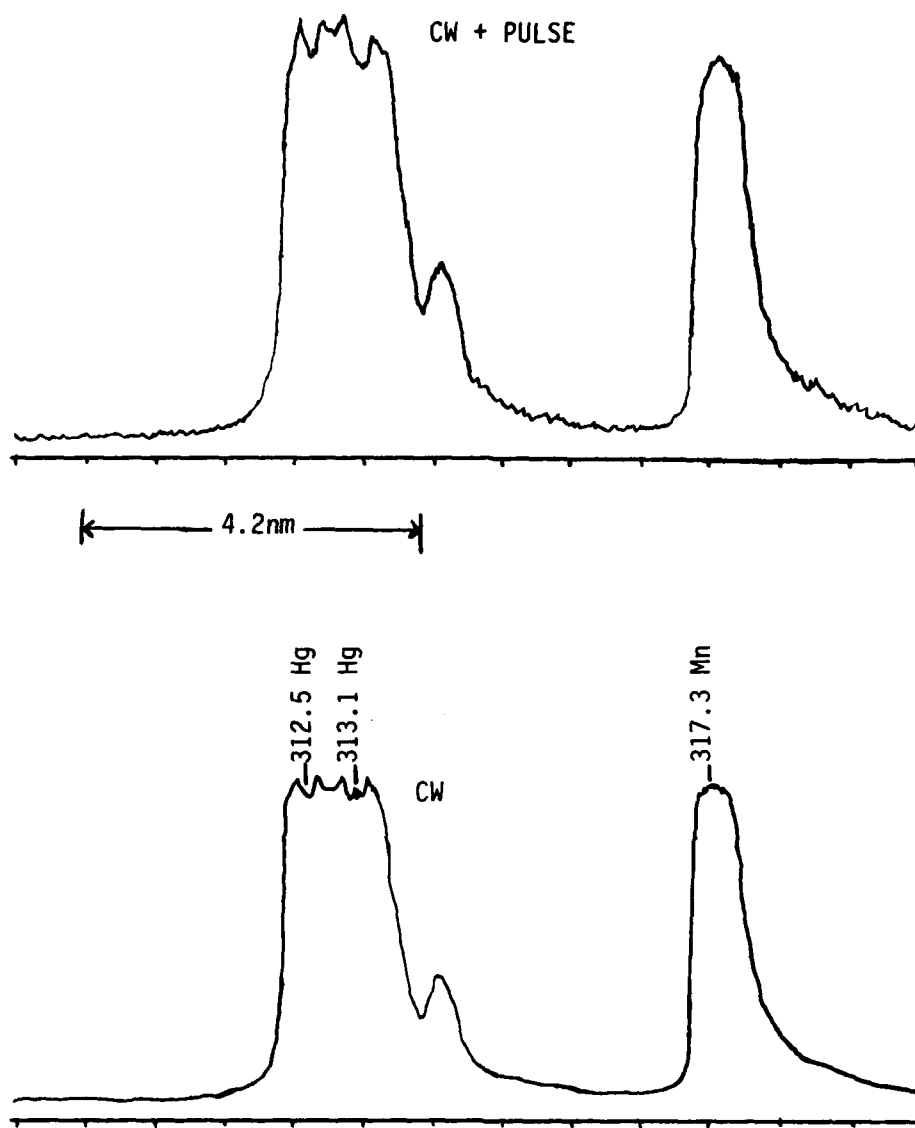
FIGURE 28  Self Absorption of 313.1nm Hg Line.

65

for the fact that the pulsed light output of the discharge tube measured for a 0.5 μsec sample time is not escaping the tube, but rather is trapped and emitted over a relatively long period of time. Some of the trapped radiation will be lost to relaxation and not emitted at all.

## 2. MERCURY BROMIDE

One of the available mercury bromide tubes contained 200 torr of helium and sufficient HgBr to produce a pressure of 3.6 torr upon complete vaporization at 160°C. It was found that high continuous microwave power input completely dissociated the molecules and the spectrum observed was that of atomic mercury.

A molecular spectrum obtained in the twin antenna irradiator with high pulsed power but minimum cw power was identical to that of Schimit-schek and Celto [8]. However, under these conditions all the cw power was absorbed at the ends of the tube resulting in a nonuniform discharge. The discharge was "slug" like, clinging to the tube walls, and not filling the tube. A discharge in pure mercury under the same conditions would completely fill the discharge tube.

HgBr lasers pumped by electrical discharge show a marked increase in efficiency and output power when nitrogen is added ot the gas mixture [9,10]. Consequently a discharge tube was made up which contained 10 torr of nitrogen, 10 torr of helium, and some mercuric bromide powder. This sealed tube was placed inside an open-ended heating tube and installed in the sandwich applicator. A variac controlled heat gun was connected to the heating tube and was used to control the vapor pressure

66

of $HgBr_2$. A thermocouple placed on the downstream end of the heating tube was used to estimate the temperature of the discharge tube.

The first results were obtained using a circular heating tube of 25 mm diameter. This tube limited the spacing of the two interdigital lines in the sandwich applicator. When no external heat source was used, a discharge could be sustained by one microsecond pulses of microwave power at a repetition rate of 1.4 kHz. However, as external heat was applied to vaporize the $HgBr_2$, the discharge could not be sustained by pulsed only microwaves. It was necessary to use some cw microwave power to maintain the plasma. In this case the discharge was localized, filling only part of the tube cross-section.

Emission due to nitrogen, atomic mercury, and HgBr was observed. In the HgBr $B \rightarrow X$ band at 500 nm, a cw photomultiplier current of 0.5 $\mu A$ and a pulsed current of 80 $\mu A$ was produced by the light emission due to cm microwave power of 300 watts and pulsed microwaves of 3960 watts respectively. The instantaneous pulsed microwave output is larger than the cw output by a factor of thirteen but the resulting fluorescence is increased by a factor of 160. These results imply the probability of formation of the HgBr (B) state increases with increasing electric field.

The circular heating tube was replaced by a rectangular heating tube of outside dimensions 13 x 26 mm. The smaller height of the rectangular tube allowed the two interdigital lines of the sandwich applicator to be placed considerably closer together which raised the microwave intensity in the plasma tube. With this configuration, it was possible to sustain a discharge with pulsed microwaves only with a substantial vapor pressure of $HgBr_2$ in the tube. The discharge appeared to fill the tube cross section. The pulsed emission on the HgBr $B \rightarrow X$ transition was larger by a factor of eight than when using the circular

67

heating tube. For the pulsed only excitation of $HgBr_2$ with the narrow interapplicator spacing the crude calibration scheme described elsewhere in this report is used to estimate that this peak photomultiplier current coresponds to an emission of $0.03$ W cm$^{-3}$ nm$^{-1}$ from the discharge tube. An approximate integration of the photomultiplier response over the volume of the discharge and over the spectral region 450 nm to 520 nm indicates a total emission of 6 watts. A total of $3 \times 10^{12}$ molecules cm$^{-3}$ emit visible radiation during the 1 μs pulse. As the molecular density was $10^{16}$ cm$^{-3}$ under the conditions of this experiment, only a fraction $3 \times 10^{-4}$ of the molecules contributed to the emission.

## 3. XENON CHLORIDE

Discharge tubes were filled containing 4% HCl, 48% Xe, and 48% Ne at a total pressure of 4.9 torr, and 8% HCl, 46% Xe and 46% Ne at a total pressure of 4.0 torr. Emission was observed from a variety of xenon lines, from the XeCl D-X transition at 236 nm and from the XeCl B-X transition at 308 nm [41, 45]. The B-X emission is approximately an order of magnitude more intense than that on the D-X transition. All the XeCl emission decayed rapidly with time, falling to 1/e of its original intensity after 10 to 15 minutes in the continuously pulsing microwave applicator. Before filling with the second gas mix mentioned above, the discharge tube was extensively baked under vacuum. The baking temperature was however limited by the teflon valve on the discharge tube. As a result of this, the decay of the XeCl emission with the second gas fill appeared slower than that with the first gas fill. Moreover the rate of decay seemed to decrease with time with the second gas fill. With

68

both gas fills the rate of decay with the microwave discharge turned off and then reactivated was much slower than with the microwaves on continuously.

Figure 29 illustrates the behavior of the pulsed component of the light emission at 308 nm for pulsed only microwaves exciting the gas, as cw microwave excitation is added, and as the cw microwaves are turned off, leaving only the pulsed excitation. Here one channel of the chart recorder plots the time averaged signal from the photomultiplier, while the other channel plots the output of a boxcar integrator which is gated on during the microwave pulse. The the boxcar integrator records the instantaneous sum of the pulsed and continuous components of the visible emission. It is seen in this figure that the average light emission is high when the cw microwaves are turned on, but decays in a few seconds to one third of its original value. When the cw microwaves are turned off, the pulsed emission reaches its highest value, but decays in a few seconds to its steady state value. When the cw microwaves are on, the pulsed component of the light signal is smaller than in the absence of cw microwaves. There is some mechanism associated with the continuous microwaves which appears to quench the pulsed light emission.

The temporal behavior of the XeCl B-X emission excited by pulsed microwaves appeared to be identical to the exciting microwave pulse.

4. THALLIUM MERCURY DISCHARGES

An examination was made of the spectrum of the plasma from a tube containing mercury and thallium iodide. For this tube a temperature of 385° C would be required to completely vaporize the mercury, providing a

69
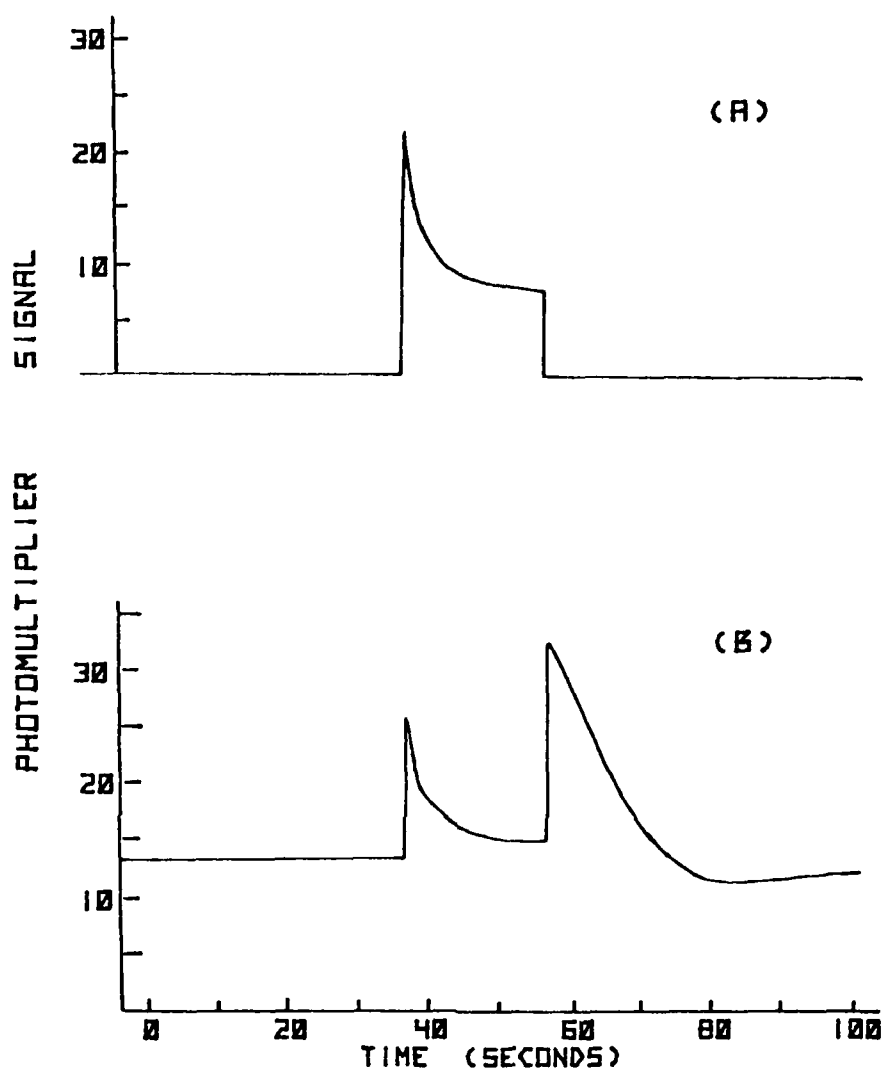
FIGURE 29 Time development of the [A] CW and [B]
CW plus pulsed emission from XeCl at
308 nm as the CW microwaves are turned
on and off again.

pressure of 1333 torr or 1.75 atmospheres. At this temperature the vapor pressure of TlI is of the order of one torr. It was found that the tube could be operated in one of two modes, similar to that of mercury filled tubes. The 'cold' mode, in which the discharge fills the entire cross section of the tube was obtained under conditions of low power loading and low setting of the external heating. The continuous microwave power absorbed was typically 40 watts, and the temperature of the gas that had flowed by the tube was 50° C. Higher power loading conditions resulted in a constricted wall stabilized discharge. The cw power in this case was typically 240 watts, the external heater was run at four times the power as that required for the cold mode, and the flowing air temperature was 160° C. To this time, this tube has not been operated with higher power loading. The power loading used has been insufficient to cause the plasma to form along the entire length of the tube, resulting in condensation of the vapours in the coolest spot on the tube walls.

The spectrum of the radiation emitted from the 'cold' plasma was due to mercury. It seems likely that under the condition in which the cold mode of operation was obtained, the vapour pressure of thallium iodide was negligible. In the wall stabilized discharge, spectral lines of thallium metal were seen in addition to the mercury atomic lines. However, no excimer or molecular emission was seen.

Over a limited range of external heating, a plasma could be obtained in this tube using the pulsed microwave sources only. Weak molecular emission could be seen in the range 444 nm to 452 nm, which is within an emission band of HgTl [17]. With this tube, raising the gas

71

density extinguished the discharge. The molecular structure at 445 nm was observed also in a discharge tube which contained mercury only. For this comparison tubes with approximately the same mercury fill were used with approximately the same power loading. The species responsible for the emission has not been identified.

Note that the tube temperatures used in these experiments are much less than those used in the literature for mercury thallium excimer lasers.

## 5. THALLIUM XENON DISCHARGES

To evaluate the potential for microwave pumping in the thallium xenon system, a discharge tube was constructed containing 1.8 mg of thallium iodide and 20 torr of xenon. Intense emission was observed from atomic iodine and from the xenon iodide excimer, as shown in Figure 30. The iodine line at 178.29 nm is not observed due to cutoff of the photo-multiplier response. The relative intensity of the XeI B-X and B-A emission and the shape of the envelope of the B-A emission depended upon the excitation conditions, in particular on the discharge tube temperature. Emission from atomic thallium was observed at the maximum temperatures used in these experiments. The dependence of emission from the various species on tube temperature is illustrated in Figure 31. This data was quantitatively nonreproducable and appeared to depend on the immediate past history of the discharge tube. It appears likely that the back reaction of thallium with iodine is relatively slow under the conditions of our experiments. In the experiments described in [22] which employed much higher temperatures, no emission from atomic iodine or from XeI was observed.

72

## FIGURE 30

Spectra from a microwave excited
xenon thallium iodide discharge
tube in the range 175-350 nm.
The iodine and XeI B→X emission
is offscale. Wavelengths are in-
dicated in nanometers.
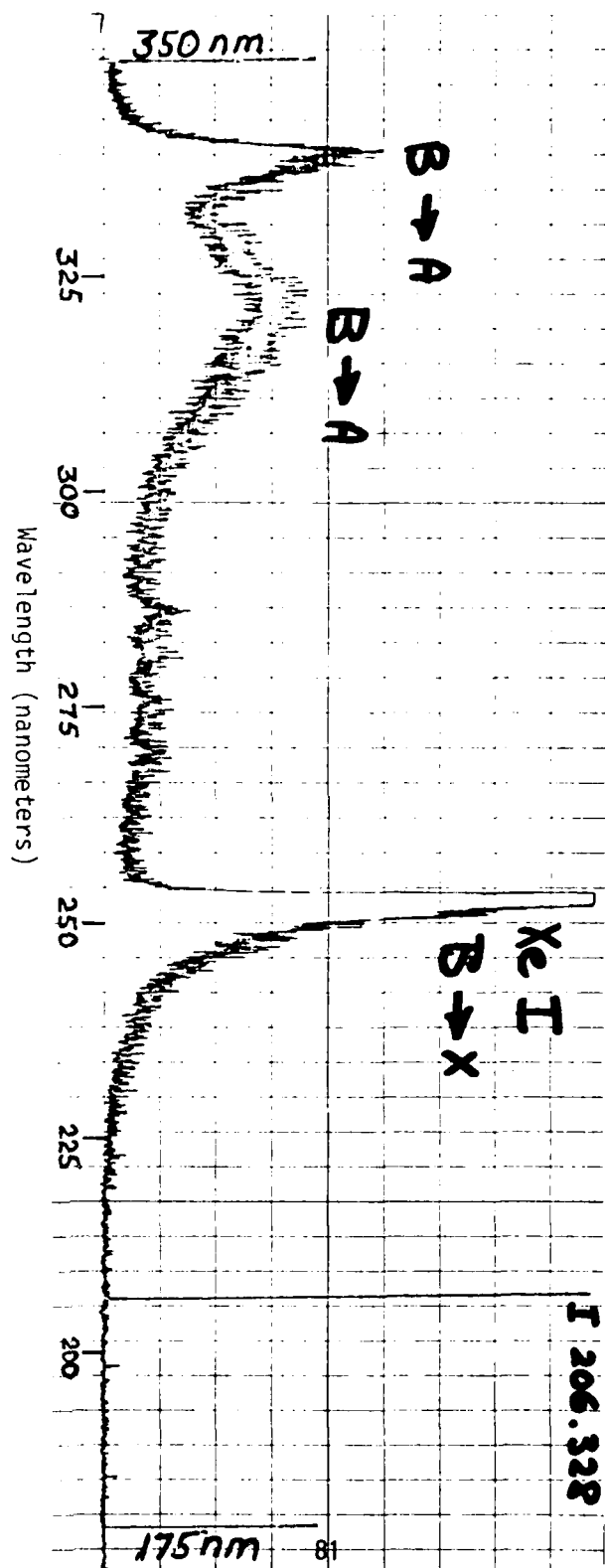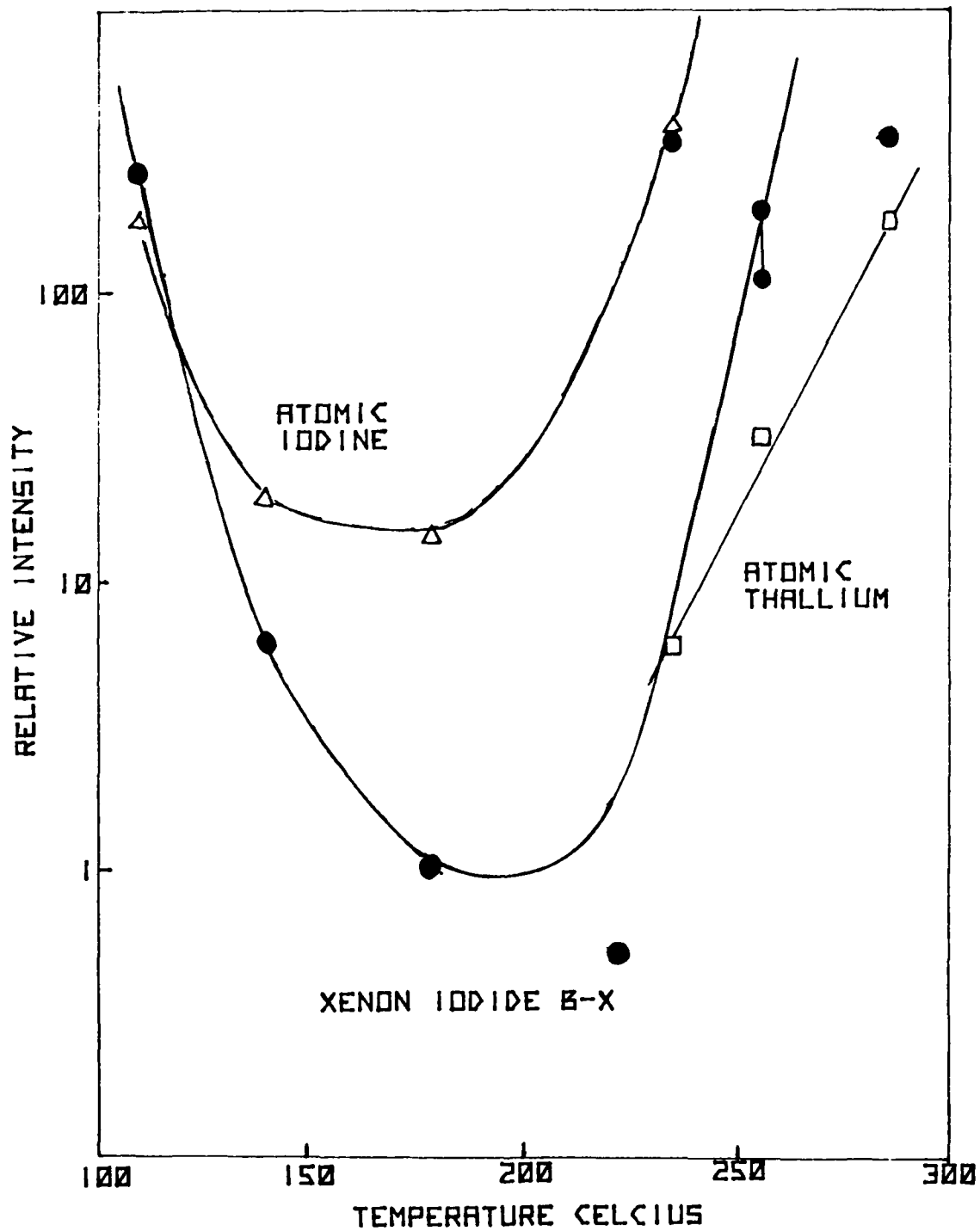
FIGURE 31    Temperature dependence of emission from various
             atomic and molecular species in a xenon thallium
             iodide discharge tube.

74

In these experiments, no emission from the thallium xenon excimer was observed. Thallium in the $7^2S_{1/2}$ excited state can radiate at 535 nm to the $6^2P_{3/2}$ state at a rate of 6.25 x $10^7$ sec$^{-1}$ or radiate at 377.6 nm to the $6^2P_{1/2}$ ground state at a rate of 7.05 x $10^7$ sec$^{-1}$ [22]. Alternately, the excited thallium can form the thallium xenon excimer in the B state in a three body collision with xenon atoms at a rate of 5 x $10^{-31}$ cm$^6$ sec$^{-1}$ [22]. For the excimer formation to dominate over radiative loss of the excitation requires a xenon density greater than 1.6 x $10^{19}$ cm$^{-3}$. This corresponds to a pressure of 400 torr at room temperature. Similarly a xenon density greater than 6.6 x $10^{18}$ cm$^{-3}$ (200 torr at room temperature) is required for formation of the excimer in the C state. Thus the excimer emission will not be observed with the existing discharge tube.

6.  SULFUR

Discharges in sulfur in the twin antenna applicator were nonuniform along the length of the plasma tube. The visible and ultraviolet emission occurs predominately at the position in which the microwaves were injected and decreases down the tube. This is illustrated in Figure 32 for a specific case. The spatial decay of the emission is related to the spatial decay of the microwave intensity and is found to depend on the wavelength being monitored. This indicates that the vibrational population distribution is influenced by the microwave intensity.

It was found that more uniform discharges in sulfur tubes could be obtained when using the sandwich applicator. The pressure of sulfur in
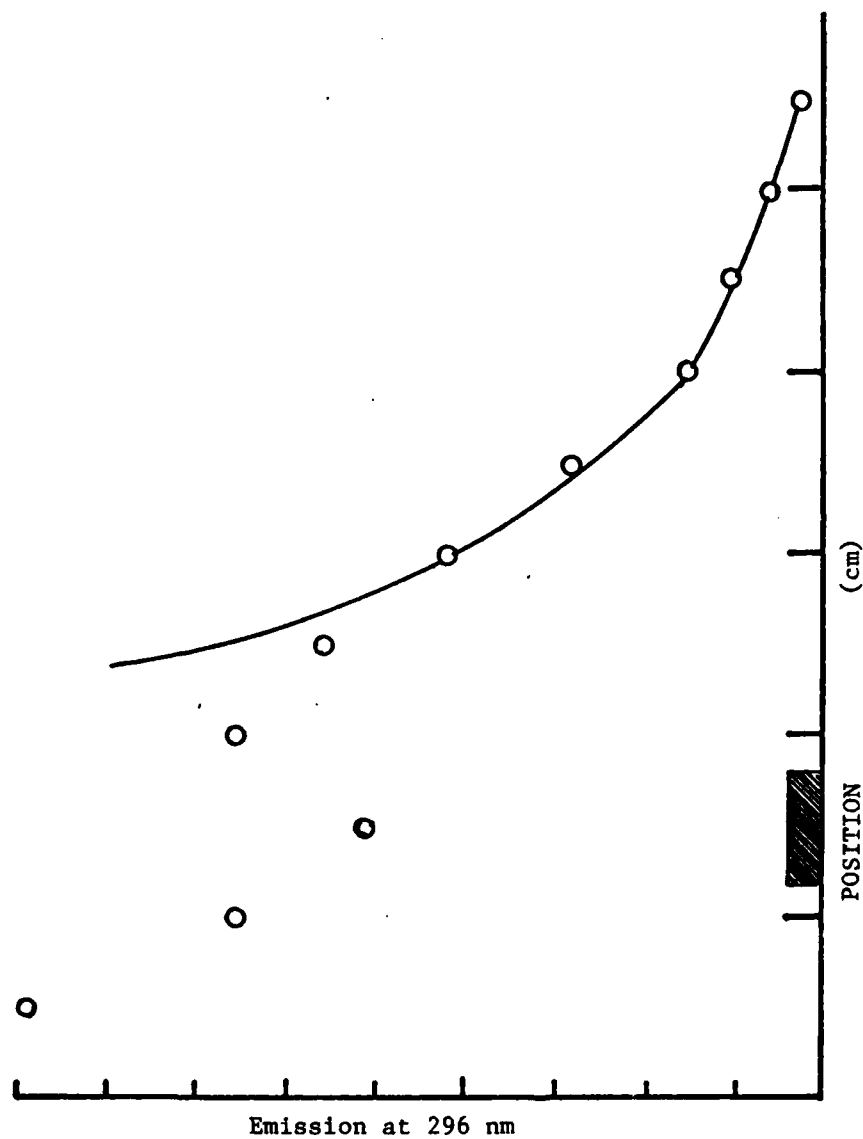
FIGURE 32    Dependence of emission intensity of 295.8 nm on the position on the applicator monitored by the spectrometer and photomultiplier. The shaded portion of the abscissa indicates the position at which microwaves were injected into the applicator.

the gas phase was determined largely by the power input to the discharge.

Characteristics of the emission under these excitation conditions are shown in Figure 33. Curve A of this figure clearly indicates that emission efficiency and intensity decreases with increasing power into the discharge. Clearly as power input increases, the electrical power is deposited into something other than electronically excited $S_2$. However no spectral lines were observed which could be attributed to anything other than $S_2$.

Curves B, C, and D of Figure 33 indicate a change in the vibrational distribution of electronically excited sulfur as power loading is increased. Curve B is the ratio of the emission on the v'=8 to v"=0 transition to that on the v'=9 to v"=0 transition. Curve C is the ratio of the emission on a spectral peak predominantly due to the v'=7 to v"=0 transition to that on the v'=9 to v"=0 transition. Curve D is the ratio of the emission at 374 nm to that on the v'=9 to v"=0 transition. Several vibrational transitions overlap at 374 nm. However, the strongest transition is v'=0 to v"=7 and all of the overlapping transitions originate from low-lying vibrational states. Thus the curves B, C, and D correspond to transitions originating from successively lower values of the upper state vibrational excitation. Lower values of vibrational excitation are clearly favored at high power levels.

Since in this configuration an increase in power loading results in an increase in gas density, the behavior of E/N with increases in power loading is not obvious. However, vibrational relaxation does occur at a faster rate as the power loading is increased. The results

77
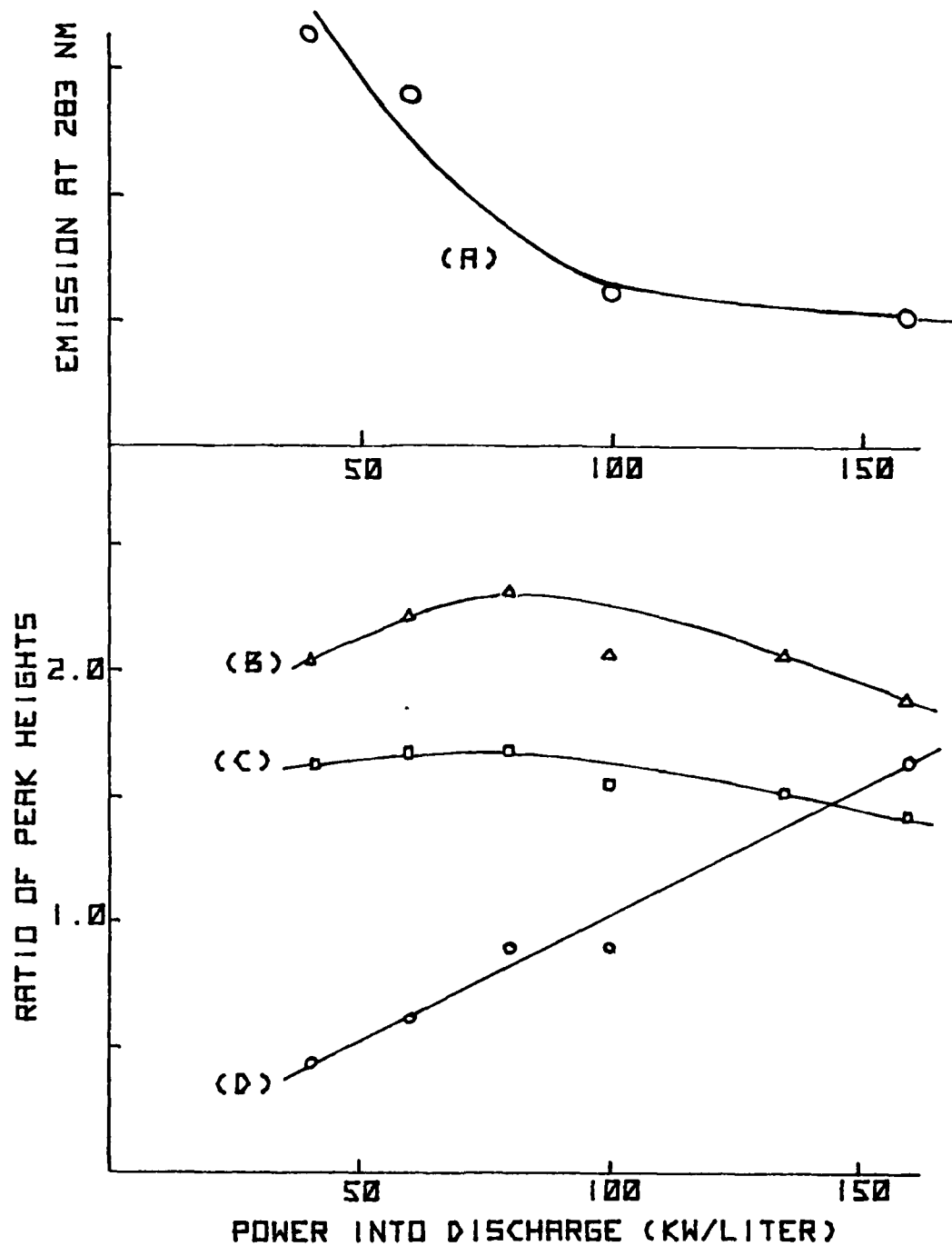
FIGURE 33    Characterization of the emission
from a sulfur discharge tube without
external heating of the discharge tube.

78

of Figure 33 are consistent with the electronically excited sulfur
being formed in a high vibrational level. As power loading and the
rate of vibrational relaxation increases, a larger fraction of the $S_2$
molecules are transferred into vibrational levels from which predissocia-
tion occurs, leading to a decreased overall signal. In addition, more
$S_2$ molecules are transferred into low lying vibrational levels as
indicated in Figure 33.

A systematic study was undertaken of the effect of the pressure
of sulfur, the nature of the gas with which tubes were backfilled, and
the pressure of the background gas. For this study, the discharge tube
was located at an angle to the applicator axis so the tube extended
beyond the region of high microwave field. As discussed earlier, this
configuration means that the gas pressure is determined primarily by
the external source of heat and not to a very great extent by the
microwave power absorbed. For this systematic study, the microwave
power levels were kept at the same value as determined using a digital
volt meter on the output of the power monitors.

In spite of the efforts to keep the experimental conditions
constants, there was a great discrepancy between readings taken under
apparently identical conditions. For example, Figure 34 shows the
spectrally integrated emission from a sulfur discharge tube with a
backfill of 50 torr argon. "Spectrally integrated" means that the data
acquisitions system described earlier was used to integrate the measured
data over the entire frequency range in which emission occurred, after
first correcting the data for the wavelength dependence of the response
of the photomultiplier-spectrometer detection system. The difference

79

FIGURE 34    Integrated CW emission as a function
of sulfur pressure, showing non-
reproducibility of the data.

△ 21 April 1980
○ 28 April 1980
○ 1 May 1980
□ 7 May 1980

**Sulfur pressure   (Torr)**

Spectrally Integrated Emission  (Arbitrary Units)
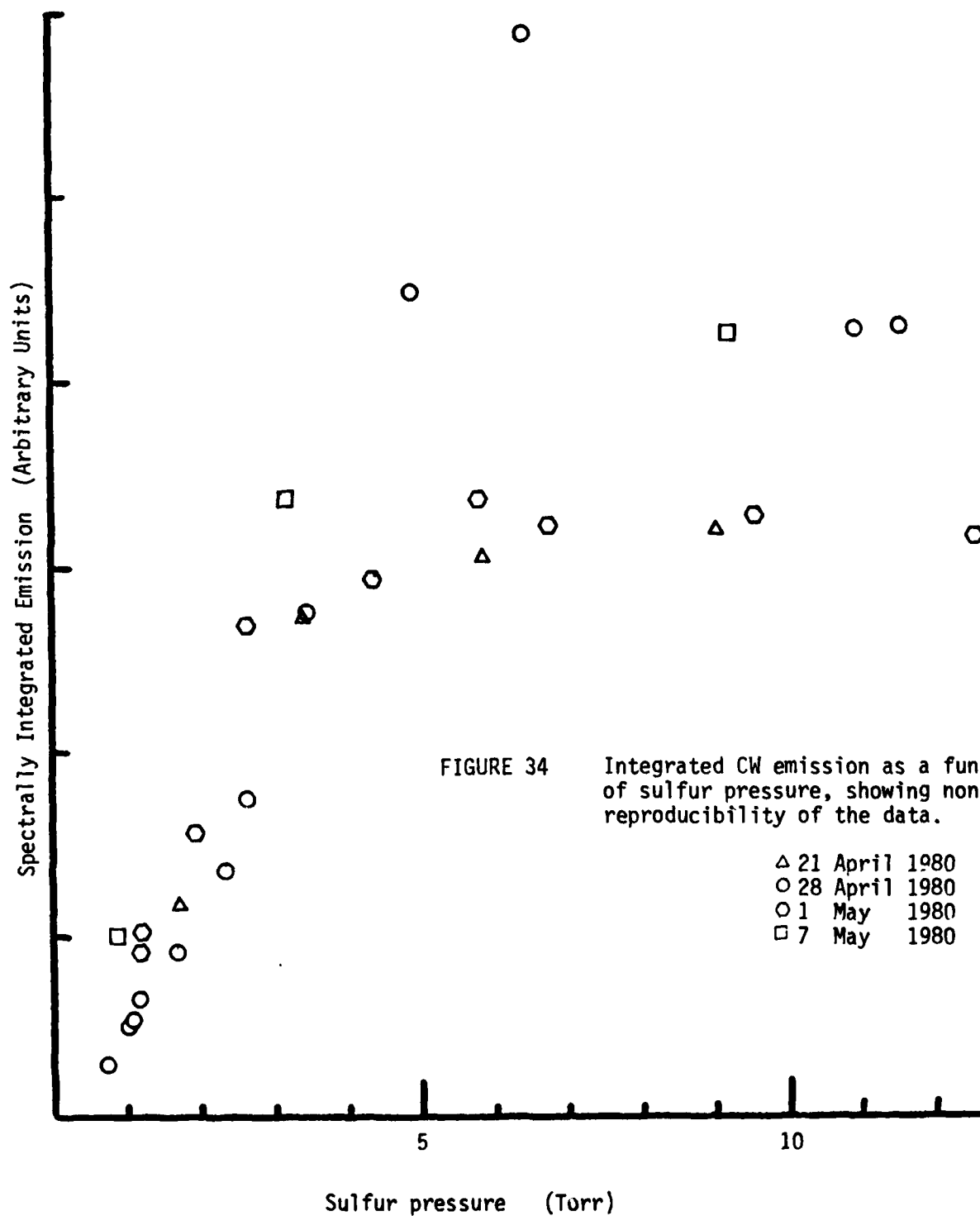
between measurements taken on successive days was as much as a factor of two. In some cases in a series of measurements, a final measurement would be much lower, in some cases higher. When an initial reading taken under the same conditions and on the same day, it was initially thought that some chemical effects between the sulfur and the quartz discharge tube may be responsible for the inconsistencies. To investigate this possibility, a tube was "cycled": after measurements were taken at a low operating pressure, the tube was heated to a high temperature and pressure with the microwave level held constant. The tube was allowed to cool to the original pressure and after a steady state was reached, another measurement was taken. The process was then repeated. In this test the measurements agreed to within a few percent. The cause of irreproducibility in other measurements remains a mystery.

The time averaged spectrally integrated emission is plotted as a function of the pressure of sulfur and the backfill gas in Figures 35 and 36 for helium and argon respectively as the backfill gas. Some nonreproducibility of the measurements is also evident in these graphs. In view of the scatter in the measurements, conclusions drawn from these graphs may be arguable. The trends in the data indicate that the emission from tubes with a high pressure of background gas is definitely lower than that with a lower pressure. Optimum results are obtained with 0.5 torr of helium or with 5.0 torr of argon. For a given backfill pressure, as the sulfur pressure is increased the emission increased, goes through a maximum, and then decreases. The maximum is at about 2 torr with a low pressure (~0.5 torr) of backfill gas and at about 5 torr when 5 torr of backfill gas is used.

81

FIGURE 35    Time averaged component of visible emission from sulfur vapor irradiated by CW and pulsed microwaves.

Sulfur plus   △ 0.59 Torr argon
              ○ 5.02 Torr argon
              □ 49.4 Torr argon

Spectrally integrated emission

Sulfur pressure  (Torr)

82

FIGURE 36    Time averaged component of visible emission from sulfur vapor irradiated by pulsed and and CW microwaves.

Sulfur plus    △ 0.51 Torr helium
               ○ 4.91 Torr helium
               □ 50.2 Torr helium

Spectrally integrated emission

Sulfur pressure  (Torr)

83

The pulsed component of the visible emission was measured simultaneously with the time averaged emission discussed above. Figures 37 and 38 present these results for sulfur-helium and sulfur-argon discharge tubes repsectively. For 0.5 torr and for 50 torr of back fill gas, there is little difference between the measured emission when using the two different gases. However the emission seemed considerably higher when using 5 torr of helium than when using 5 torr of argon.

The role of argon and helium in collisions with excited sulfur molecules has not been completely elucidated. Durands [46] and McGee and Weston [47] report that argon and helium can either lead to vibrational relaxation or electronic quenching with the cross sections for both processes being approximately gas kinetic. The quenching of the electronic energy probably occurs because the molecule is collisionally excited to vibrational states with $v' \geq 10$. These states spontaneously dissociate into sulfur atoms as a result of the crossing of the potential curve for the B state with that of an unbound electronic state (Figure 7). However, Caughey and Crosley [48] report that collisions with the rare gases lead primarily to vibrationally and rotationally relaxed B-state $S_2$. The data of reference [48] is used to calculate the frequency of collisions between vibrationally excited sulfur and the back fill gas that lead to vibrational relaxation, and the frequency of collisions between excited state sulfur and ground state sulfur that lead to quenching.

It was found that at one torr of sulfur, quenching collisions were as frequent as relaxational collisions in tubes with 5 torr of back fill

FIGURE 37    Pulsed component of visible emission from sulfur vapor irradiated by CW and pulsed microwaves:

Sulfur plus    △0.59 Torr argon
○5.02 Torr argon
□49.4 Torr argon

85

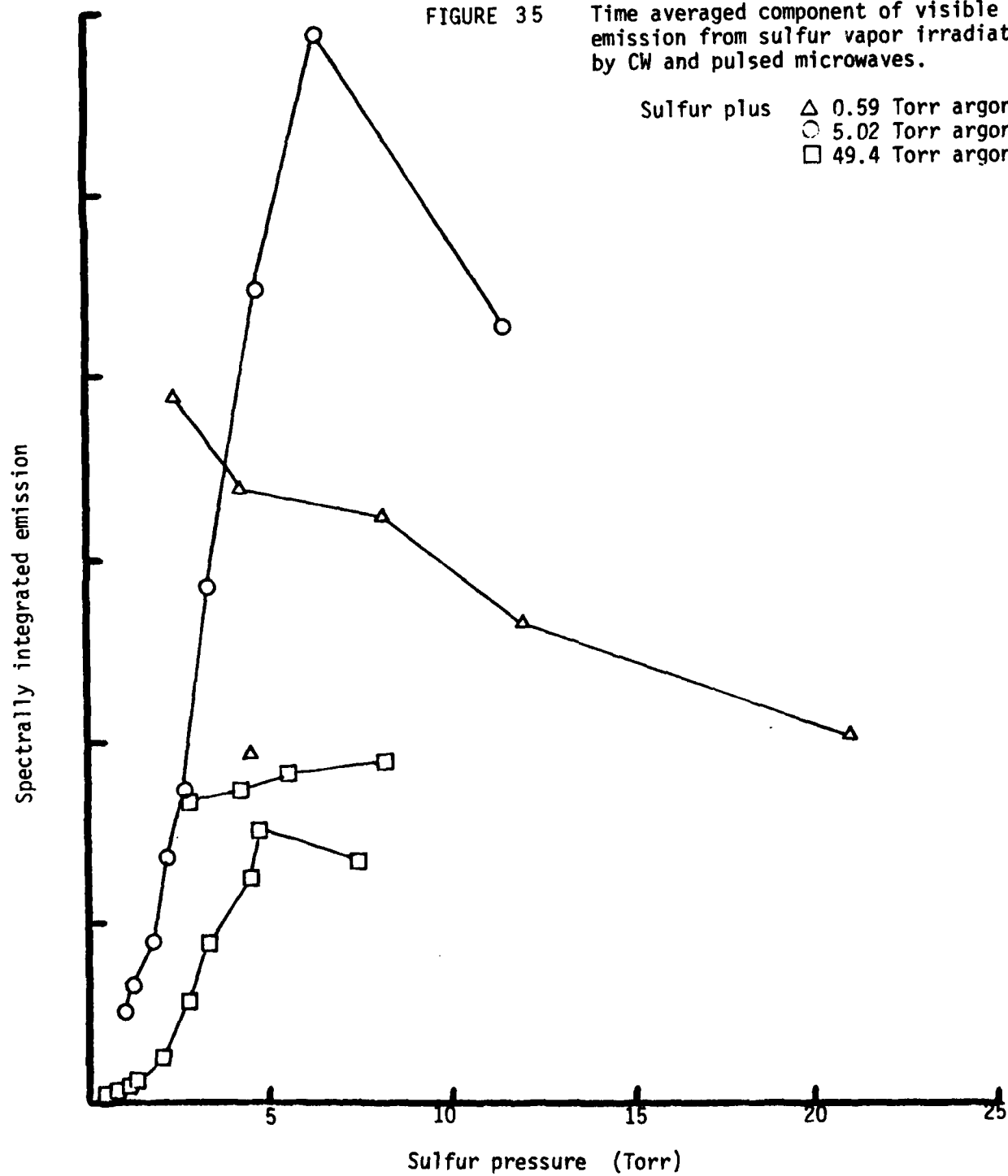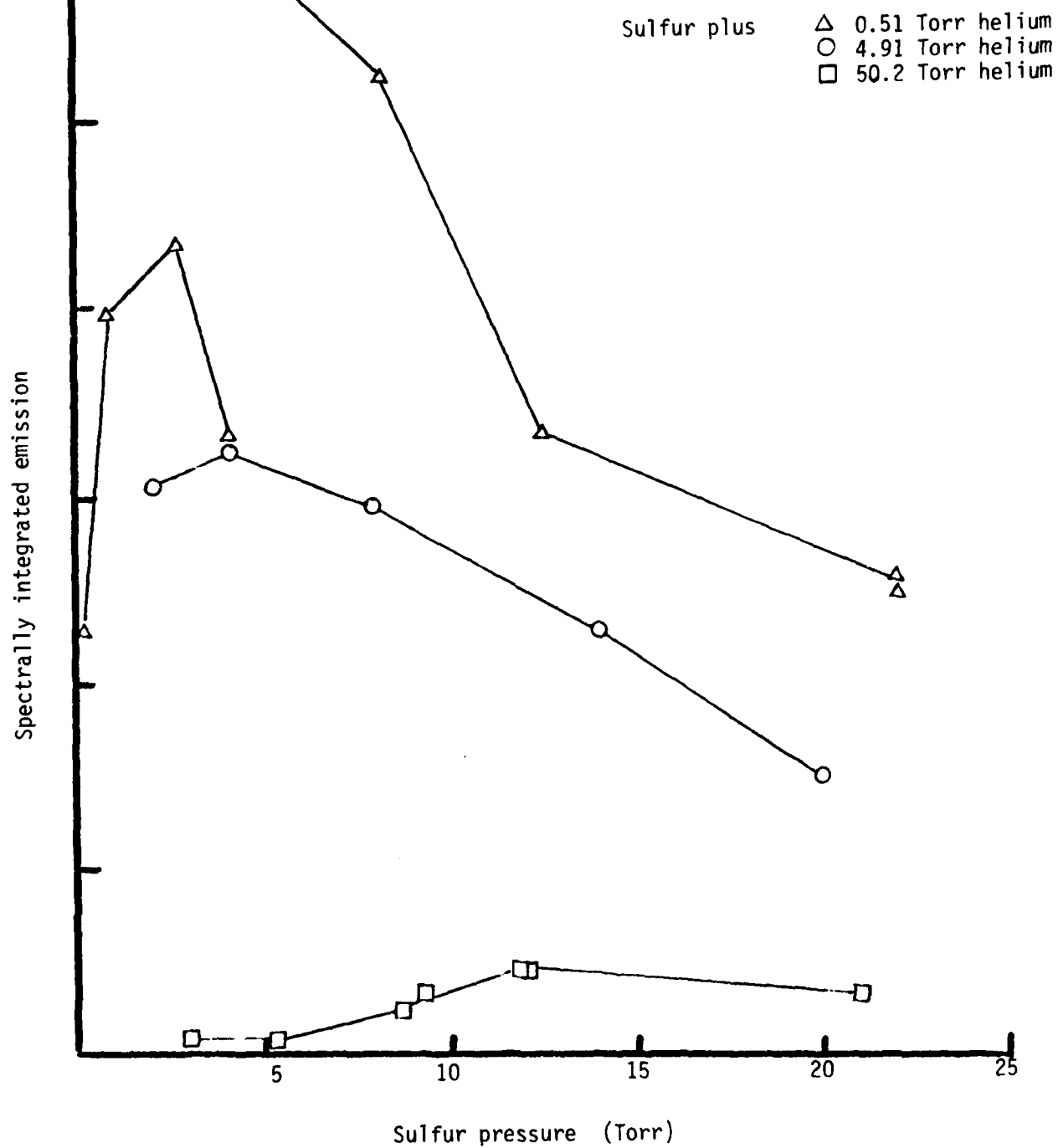FIGURE 38   Pulsed component of visible emission from sulfur vapor irradiated by CW and pulsed microwaves:

Sulfur plus  △ 0.51 Torr helium
             ○ 4.9  Torr helium
             ☐ 50.2 Torr helium

86

gas, either helium or argon, and much more frequent in tubes with 0.5 torr of back fill gas. At 10 torr of sulfur, quenching collisions were as frequent as relaxational collisions in tubes with 50 torr of back fill gas and much more frequent in tubes with 0.5 or 5 torr of gas.
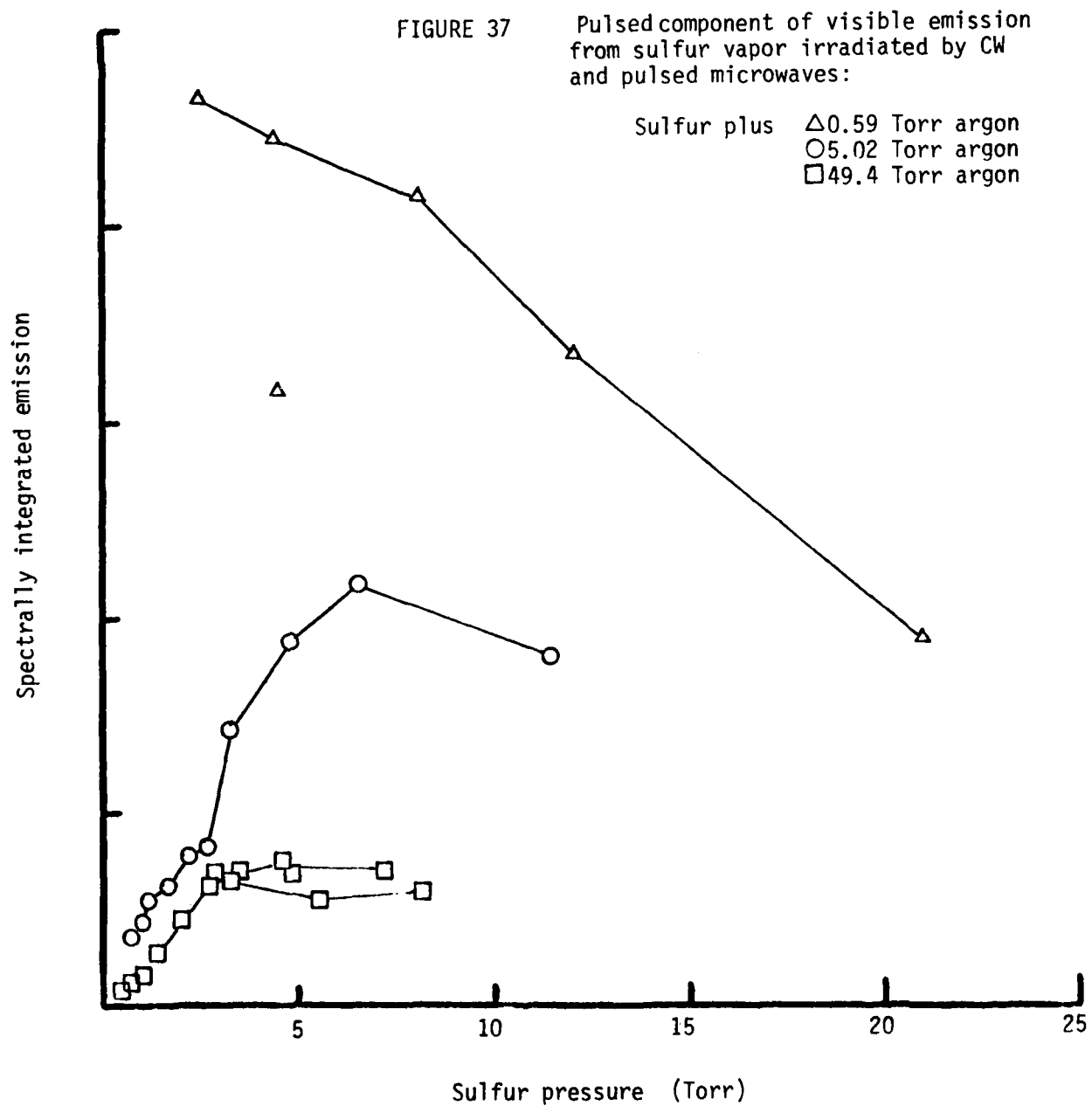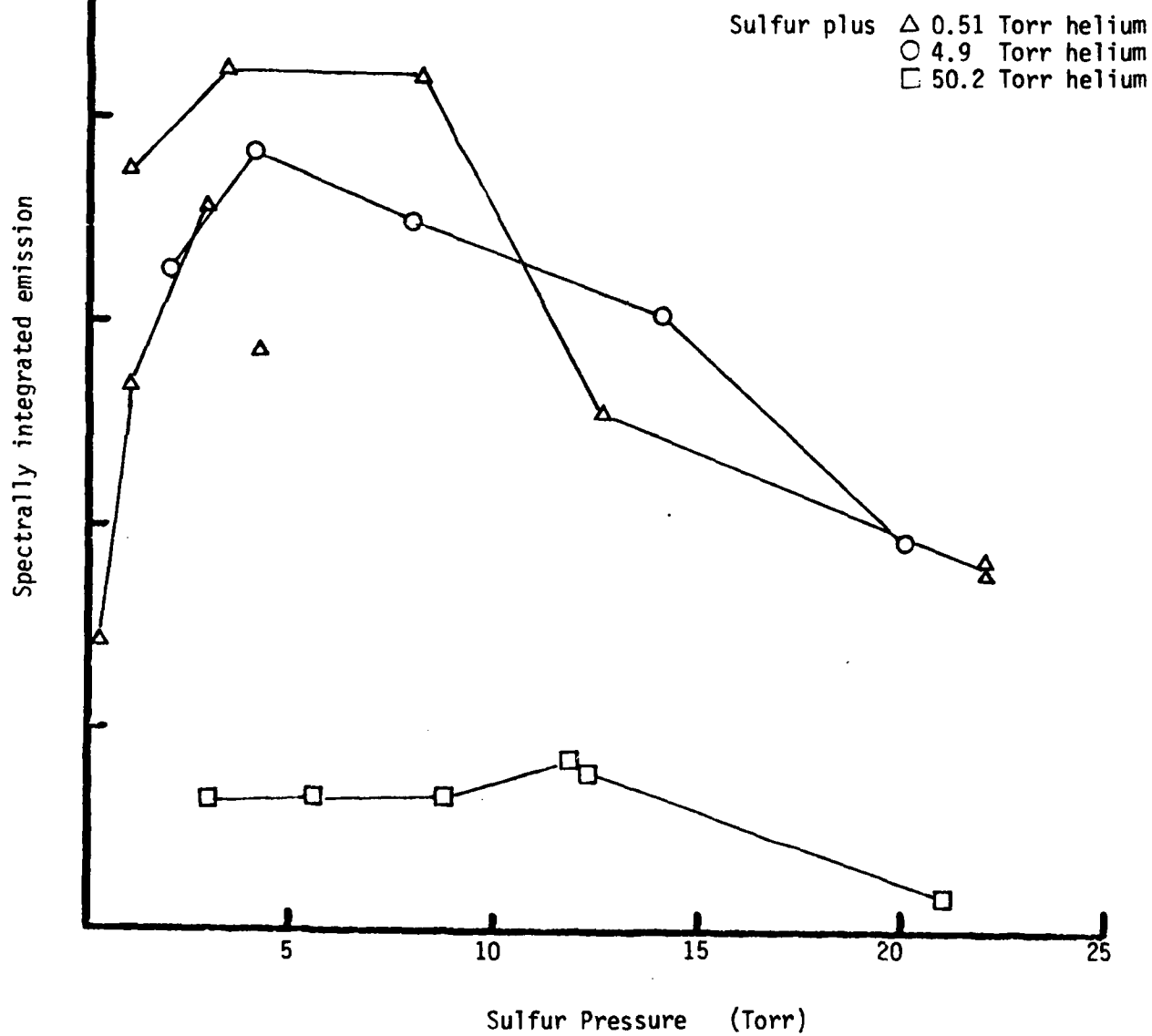
The results (Figures 35 to 38) show there to be no significant difference between the dependence on sulfur pressure when the backfill gas is 0.5 torr of either helium or argon. However there is wide differences between the curves for 5 torr of backfill gas.

In the above measurements, the incident microwave power was held at a constant value throughout. In different tubes and as the sulfur pressure was varied, the ratio of electric field to number density, E/N, is a variable quantity. The dependence of emission intensity on gas pressure (Figures 35 to 38) will be partially due to the probability of quenching collisions but will also be influenced by the dependence of excitation probability on E/N. As the sulfur pressure was increased, the fraction of the incident power that was absorbed by the plasma decreased. The dependence of absorption on sulfur pressure was stronger for the cw power than for the pulsed power, and was stronger in tubes with 50 torr of backfill gas than in tubes with a lower helium or argon pressure.

The extent of the discharge when the discharge tube was mounted at an angle to the applicator was in principle limited by the length of overlap between the tube and the region of high microwave intensity. In practice the extent of discharge was found to decrease with increasing sulfur pressure and with increasing pressure of the backfill gas.

The spectral distribution of the radiation emitted by the sulfur plasma is shifted to longer wavelengths as the pressure of backfill gas

87

was increased, as illustrated in Figure 39.    For low background gas
pressures, emission is greatest for wavelengths shorter than 320 nm.
As shown in Figure II-8, primarily higher vibrational states of $S_2$:B
contribute to emission in this spectral region.  For wavelengths in the
range 340 - 410 nm, the largest contribution to the emission comes from
low lying vibrational levels of the excited electronic state.  Tubes
with a higher pressure of background gas give the largest contribution
in this spectral region, indicating that in these tubes vibrational
relaxation has occurred before emission.  This is verified in Figure
40 which  gives the results of the computation of populations of
vibrational states from the spectral distribution of the emission. The
results of the calculation are not spectacularly impressive; a "jagged"
dependence on vibrational quantum number is produced rather than a smooth
curve, as a result  inaccuracies in some of the data that had been
input to the computer calculation.  Nevertheless, the trends in the
populations do indicate increasing relaxation with increasing pressure
of buffer gas.  For low pressure of argon, the population distribution
is approximately constant with a tendency to increase at higher vibra-
tional levels.  At higher argon pressures, a larger fraction of the
population is in low lying vibrational levels.

In low pressure discharges in sulfur, spectral lines of atomic
sulfur was observed.  Emission at 468 nm is due to the $^5$P to $^5$S and
that at 528 nm is due to $^3$P to $^3$S transitions [26].  In both cases, the
upper level for the observed transactions is at 74000 cm$^{-1}$ or about 6 eV
above the ground state of atomic sulfur.  The dependence of the emission
on the pressure of sulfur gas is illustrated in Figure 31.    From

88

FIGURE 39   Dependence on gas mix of
spectrally resolved emission

2.7 Torr Sulfur plus

△ 0.59 Torr argon
○ 5.02 Torr argon
□ 49.4 Torr argon

89
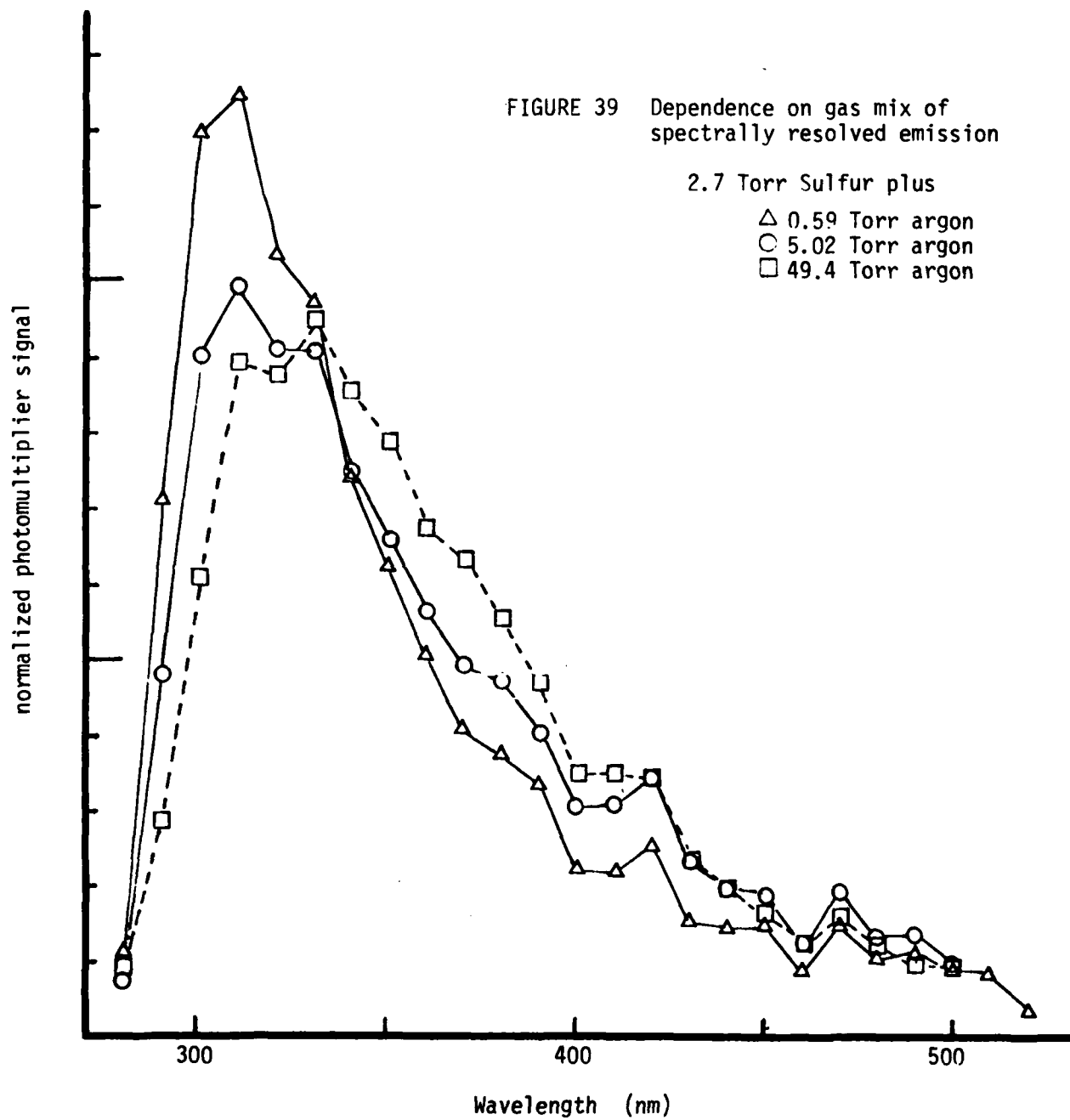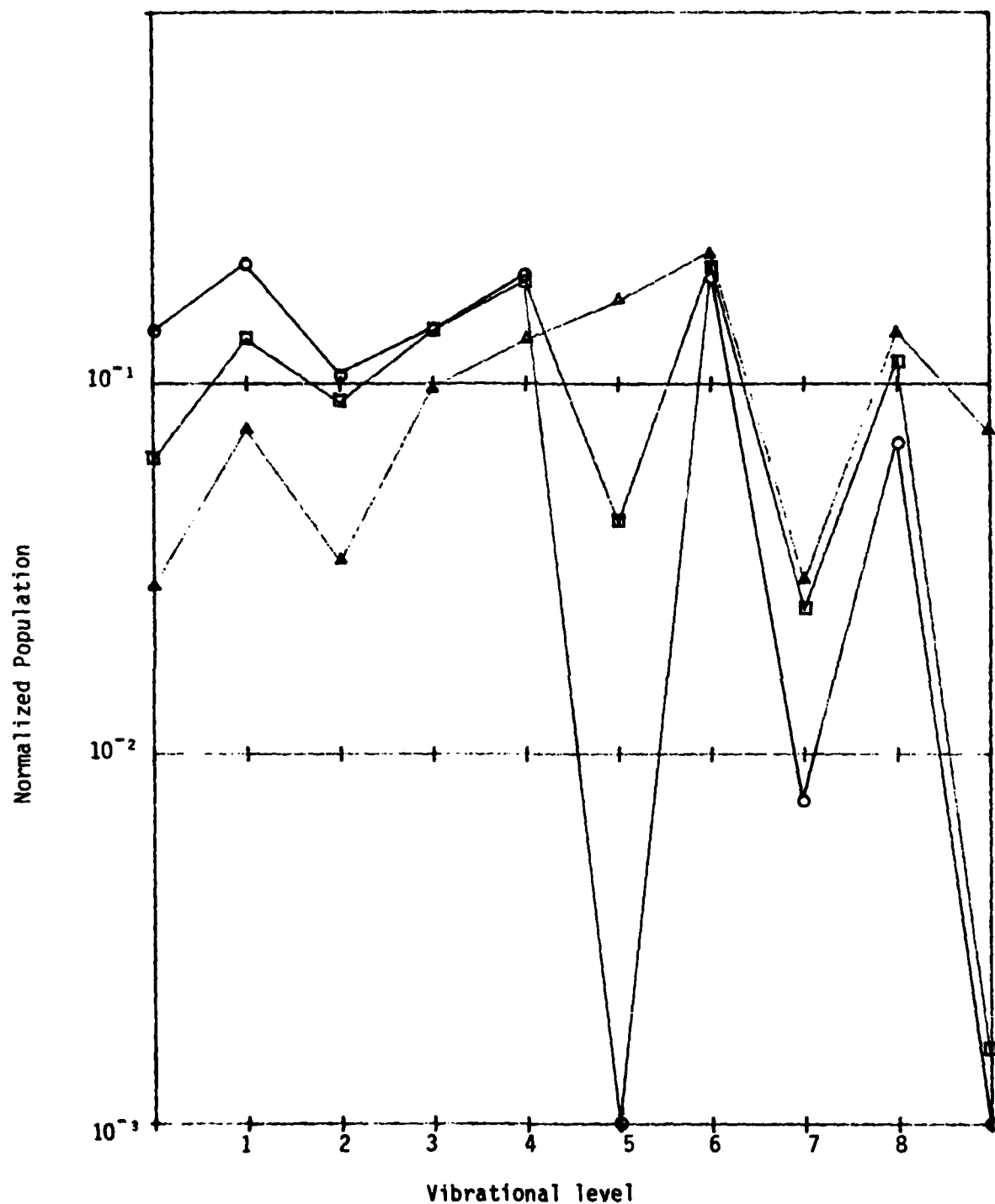
FIGURE 40    Population of Vibrational levels for plasmas in
discharge tubes with 2.7 Torr sulfur and (○) 49.4
Torr, (□) 5.02 Torr, or (▲) 0.59 Torr of Argon
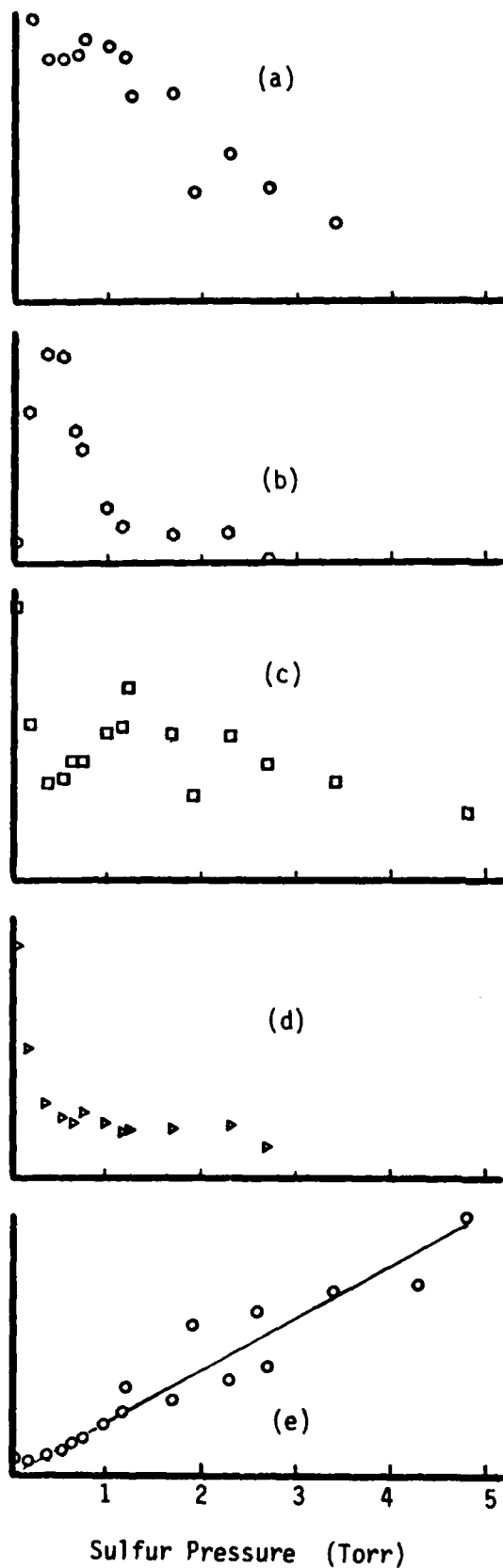
FIGURE 41

Dependence on sulfur pressure of emission intensity on atomic and impurity lines. Note the vertical axis units are not the same for each graph.

(a) atomic sulfur at 468 nm

(b) hydrogen β at 486 nm

(c) CS at 256 nm

(d) argon at 415 nm

(e) total emission 275-515 nm, primarily from diatomic sulfur.

Sulfur Pressure (Torr)

Figure 7 it is observed that diatomic sulfur in the excited electronic state $B^3\Sigma$ predissociates into ground state atomic sulfur. Therefore, the decrease in emission from atomic sulfur as the gas pressure is increased does not necessarily mean that dissociation is no longer taking place. The decrease in emission may be because at high gas pressures the electron energy is too low to electronically excite the atomic sulfur produced by predissociation.

## 7. IMPURITIES IN SULFUR DISCHARGES

The first plasma in a newly made sulfur discharge tube, when no external heat was applied, gave a spectrum in which all lines were identified as due to the backfill gas, either helium or argon. With several hundred watts of continuous power the discharge comes blue and contains spectral lines of $S_2$ and the radical CS, with atomic lines of C (248 nm) and S (469 nm) appearing weakly. The helium lines are absent under these conditions. As the external heating is turned on to heat the tube, the atomic lines weaken and the $S_2$ emission becomes stronger with respect to the CS impurity. Several tubes were run with continuous microwave inputs of greater than 700 watts. However, under these conditions the quartz walls of the tube could be seen to be glowing when the microwave discharge was suddenly extinguished. After this, a discharge run under the same conditions that were previously used to record a helium spectrum now was a bright red colour and gave the spectrum of atomic hydrogen in addition to that of helium. With slightly higher cw power, but without external heating, the spectrum of CO was obtained. It appears that the extreme heat of the discharge under high power conditions

dissociated some impurity species that had previously not contributed to the emission.

The CS impurities were observed in all the discharge tubes, although the emission was weakest in discharge tubes in which extraordinary care was taken concerning purity. The mechanism by which carbon is admitted to the tubes is not known. The CS emission probably results from discharge induced dissociation of $CS_2$, a stable molecule which may be formed from the unknown carbon source in the first discharge in each new tube. The amount of $CS_2$ in the tube may be quite small but it would dominate the sulfur emission at low power levels or with little external heating since the vapour pressure of sulfur is very much lower than that of $CS_2$. As the tube temperature is increased, the emission from $S_2$ dominates that from CS. Because of this, the presence of impurities in the tube is not considered an important factor.

Figure 42 indicates that the sulfur monoxide spectrum was present along with the $S_2$ spectrum in some cases. The SO emission appeared to get progressively stronger as the tube was run for long periods of time under high power loading conditions. When a discharge tube in which SO appeared was run at low powers with little external heating, in some cases the SO emission completely dominated the $S_2$ emission. The spectrum of OH often appeared under the same conditions as that of SO.

The SO and OH emission would never appear in a tube operated only under moderate power input, for example, with about 150 watts continuous incident on the plasma.

SO(1,4)

SO(2,5)

SO(0,4)

SO(1,5)

SO(2,6)

SO(0,5)

$S_2(9,0)$

$S_2(8,0)$
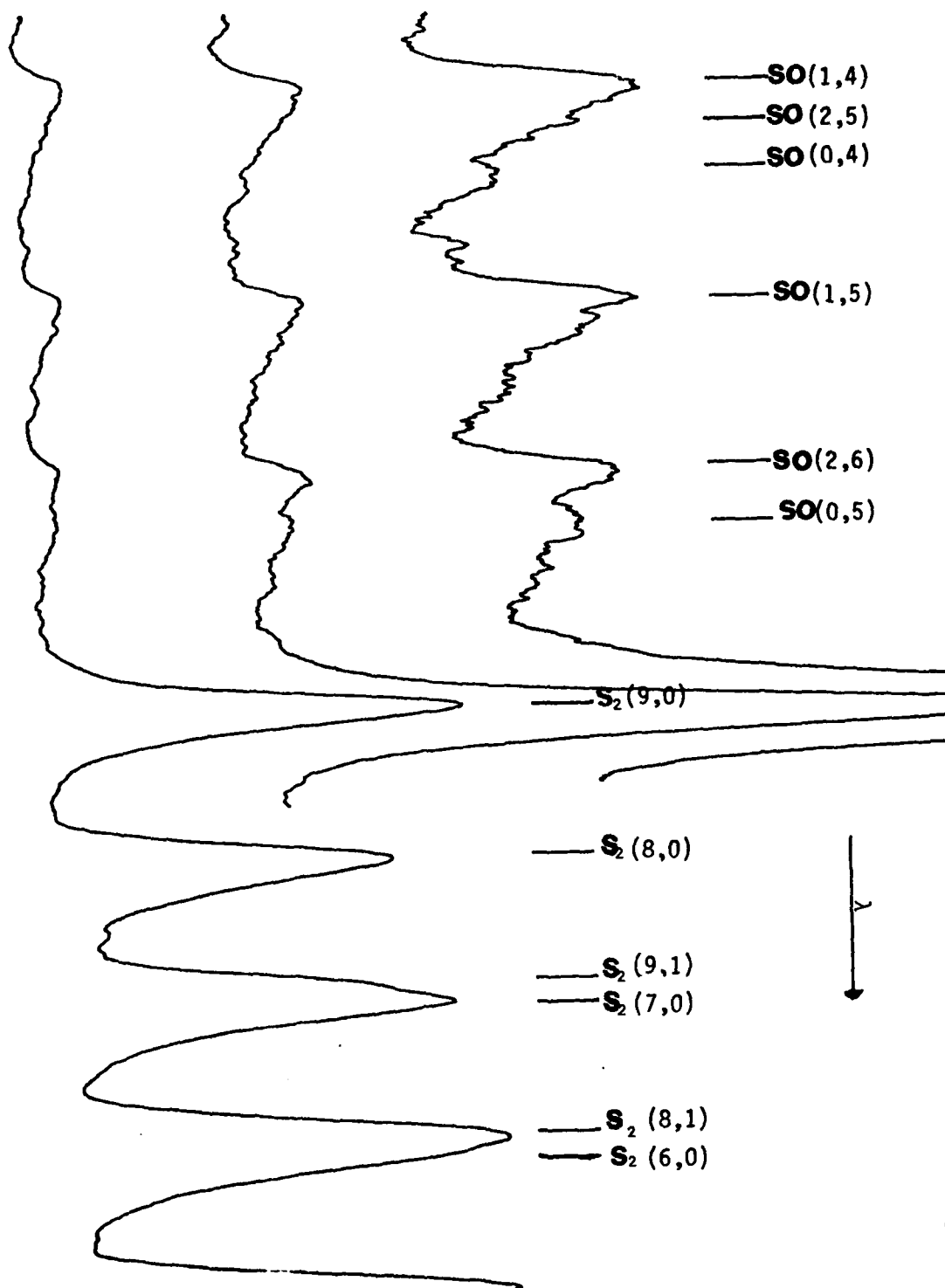
$S_2(9,1)$

$S_2(7,0)$

$S_2(8,1)$

$S_2(6,0)$

FIGURE 42

Emission from a sulfur discharge tube in the range
266 to 296 nm, showing SO as well as $S_2$ emission.
The three figures are on progressively increasing
gains of the chart recorder.

94

The source of the hydrogen and oxygen which appears in observed spectra is believed to be the fused silica discharge tubes. The "Suprasil" fused silica, supplied by Heraeus Amersil, Inc., used in the fabrication of discharge tubes contains greater than 0.1% by weight of the hydroxyl (OH) group [49]. Grades of fused silica containing a lower OH concentration are commercially available; however, they generally contain a higher concentration of metallic impurities that reduce the ultraviolet transmittivity.

The heating of fused silica by a gas torch will cause the release of the OH, and the formation of water droplets on a cooler portion of the inside wall of the tube. Moreover a white ring will form on the tube wall a short distance away from the spot in which the torch is applied. The white deposit is silicon monoxide formed as a result of the dissociation of the silica (silicon dioxide). Evidently oxygen must be released also. In an earlier study of absorption and radiative lifetimes in a sealed quartz cell [50], the presence of $SO_2$ and possibly of $H_2S$ was observed. In this case the gas of sulfur molecules was not exposed to an electrical discharge but was kept at elevated temperatures for extended periods of time before the impurities were detected. In this experiment as well as in those described in this report, the impurity species most probably result from the reaction of the hot sulfur with the quartz.

## REFERENCES

1.  J. S. Whittier, M. L. Lindquist, A. Ching, G. E. Thornton, R. Hofland, Jr., "Dissociation Efficiency of Electron-Beam-Triggered Discharges for Initiating Atmospheric-Pressure $H_2$-$F_2$ Lasers", J. of App. Phys., 47, 3542 (1976).

2.  Fusion System Corporation, Bulletin RAD-2, S.

3.  S. L. Bellinger, General Electric Review, 47, 31 (1944).

4.  R. Darrah, "Large Volume Plasma Production by 2.45 GHz Microwaves", Technical Report AFAPL-TR-77-85.

5.  J. F. Waymouth, Electric Discharge Lamps, (M.I.T. Press, Cambridge, Mass., 1971).

6.  J. F. Waymouth, "Metal Halide Lamps", Proc. IEEE 59, 629 (1971).

7.  E. J. Schimitischek, J. E. Celto, and J. A. Trias, "Mercuric Bromide Photodissocation Laser", Appl. Phys. Lett. 31, 608 (1977).

8.  E. J. Schimitischek and J. E. Celto, "Mercuric Bromide Dissociation Laser in an Electric Discharge", Optics Letters 2, 64 (1978).

9.  R. Burnham, "Discharge Pumped Mercuric Halide Dissociation Lasers", Appl. Phys. Lett. 33, 156 (1978).

10. E. J. Schimitischek and J. E. Celto, "The Effect of Nitrogen on the Extraction Efficiency of a $HgBr_2$ Dissociation Laser", Paper ThB3, Topical Meeting on Excimer Lasers, Charleston, September 1979.

11. W. L. Nighan, "Kinetic Processes in Electrically Excited Mercuric-Halide Dissociation Lasers", Paper ThB4, Topical Meeting on Excimer Lasers, Charleston, Setpember 1979.

12. N. Djeu and C. Mazza, "Laser Induced Fluorescence Measurement of HgBr (B→X) Radiative Lifetime", Chem. Phys. Lett. 46, 172 (1977).

13. Ch. A. Brau, "Rare Gas Halogen Excimers", in Excimer Lasers edited by Ch. K. Rhodes(Springer-Verlag, New York, 1979).

14. L. Burlamacchi, P. Burlamacchi, and R. Salimbeni, "Long-Life Operation of an XeCl Excimer Laser", Appl. Phys. Lett. 34, 33 (1979).

15. W. L. Nighan and R. T. Brown, "Efficient XeCl(B) Formation in an E-Beam Assisted Xe/HCl Discharge," Appl. Phys. Lett. 36, 498 (1980).

16. L. A. Schlie, L. E. Jusinski, R. D. Rathge, R. A. Hamil, and D. L. Drummond, "Strong Tl-Hg Band Emission at 4590 and 6560 A via Electron Beam Initiated Discharges in TlI and Hg Mixtures", J. Chem. Phys. 72, 4549 (1980).

17. D. Drummond and L. A. Schlie, "The Thallium Mercury Excimer and Its Potential as a Laser", J. Chem. Phys. 65, 3454 (1976).

18. R. A. Hamil, D. L. Drummond, L. A. Schlie, and R. P. Benedict, "UV Preionized Thallium-Mercury Discharge", J. Appl. Phys. 50, 637 (1979).

19. S. Chilukuri and M. H. Nayfeh, "Emission and Gain Studies of the Tl-Hg Excimer", J. Appl. Phys. 49, 5378 (1978).

20. D. J. Ehrlich, J. Maya, and R. M. Osgood, Jr., "Efficient Thallium Photodissociation Laser", Appl. Phys. Lett. 33, 931 (1978).

21. B. Cheron, R. Scheps, and A. Gallagher, "Continuum Radiation and Potentials of Tl-Noble Gas Molecules", J. Chem. Phys. 65, 326 (1976).

22. L. A. Schlie, L. E. Jusinski, R. D. Rathge, R. A. Hamil, and D. L. Drummond, "Strong Tl-Xe Excimer Band Emission Via Electron Beam Initiated Discharges in TlI and Xe Mixtures", J. Chem. Phys. 72, 4529 (1980).

23. S. R. Leone and K. G. Kosnik, "A Tunable Visible and Ultraviolet Laser on $S_2$ (B-X)", Appl. Phys. Lett. 30, 346 (1977).

24. B. Wellegehausen, "Optically Pumped CW Dimer Lasers", IEEE J. Quant. Elect. QE-15, 1108 (1979).

25. H. Rau, unpublished results quoted in Sulphur Energy and Environment, B. Meyer (Elsevier Scientific Publishing Co., 1977).

26. "Pure Sulphur Discharges and Associated Spectra", D. A. Peterson, MSc. Thesis, Air Force Institute of Technology.

27. D. A. Peterson and L. A. Schlie, "Stable Pure Sulfur Discharges and Associated Spectra", unpublished manuscript.

28. H. Rau, T. R. N. Kutty and J. R. F. Guedes de Carvalko, "Thermodynamics of Sulphur Vapour", J. Chem. Thermodynamics 1973, 833.

29. J. Berkowitz, "Molecular Composition of Sulfur Vapor", in Elemental Sulfur ed. by B. Meyer (Interscience Publishers, New York, 1965).

30. R. F. Barrow and R. P. de Parcq, "Electronic Spectrum and Electronic States of $S_2$", in Elemental Sulfur, ed. by B. Meyer (Interscience Publishers, New York, 1965).

31. J. M. Ricks and R. F. Barrow, "The Dissociation Energy of Gaseous Diatomic Sulfur", Canad. J. Phys. 47, 2423 (1969).

32. W. R. Anderson, D. R. Crosley, J. E. White, Jr., "Franck-Condon Factors for the B-X System of $S_2$", J. Chem. Phys. 71, 821 (1979).

33. T. H. McGee and R. E. Weston, Jr. "Lifetime of the B $^3\Sigma_u^-$ State of $S_2$", Chem. Phys. Lett., 47, 352 (1977).

34. B. H. Armstrong and R. W. Nicholls, Emission, Absorption and Transfer of Radiation in Heated Atmospheres (Pergamon Press, Oxford, 1972).

35. V. E. Merchant, "Manual for Operating Microwave Irradiation Facility," USAF-APL Contract F33615-77C-3113.

36. R. W. B. Pearse and A. G. Gaydon, The Identification of Molecular Spectra, 4th Edition (John Wiley and Sons, New York, 1976).

37. V. E. Merchant and M. L. Andrews, "Rotational Temperature of Diatomic Sulphur in Microwave Discharges", presented at 1979 Annual Meeting of the Optical Society of America, Rochester, New York, October 1979.

38. V. E. Merchant and M. L. Andrews, "Technique for Measuring Rotational Temperature of Microwave Excited Diatomic Sulfur", accepted for publication in Applied Optics.

39. G. Herzberg, Spectra of Diatomic Molecules (Van Nostrand Reinhold Co., New York, 1950), p. 271.

40. J. B. Tatum and J. R. G. Watson, "Rotational Line Strengths in $^3\Sigma^\pm - ^3\Sigma^\pm$ Transitions With Intermediate Coupling", Canad. J. Physics 49, 2693 (1971).

41. K. P. Huber and G. Herzberg, Molecular Spectra and Molecular Structure: Constants of Diatomic Molecules (Van Nostrand Reinhold Company, New York, 1979).

42. K. A. Meyer and D. R. Crosley, "Rotational Satellite Intensities and Triplet Splitting in the B $^3\Sigma_u^-$ State of $S_2$", Canad. J. Phys. 51, 2119 (1973).

43. J. E. Meakin and R. F. Barrow, "The Electronic Spectrum of $S_2$", Canad. J. Phys. 40, 377 (1962).

44. L. A. Schlie, private communication.

45. J. E. Velazco and D. W. Setser, J. Chem. Phys. 62, 1990 (1975).

46. E. Durand, "Quenching and Vibrational Energy Transfer in the Fluorescente Spectrum of $S_2$", J. Chem. Phys. 8, 46 (1940).

47. T. H. McGee and R. E. Weston, Jr., "Collisional Quenching of Fluorescence from $S_2$ (B $^3\Sigma_u^-$)", J. Chem. Phys. 68, 1736 (1978).

48. T. A. Caughey and D. R. Crosley, "Coherence Retention During Rotationally Inelastic Collisions of Selectively Excited Diatomic Sulfur", Chem. Phys. 20, 467 (1977).

49.  W. H. Dumbaugh, Jr., and J. W. Malonendier, "Refractory Oxides", in
     <u>High Temperature Oxides Part IV</u>, Ed. by A. M. Alper (Academic Press,
     New York, 1971).

50.  K. A. Meyer, "Some Radiative Properties of the B $^3\Sigma_u^-$ State of Diatomic
     Sulfur", Ph.D. Thesis, University of Wisconsin-Madison, 1976.